University of Trento

Center for Mind/Brain Sciences

Doctorate School in Cognitive and Brain Sciences: XXIV cycle

Doctoral Dissertation

Computational Methods for the Assessment of Brain Connectivity in Visuo-Motor Integration Processes

Silvia Erla

2011

Computational Methods for the Assessment of Brain Connectivity in Visuo-Motor Integration Processes

© 2011, Silvia Erla.
All rights reserved. No part of this publication may be reproduced or transmitted in any form or by any means, without permission of the author.
Printed in Italy, Trento.
November 2011.

Author's Adress:

Erla Silvia
Center for Mind/Brain Sciences
University of Trento
Via delle Regole 101
38123 Mattarello, Trento, Italy.

email: silvia.erla@gmail.com, silvia.erla@unitn.it

University of Trento
Center for Mind/Brain Sciences
Doctorate School in Cognitive and Brain Sciences: XXIV cycle

Computational Methods for the Assessment of Brain Connectivity in Visuo-Motor Integration Processes

Silvia Erla

Advisor: PhD Giandomenico Nollo
Co-Advisor: Prof. Christoph Braun

Examination commission:
Prof. Fabio Babiloni
Prof. Maria Concetta Morrone
Prof. Costanza Papagno
Prof. Lucia Regolin

Date of the oral defense: 12 December 2011

The dataset was recorded at the Institute of Medical Psychology and Behavioral Neurobiology/MEG Center of the University of Tübingen.
Data analysis was performed at the Physics Department, BIOtech Research Center of the University of Trento.

to my grandmother, Maria

Abstract

The identification of the networks connecting different brain areas, as well as the understanding of their role in executing complex behavioral tasks, are crucial issues in cognitive neurosciences. In this context, several time series analysis approaches are available for the investigation of brain connectivity from non-invasive electroencephalographic (EEG) and magnetoencephalographic (MEG) recordings. Among them, multivariate autoregressive (MVAR) models, studied in the frequency domain, allow quantitative assessment of connectivity separately for each specific brain rhythm. In spite of its widespread utilization and great potential, MVAR-based brain connectivity analysis is complicated by a number of theoretical and practical aspects. An important issue is that the MVAR model, commonly applied to neurophysiological time series, accounts only for lagged effects among the series, forsaking instantaneous (i.e., not lagged) effects. Despite this, instantaneous correlations among EEG/MEG signals are largely expected, mainly as a consequence of volume conduction, and the impact of their exclusion on frequency-domain connectivity measures has not been investigated yet.

The aim of the present thesis was to introduce and validate a new methodological framework for the frequency-domain evaluation of brain connectivity during visuo-motor integration processes. To this end, we provided first a comprehensive description of the most common MVAR-based connectivity measures, enhancing their theoretical interpretation. Then, we introduced an extended MVAR (eMVAR) model representation explicitly accounting for instantaneous effects. Accordingly, new frequency-domain connectivity measures were defined, and procedures for improving model identification and significance assessment were given. The proposed approach was validated on theoretical illustrative examples, and then applied to EEG and MEG multichannel data recorded from subjects performing a visuo-motor task combining precise grip motor commands with sensory visual feedback.

The theoretical validation showed that, in the presence of significant instantaneous correlations, the traditional MVAR formulation may yield misleading connectivity patterns, while the correct patterns can be detected from the new measures based on eMVAR model identification. The practical application showed that instantaneous correlations are non negligible in the considered neurophysiological recordings, strongly suggesting the necessity of using the proposed eMVAR model in place of the traditional one. Results showed that execution of the visuo-motor task evokes the activation of a specific network subserving sensorimotor integration, which involves

occipito-parietal and precentral cortices. The new connectivity measures revealed connections which were peculiar of different brain rhythms. Specifically, in the alpha frequency band (8-13 Hz) we documented an enhanced driving role of the visual cortex on the left motor cortex, suggesting a relation between this rhythm and the lateralization of the visuo-motor task. In the beta band (13-30 Hz), task-induced connectivity changes were bilateral, suggesting an involvement of both hemispheres. In both alpha and beta bands, the new connectivity measures suggested an important role for the parietal cortex in mediating the information flow from visual to motor areas, confirming previous evidences from invasive studies based on intra-cranical recordings, TMS or PET examinations.

List of Abbreviations and Acronyms

MVAR	multivariate autoregressive
eMVAR	extended multivariate autoregressive
EEG	electroencephalographic
MEG	magnetoencephalographic
FT	Fourier Transform
COH	coherence Γ
PC	partial coherence Π
DC	directed coherence γ
DTF	directed transfer function δ
PDC	partial directed coherence
gPDC	generalized partial directed coherence π
sPDC	squared partial directed coherence
eDC	extended directed coherence ξ
ePDC	extended partial directed coherence χ
iDC	instantaneous directed coherence $\tilde{\gamma}$
iPDC	instantaneous partial directed coherence $\tilde{\pi}$
ROIs	regions of interest
ERFs	event related fields
ERPs	event related potentials
VM	visuo-motor task

V+M	visual plus motor task
V	visual task
M	motor task
SAM	Synthetic Aperture Magnetometry
TMS	transcranial magnetic stimulation
fMRI	functional magnetic resonance imaging
PET	positron emission tomography

Contents

Chapter 1

Introduction

In the past two decades, functional neuroimaging techniques allowed to detect the relationship between various brain regions and their specific sensory-motor or cognitive functions. The role of each area was identified on the basis of its activation during specific experimental paradigms in healthy subjects and patients. Hence, the specialization of various cortical and subcortical brain regions in isolation, also known as functional segregation, was indicated as one of the main mechanisms for the human brain organization [1]. Recently, researchers realized that the analysis of neural activity based solely on functional specialization provides only a limited account of the neuronal substrate of the investigated processes [2]. In fact, real world situations often require that our brain analyses concurrently several stimulations coming from different sensory modalities, matching them in order to take a decision or to make a movement [3]. This implies that the involved brain systems communicate with each other. The characterization of brain activity in terms of functional specialization does not reveal anything about the interplay between different areas of the extended network. Therefore, it is common opinion that functional segregation cannot be the sole mechanism for brain organization and that connectivity within and between functionally specialized areas has also to be considered [2, 3].

1.1 Brain connectivity

Brain connectivity is nowadays one of the most influential concepts in modern cognitive neurosciences. Many studies have been carried on involving different spatial and temporal resolutions and focusing on different descriptive levels, from the activity of individual neurons to the large-scale activations, by means of specific computational algorithms (see for example [4, 5, 6, 7, 8]). Despite this, a complete framework on this topic is not yet available and further theoretical and methodological clarifications are required [9].

To understand how different areas of the brain communicate in everyday life actions or in pathological states, three main approaches were proposed. The first one consists in analyzing the *neuroanatomical connectivity*. It was shown that many anatomical

modifications can be strictly associated to functional information. For example, it was observed that new connections can be generated, or already existing connections are eliminated, as a consequence of the executed functions (brain plasticity) [10]. Despite this, it is important to notice that plasticity is a slow process, in which the brain changes its organization at the neurons level. For this reason it cannot fully explain brain communication. In fact, our perceptions and cognition processes are often fast (in the order of fractions of a second) and sometimes unique (we can perceive objects that we see only once). These processes can be explained by studying *functional connectivity* and *effective connectivity*. Functional connectivity is defined as the temporal correlation between spatially remote neurophysiological events [11]. Effective connectivity is the influence that one neural system exerts over another, either directly or indirectly [12]. These definitions emphasize different aspects of brain interactivity: the description of patterns of neural activity (what the brain does) and the possible explanation of their origins (theory of how it does). The evaluation of the functional connectivity is based on testing the null hypothesis that the activity recorded from two regions is statistically independent. Statistical dependence is usually estimated by measuring correlation, covariance, spectral coherence or phase-locking. This approach does not require any assumption on the underlying system generating the data ("data-driven" approach). In contrast, to characterize the effective connectivity a model is required, describing the data to explore the concept of causality information (who drives who) or in which regions and connections of interest are specified a priori by the researcher (usually constrained by neuroanatomical or neuropsychological data), and which would produce the same temporal relationships as observed experimentally ("model-driven" approach) [2].
Obviously, to obtain a full understanding of brain connectivity mechanisms, the analysis of all the above mentioned aspects is required. Furthermore, knowledges coming from the different technologies and analysis approaches have to be integrated and compared. This is still a tricky issue, mainly because the three definitions of connectivity are applied in multiple types of data (e.g., magnetic resonance imaging, diffusion tensor imaging, positron emission tomography, functional magnetic resonance imaging, electroencephalography, magnetoencephalography), with different spatial and temporal resolution and because the actual computational algorithms, that are used to determine them, differ among investigators, even for the same data type [13]. A necessary step is therefore to clearly define connectivity every time we refer to this concept, carefully considering the applied technology and methods. Moreover, the adopted methodological approaches have to be robust and rigorous.

In this work, methods for the study of both functional and effective connectivity will be proposed and applied. These approaches are devoted to the study of specific and fast cognitive processes, which temporal scale do not involve plasticity. As an example of possible application, we propose a visuo-motor force-tracking experimental paradigm, which evokes visual perception, motor action, and visuo-motor performance. Visuo-motor force-tracking is a good example of functional cooperation between visual and motor regions, since it asks the brain for both the continuous visual inspection of the signal representing requested and actually generated force

discrepancy, and the generation of an adequate response. The actual cooperation processes between different specialized brain areas will be indicated as integration processes, to stress the fact that information coming from different sensory modalities and driving movements are used together to execute the task, and that the communication among the involved brain areas has this specific functional aim.
To avoid misunderstandings on the interpretation of our results, the meaning of the term brain connectivity will be clarified in the following paragraphs on the basis of the analyzed data and computational methods.

1.2 Detecting brain connectivity

In general, neurons communicate by sending messages (encoded in rate or synchronization of action potentials) to all the neurons to which they are anatomically connected, and the receiving neurons combine (sum and threshold) all these inputs. Besides this anatomical communication model, the data available so far support the hypothesis that synchronization of neural firings might play a crucial role in functional connectivity between different brain regions (hypothesis of the "communication-through-coherence") [14, 15, 16]. This hypothesis is based on two observations: (i) activated neuronal groups have the intrinsic property to oscillate; (ii) neuronal excitability is rhythmically modulated and this affects both the likelihood of spike output and the sensitivity to synaptic input. When two or more neuronal groups oscillate coherently (are phase-locked), the communication is effective (i.e., their communication windows for input and for output are open at the same times) [17].

A common way of eliciting information about a neurophysiological system is to study the features of one or more signals recorded from it. If we adopt the "communication-through-coherence" as a mechanism for connectivity, the recorded signals have to be sensitive to coherently oscillating neuronal groups. A widely used technique is the recording of Local Field Potentials (LFPs). Nevertheless, LFPs provide only a partial view of the electrical activity of the brain in the strict locality of the tip of the needle electrode [Erla et al., 2011a] and are not suitable for studying healthy subjects. As an alternative, non-invasive techniques such as electroencephalography (EEG) and magnetoencephalography (MEG) are widely adopted in neuroscience. In fact, the effects of synchronized oscillations observed on these recordings result from changes in both oscillatory power and phase coherence within the underlying neuronal population [15]. Moreover, EEG and MEG signals provide a direct measure of the ongoing brain activity with excellent temporal resolution (in the millisecond range), which is optimal for studying coupled oscillatory activities [18].

1.3 EEG and MEG signals

EEG and MEG are non-invasive neuroimaging techniques used to record the electromagnetic fields generated by the electrical activity within the brain. EEG measures the variation over time of the differences of electric potential between two electrodes

located on the scalp, while MEG captures the variation over time of the magnetic fields generated orthogonally to the neural currents, according to Biot-Savart's law.

EEG and MEG signals derive from ionic currents flowing at the same time in thousands of dendrites of cortical pyramidal neurons during synaptic transmission. The scalp electric potentials producing EEG come from the extracellular ionic currents caused by dendritic electrical activity (secondary currents), whereas the principal component of the the fields producing MEG signals is associated with intracellular ionic currents (primary currents).
EEG signals amplitude usually varies approximately in the range $\pm 100\ \mu V$. The weak magnetic field caused by the current flowing in the brain has amplitudes around 100 fT, which can be detected only using highly sensitive superconducting sensors (called Superconducting Quantum Interference Devices - SQUIDs- magnetometers), arranged in a dewar in whose vicinity the subject's head is placed.

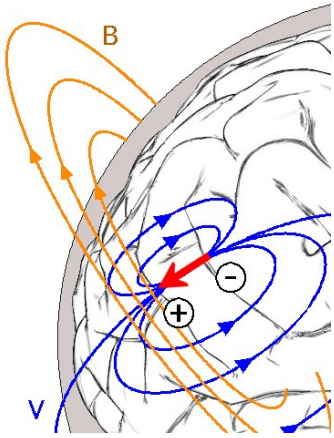

Figure 1.1: Schematic representation of fields generation in the brain.

Although EEG and MEG are similar for many aspects and are generated by the same neurophysiologic processes, there are some differences to notice. Differently from electric fields, magnetic fields are less distorted by the impedance of the skull and scalp, and for this reason MEG spatial resolution is higher. Electric and magnetic fields are oriented perpendicular to each other, so that the directions of highest sensitivity are orthogonal to each other. Scalp EEG is sensitive to both tangential and radial components of a current source, MEG detects only its tangential components (activity of the sulci). Morover, the decay of magnetic fields as a function of distance is larger than for electric fields. MEG is therefore more sensitive to superficial cortical activity. Finally, MEG is reference-free differently from EEG that requires a reference electrode.

1.4 Studying connectivity in neurophysiological signals

Given the assumption that synchronized oscillations might provide a mechanism for brain connectivity, a set of mathematical tools is required to quantify the task-related transiently formed functional networks.
By considering the temporal evolution of each signal recorded from the brain as a numerical time series, quantitative indexes can be obtained through the application of time series analysis techniques [19]. Historical approaches to time series analysis were addressed to the study of a single signal (univariate analysis). However, an increasing number of experiments are being carried out in which several neurophysiological signals are simultaneously recorded. Recent advances have made it possible to study collectively the behavior of several signals measured simultaneously from the considered system (multivariate time series analysis) [20]. The intro-

duction of these new analytical tools make it possible to extract more meaningful information from the recordings of the brain electro-magnetic activity. This is one of the main reason for the renewed interest in neurophysiological techniques such as electroencephalographic (EEG) and magnetoencephalographic (MEG), which are suitable to capture the macroscopic spatio-temporal dynamics of the brain fields at different locations of the scalp [21].
Multivariate time series analysis allows the detection of both coupling (functional connectivity) and driver-response causality relationships (effective connectivity) between the considered time series. Methods for the assessment of coupling and causality can be divided into two main branches: (i) linear time series approaches, in which a linear model is supposed to underlie the generation of temporal dynamics and interactions of the considered signals and (ii) nonlinear methods [22, 23]. Even though the nonlinear approaches are continuously under development (see for example [20, 24],[Faes et al., 2010b]), traditional linear methods are very important in the study of neurophysiological data, mainly because of their strict connection to the frequency-domain representation of the signals, which are rich of oscillatory content within the frequency bands from delta to gamma [18]. In this thesis we will focus on linear approaches.
Several frequency-domain measures of coupling and causality have been introduced and applied in recent years (see [25, 26, 27, 28, 29, 30, 31] and [Erla et al., 2009]). Despite the recent success and diffusion of many frequency-domain measures for the evaluation of coupling and causality, several aspects have to be carefully considered for a correct application and many open issues need to be addressed.

1.5 Aims of the thesis

- To give a comprehensive framework for measuring functional and effective connectivity, based on linear time series analysis methods, for the application to neurophysiological signals like EEG and MEG;
- to improve crucial aspects of the existing frequency-domain connectivity measures, such as model parameters setting procedures and assessment of the significance of the calculated frequency-domain measures of coupling/causality;
- to address the possible influences on coupling and causality measures of instantaneous (i.e., non-lagged) correlations, commonly not modeled, even if possibly occurring across the measured time series.
- to apply the presented theoretical framework on a cognitive paradigm, involving visuo-motor integration processes, in order to test the proposed methods, to discuss possible advantages and limitations and to further elucidate the neuronal mechanisms underlying visuo-motor integration.

The following part of the manuscript is divided into two main parts. The first part discusses the state of art of methods and improvements for the calculation of coupling and causality measures. In the second part, the presented theoretical approach is applied to the study of the mechanisms underlying visuo-motor integration.

Chapter 2

Coupling and causality measures

In this chapter the theoretical basis for coupling and causality analysis of multiple time series is presented. The available frequency-domain measures are detailed and some theoretical advancements and improvements are proposed and discussed: approaches for model identification, inclusion in the model of instantaneous causality effects and validation for significance through surrogate data analysis for causality. The chapter is divided into four main sections. In the first one, the definitions of coupling and causality are given for multivariate processes. The second part provides a common framework for the definition of the available frequency-domain measures of coupling and causality based on multivariate autoregressive (MVAR) models. Section three introduces a new approach, leading to the definition of novel frequency-domain causality measures, which consider significant instantaneous correlations of the observed process. In the last part, the practical application of these methods is treated, step by step, for physiological time series such as EEG or MEG signals.

2.1 Multivariate analysis of coupling and causality

2.1.1 Coupling

Consider a joint observation of time series $\mathbf{Y}(n) = [y_1(n) \cdots y_M(n)]^T$ recorded on the scalp by means of M EEG or MEG derivations. These series, distributed in space and time over the cortical surface, can be described as the realization of a stochastic process [18]. To test the hypothesis that the similarities between series recorded from different locations reflect interactions between different brain regions, the spatial properties of the stochastic activity have to be analyzed [32].
A straightforward approach to investigate dependence between signals is the conventional statistical analysis of the multivariate correlation structure of the observed processes [33]. The $M \times M$ correlation matrix and its inverse are defined, for each lag k, as:

$$\mathbf{R}(k) = E\left[\mathbf{Y}(n)\mathbf{Y}^T(n-k)\right] \quad \text{and} \quad \mathbf{P}(k) = \mathbf{R}(k)^{-1}. \tag{2.1}$$

From these definitions it is possible to extract the so called correlation coefficient and partial correlation coefficient:

$$\rho_{ij}(k) = \frac{r_{ij}(k)}{\sqrt{r_{ii}(k)r_{jj}(k)}} \quad \text{and} \quad \eta_{ij}(k) = -\frac{p_{ij}(k)}{\sqrt{p_{ii}(k)p_{jj}(k)}}, \tag{2.2}$$

with $r_{ij}(k)$ and $p_{ij}(k)$ being the i-j elements $(i, j = 1, \ldots, M)$ of $\mathbf{R}(k)$ and of $\mathbf{P}(k)$, respectively. The correlation coefficient is a normalized measure of the linear interdependence existing between $y_i(n)$ and $y_j(n-k)$ (named *correlation*), while the partial correlation coefficient is a normalized measure of the so called *direct correlation*, i.e., the linear interdependence between $y_i(n)$ and $y_j(n-k)$ after removing the effects of all remaining processes (i.e., effects of the other co–recorded channels on the specific pair i-j).

The frequency-domain analogous of the covariance approach is coherence analysis. The multivariate process $\mathbf{Y}(n)$ can be represented in the frequency domain by its $M \times M$ spectral density matrix:

$$\mathbf{S}(f) = \begin{pmatrix} S_{11} & S_{12} & \cdots & S_{1M} \\ S_{21} & S_{22} & \cdots & S_{2M} \\ \vdots & \vdots & \vdots & \vdots \\ S_{M1} & S_{M2} & \cdots & S_{MM} \end{pmatrix}, \tag{2.3}$$

where the diagonal terms contain the auto-spectra of each considered series y_i, while the off-diagonal terms contain the cross-spectra between y_i and y_j $(i, j = 1, \ldots, M)$. $\mathbf{S}(f)$ is defined as the Fourier transform (FT) of the correlation matrix $\mathbf{R}(k)$ [22]. Starting from the spectral matrix $\mathbf{S}(f)$ and its inverse $\mathbf{P}(f) = \mathbf{S}(f)^{-1}$, it is possible to provide frequency-domain measures of coupling and direct coupling. Hence, the *coherence* (COH) and the *partial coherence* (PC) functions are defined [34]:

$$\Gamma_{ij}(f) = \frac{S_{ij}(f)}{\sqrt{S_{ii}(f)S_{jj}(f)}}, \quad \Pi_{ij}(f) = -\frac{P_{ij}(f)}{\sqrt{P_{ii}(f)P_{jj}(f)}}. \tag{2.4}$$

Since the functions in 2.4 are complex-valued, usually their squared values $|\Gamma_{ij}(f)|^2$ and $|\Pi_{ij}(f)|^2$ are adopted for the estimation of coupling and direct coupling. Their range varies between 0 for uncoupling (random relations of power and phase between signals) and 1 for full coupling (linear relation of power and phase between the two signals).

EEG and MEG coherence is often used to measure the functional association between two brain regions [35, 18]. Several cognitive and clinical studies describe it as a sensitive measure that can reveal aspects of the network dynamics of the brain, complementary to the data obtained by power spectral analysis (see, for example, [36, 37, 38, 27, 39, 40, 41, 42]).
To correctly interpret the neurophysiological results of EEG/MEG coherence analysis, the dependence of coherence estimate both from power and phase dynamics of the signals has to be considered. In fact, unlike correlation, coherence analysis does not provide direct information on phase relations. Nevertheless, it depends on the stability of phase relations [32]. In addition, cortico-cortical connectivity studies have to seriously consider the physical constrains of scalp recordings [43, 44], e.g., volume conductor and reference issue.
Finally, it is worth to notice that coherence and partial coherence have symmetrical nature. Therefore, they cannot provide information about causality. Such an information can be extracted, as explained in the following paragraphs, from the coefficients of a parametric representation of the time series.

2.1.2 Causality

The concept of causality in the context of linear models of stochastic processes was first formulated by Sir Clive William John Granger in 1969 [45]. He won a Nobel Memorial Prize in Economic Sciences for this discovery, which has played a considerable role in investigating the relations among stationary time series. The original definition, named *Granger causality*, is based on the concept of improvement in predictability of a time series (i.e. reduction of the variance of the predictive error) resulting from incorporating the past of a second series, above the predictability based solely on the past of the first series. Anyway, this definition involves only the relation between pairs of time series, and may produce misleading results (spurious or indirect causality relations) when the true network involves three or more variables, as shown in Fig. 2.1. To overcome this issue, the *conditional Granger causality* (or *prima facie causality*) was defined [47]: Y is a prima facie cause of X, if lagged observations of Y helps to predict X when lagged observations of the other series Z are also considered [46, 48].

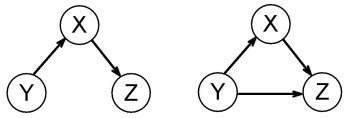

Figure 2.1: A pairwise causality analysis cannot distinguish these two connectivity patterns. Adapted from [46].

Given a multivariate stochastic process $\mathbf{Y}$, composed of M scalar processes of zero mean, $\mathbf{Y} = [y_1, \ldots, y_M]^T$, defined at discrete time ($y_m = y_m(n)$; e.g., sampled ver-

sions of the continuous time processes $y_m(t)$, taken at the times $t_n = nT$, with T the sampling period), we indicate the set of p past values of $y_m(n)$ $(m = 1, \ldots, M)$ as $Y_m = \{y_m(n-1), \ldots, y_m(n-p)\}$, and the set of the past values of all processes except y_m as $Z_m = \{Y_l | l = 1, \ldots, M, l \neq m\}$. Two different definitions of causality from the process y_j to the process y_i $(i, j = 1, \ldots, M; i \neq j)$ can be formalized:

- direct causality from y_j to y_i, $y_j \rightarrow y_i$, exists if the prediction of $y_i(n)$ based on Z_j and Y_j is better than the prediction of $y_i(n)$ solely based on Z_j;
- causality from y_j to y_i, $y_j \Rightarrow y_i$, exists if a cascade of L direct causality relations occurs such that $y_j \rightarrow y_m \cdots \rightarrow y_i$ for at least one value m in the set $(1, \ldots, M)$.

It is worth noticing that, for a bivariate process $(M = 2)$, causality reduces to direct causality and that they correspond to the original Granger definition [45], while for a multivariate process, direct causality corresponds to *prima facie* causality [47]. Furthermore, it is worth to emphasize that the definitions of coupling, accounting for the presence or absence of an interaction between processes but not for the directionality of such interaction, can be derived from the causality definitions as follows [49]:

- direct coupling between y_i and y_j, $y_i \leftrightarrow y_j$, exists if $y_i \rightarrow y_m$ and $y_j \rightarrow y_m$; the most obvious case is when $m = i$ or $m = j$, but two processes are considered as directly coupled also when they both directly cause a third common process $(m \neq i,\ m \neq j)$;
- coupling between y_i and y_j, $y_i \Leftrightarrow y_j$, exists if $y_m \Rightarrow y_i$ and $y_m \Rightarrow y_j$; coupling may arise when one of the two processes causes the other $(m = i$ or $m = j)$, or when both processes are caused by other common processes $(m \neq i,\ m \neq j)$.

To conclude this paragraph, we present a graphical and intuitive representation of the above causality and coupling definitions for an example of network with 4 interacting processes (Fig. 2.2).

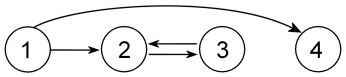

Figure 2.2: Schematic representation of a set of interactions. Nodes correspond to processes and connecting arrows depict direct causality relations.

By observing the connectivity diagram, the following relations can be listed:

- direct causality: $1 \rightarrow 2$, $2 \rightarrow 3$, $3 \rightarrow 2$, and $1 \rightarrow 4$;
- causality: $1 \Rightarrow 2$, $2 \Rightarrow 3$, $3 \Rightarrow 2$, $1 \Rightarrow 4$ (direct causality is a sufficient condition for causality) and $1 \Rightarrow 3$ (the cascade $1 \rightarrow 2 \rightarrow 3$ determines an indirect effect);
- direct coupling: $1 \leftrightarrow 2$, $2 \leftrightarrow 3$, $1 \leftrightarrow 4$ (it follows from direct causality), and $1 \leftrightarrow 3$ (common driving exerted by 1 and 3 on 2);
- coupling: $1 \Leftrightarrow 2$, $2 \Leftrightarrow 3$, $1 \Leftrightarrow 4$, $1 \Leftrightarrow 3$ (because of the causality relations), $3 \Leftrightarrow 4$ and $2 \Leftrightarrow 4$ (because of the common driving exerted by 1 respectively on 3 and 4, and on 2 and 4).

2.1.3 MVAR modeling

MVAR models are a well known method for the evaluation of linear stochastic time series [33, 50]. They describe well signals containing various oscillations (rhythms), allowing to extract from the noise frequency-specific information about the analyzed series [48]. This property makes them very useful for the study of neurophysiological signals like EEG or MEG, which show specific rhythms of a certain frequency embedded in a noisy background [51].
This parametric approach for spectral data analysis is commonly used to formalize the notions of coupling and causality in time and frequency domain, respectively through the model coefficients and through their spectral representation [22, 52, 28], as we will see in the following paragraphs.

Time domain

The data vector $\mathbf{Y}(n)$, at the time n, can be described by the sum of its linearly weighted p previous samples in the following way [22]:

$$\mathbf{Y}(n) = \sum_{k=1}^{p} \mathbf{A}(k)\mathbf{Y}(n-k) + \mathbf{U}(n), \tag{2.5}$$

where $\mathbf{A}(k)$ is the matrix of autoregressive coefficients for the kth time lag, while p is the model order that indicates the maximum number of considered time lags. $\mathbf{U}(n)$ is assumed to be composed of white and uncorrelated noises, i.e., the correlation matrix of $\mathbf{U}(n)$, $\mathbf{R}_{\mathbf{U}}(k)$, is zero for each lag $k > 0$, while it is equal to the covariance matrix $\Sigma = cov\,(\mathbf{U}(n))$ for $k = 0$.

By fitting the model to the data we estimate a set of coefficients (see Sec. 2.4.4 for identification approaches):

$$\mathbf{A}(k) = \begin{bmatrix} A_{11}(k) & A_{12}(k) & \cdots & A_{1M}(k) \\ \vdots & \vdots & \vdots & \vdots \\ A_{M1}(k) & \cdots & \cdots & A_{MM}(k) \end{bmatrix}, \tag{2.6}$$

describing properties of the joint description of the processes. In fact, the i–j element of $\mathbf{A}(k)$, $A_{ij}(k)$, quantifies the causal linear interaction effect occurring at lag k from y_j to y_i. As a consequence, the definitions of coupling and causality provided above (Sec. 2.1.2) for a general multivariate process can be specified for a MVAR process in terms of the off-diagonal elements of $\mathbf{A}(k)$ as follows [49],[Faes et al., 2011b]:

- direct causality $y_j \rightarrow y_i$ exists if $A_{ij}(k) \neq 0$ for at least one $k = 1, \ldots, p$;
- causality $y_j \Rightarrow y_i$ exists if $A_{m_s m_{s-1}}(k_s) \neq 0$ for at least a set of $s = 1, \ldots, L-1$ values, with $L \geq 2$ (with $m_{L-1} = i$, $m_0 = j$) and a set of lags k_s with values in $(1, \ldots, p)$;
- direct coupling, $y_j \leftrightarrow y_i$ exists if $A_{mi}(k_1) \neq 0$ for at least one k_1 or $A_{mj}(k_2) \neq 0$ for at least one k_2;

- coupling, $y_j \Leftrightarrow y_i$ exists if $A_{m_s m_{s-1}}(k_s) \neq 0$ for at least a set of $s = 1, \ldots, L-1$ values, with $L \geq 2$ (either with $m_0 = m, m_{L-1} = i$ or with $m_0 = m, m_{L-1} = j$) and a set of lags k_s.

Frequency domain

The Fourier Transform of Eq. 2.5 gives the spectral representation of a MVAR process [22, 50]:

$$\mathbf{Y}(f) = \mathbf{A}(f)\mathbf{Y}(f) + \mathbf{U}(f) = \mathbf{H}(f)\mathbf{U}(f), \tag{2.7}$$

where $\mathbf{Y}(f)$ and $\mathbf{U}(f)$ are the FTs of $\mathbf{Y}(n)$ and $\mathbf{U}(n)$ and the $M \times M$ coefficient matrix is defined in the frequency domain as:

$$\mathbf{A}(f) = \sum_{k=1}^{p} \mathbf{A}(k) e^{-j2\pi fkT}. \tag{2.8}$$

The matrix $\mathbf{H}(f)$ is called transfer matrix of the system. It contains frequency-dependent information about the relations between channels, since it is linked to the coefficients matrix by:

$$\mathbf{H}(f) = [\mathbf{I} - \mathbf{A}(f)]^{-1} = \bar{\mathbf{A}}(f)^{-1}. \tag{2.9}$$

This relation is the basis to define various frequency-domain estimates of coupling and causality in terms of the MVAR representation. It provides a useful link between the *cross-spectral density matrix* $\mathbf{S}(f)$ and its inverse $\mathbf{P}(f)$. In fact, it is possible to demonstrate [22] that for a MVAR process:

$$\mathbf{S}(f) = \mathbf{H}(f)\Sigma\mathbf{H}^H(f), \quad \mathbf{P}(f) = \bar{\mathbf{A}}^H(f)\Sigma^{-1}\bar{\mathbf{A}}(f), \tag{2.10}$$

where the superscript H stands for the Hermitian transpose and Σ is the covariance matrix of $\mathbf{U}(n)$, describing the frequency-independent variance of the process. For the sake of simplicity, from now we will consider the i–jth elements of $\mathbf{S}(f)$ and $\mathbf{P}(f)$:

$$S_{ij}(f) = \mathbf{h}_i(f)\Sigma\mathbf{h}_j^H(f), \quad P_{ij}(f) = \bar{\mathbf{a}}_i^H(f)\Sigma^{-1}\bar{\mathbf{a}}_j(f), \tag{2.11}$$

where $\mathbf{h}_i(f)$ is the i–th row of the transfer matrix $\mathbf{H}(f) = [\mathbf{h}_1(f) \cdots \mathbf{h}_M(f)]$ and $\bar{\mathbf{a}}_i(f)$ is the i–th column of the coefficient matrix $\bar{\mathbf{A}}(f) = [\bar{\mathbf{a}}_1(f) \cdots \bar{\mathbf{a}}_M(f)]$.

If the input white noises $\mathbf{U}(f)$ are uncorrelated even at lag zero, their covariance is a diagonal matrix, $\Sigma = diag(\sigma_i^2)$, as also its inverse $\Sigma^{-1} = diag(1/\sigma_i^2)$ is, with σ_i^2 variance of u_i. In this case, the Eq.2.11 can be expressed as:

$$S_{ij}(f) = \sum_{m=1}^{M} H_{im}(f)\sigma_m^2 H_{jm}^*(f), \quad P_{ij}(f) = \sum_{m=1}^{M} \bar{A}_{mi}^*(f)\frac{1}{\sigma_m^2}\bar{A}_{mj}(f). \tag{2.12}$$

Using the latter, it is possible to express the measures of coupling and direct coupling (Eq. 2.4) in terms of directional information from one process to another.

The coherence between y_i and y_j can be written as:

$$\Gamma_{ij}(f) = \frac{S_{ij}(f)}{\sqrt{S_{ii}(f)S_{jj}(f)}} = \sum_{m=1}^{M} \frac{\sigma_m H_{im}(f)}{\sqrt{S_{ii}(f)}} \frac{\sigma_m H_{jm}^*(f)}{\sqrt{S_{jj}(f)}} = \sum_{m=1}^{M} \gamma_{im}(f)\gamma_{jm}^*(f), \quad (2.13)$$

in order to decompose it into a forward and a backward part. Hence, *directed coherence* (DC) can be defined [53, 52]:

$$\gamma_{ij}(f) = \frac{\sigma_j H_{ij}(f)}{\sqrt{S_{ii}(f)}} = \frac{\sigma_j H_{ij}(f)}{\sqrt{\sum_{m=1}^{M} \sigma_m^2 \left|H_{im}(f)\right|^2}}. \quad (2.14)$$

Squared DC is characterized by the following normalization properties:

1. $0 \leq \left|\gamma_{ij}(f)\right|^2 \leq 1$. Hence, squared DC measures, for each frequency f, a normalized coupling strength. It is equal to 0 in absence of directed (i.e., causal) coupling and 1 for full directed coupling.

2. $\sum_{m=1}^{M} \left|\gamma_{im}(f)\right|^2 = 1$. This means that squared DC, $\left|\gamma_{ij}(f)\right|^2$, measures the coupling strength from y_j to y_i as the normalized proportion of $S_{ii}(f)$ which is due to y_j.

Moreover, expanding Eq. 2.9 as a geometric series [54], it is possible to show that the transfer function $H_{ij}(f)$ contains a sum of terms each one related to one of the (direct or indirect) transfer paths connecting y_j to y_i; therefore the numerator of Eq. 2.14 is non-zero whenever any path connecting y_j to y_i is significant, i.e., when causality occurs from y_j to y_i [Faes et al., 2011b].

By adding the additional restriction that all the input variances σ_i^2 are equal to each other ($i = 1, \ldots, M$), i.e., assuming that Σ has the sole diagonal elements, Eq. 2.14 leads to the definition of *directed transfer function* (DTF) from y_j to y_i [55, 56]:

$$\delta_{ij}(f) = \frac{H_{ij}(f)}{\sqrt{\sum_{m=1}^{M} \left|H_{im}(f)\right|^2}}. \quad (2.15)$$

Thus, the DTF can be seen as a particularization of the DC function. In the following, we will consider only DC, as it provides a similar measure of frequency-domain causality, but more general and interpretable in terms of power content.

In a similar way to that followed to decompose the coherence function, using Eq. 2.12, the partial coherence can be defined as follows:

$$\Pi_{ij}(f) = -\frac{P_{ij}(f)}{\sqrt{P_{ii}(f)P_{jj}(f)}} = -\sum_{m=1}^{M} \frac{\frac{1}{\sigma_m}\bar{A}_{mj}(f)}{\sqrt{P_{jj}(f)}} \frac{\frac{1}{\sigma_m}\bar{A}_{mi}^*(f)}{\sqrt{P_{ii}(f)}} = -\sum_{m=1}^{M} \pi_{mj}(f)\pi_{mi}^*(f). \quad (2.16)$$

In the latter the so called *generalized partial directed coherence* (gPDC) is introduced [57], defined as:

$$\pi_{ij}(f) = \frac{\frac{1}{\sigma_i}\bar{A}_{ij}(f)}{\sqrt{\sum_{m=1}^{M}\frac{1}{\sigma_m^2}\left|\bar{A}_{mj}(f)\right|^2}}. \tag{2.17}$$

Squared gPDC is characterized by the following normalization properties:

1. $0 \leq |\pi_{ij}(f)|^2 \leq 1$. Hence, squared gPDC measures, for each frequency f, the normalized direct coupling strength, quantified with values in the range $(0, 1)$.
2. $\sum_{m=1}^{M} |\pi_{mj}(f)|^2 = 1$. Squared gPDC, $|\pi_{ij}(f)|^2$, measures the interaction from y_j to y_i as the normalized proportion of $P_{jj}(f)$ which is sent to y_i.

gPDC is a measure of direct causality, because the numerator in Eq. 2.17 contains the term $\bar{A}_{ij}(f)$ $(i \neq j)$, which is non-zero only when $A_{ij}(k) \neq 0$ for at least one $k = 1, \ldots, p$, and is uniformly zero when $A_{ij}(k) = 0$ for each k [Faes et al., 2011b].

The gPDC defined as in Eq. 2.17 is different from the *partial directed coherence* (PDC) in its original version [52] and from its modification *squared partial directed coherence* (sPDC) (proposed in [58]), which did not include inner normalization by the input noise variances. The definition of gPDC follows directly from the decomposition in Eq. 2.16. Moreover, as well as coherence, partial coherence and directed coherence functions, also this definition has the important property of scale-invariance, contrary to the original PDC that may be affected by different amplitudes of the considered signals.

To summarize, it is worth listing DC and gPDC main differences, advantages and limitations.

DC measures causality as the amount of information flowing from y_j to y_i through all (direct and indirect) pathways, in respect to the total inflow entering the structure at which y_i is measured.
The DC has a meaningful physical interpretation, as it measures causality as the amount of power transferred from one process to another, but cannot distinguish between direct and indirect causal effects measured in the frequency domain.

gPDC measures direct causality as the amount of information flowing from y_j to y_i through the direct connection only, in respect to the total outflow leaving the structure at which y_j is measured.
The gPDC provides a one-to-one representation of direct causality, but is hardly useful as a quantitative measure because its magnitude quantifies the information flow through the inverse spectral matrix elements (which do not find easy interpretation in terms of power spectral density).

2.2 Instantaneous effects

From the above discussion, it is possible to notice that MVAR models accounts only for lagged effects (i.e., effects of the past of a time series on the present of another), but not for instantaneous effects (describing influences which occur within the same lag) among the series. Despite this, instantaneous correlations among the series are very common in EEG/MEG analysis, and their significance has rarely been tested in practical applications. Moreover, the possible effects on coupling and causality measures of forsaking such correlations have not been investigated thoroughly. Very recent studies have suggested that neglecting instantaneous interactions in the model representation may lead to heavily modified connectivity patterns [Erla et al., 2009, Faes et al., 2010a],[59].

Given the vector stochastic process $\mathbf{Y} = [y_1, \ldots, y_M]^T$, composed of M scalar processes of zero mean, it is possible to define $Y_m = \{y_m(n-1), \ldots, y_m(n-p)\}$ and $\acute{Y}_m = \{y_m(n), Y_m\}$ $(m = 1, \ldots, M)$, as the set of p past values of $y_m(n)$ and the set enlarged with the current value, respectively. New definitions of causality from the process y_j to the process y_i can be added to those presented in section 2.1.2, to compose this framework:

- instantaneous causality from y_j to y_i exists if $y_j(n)$ is useful to predict $y_i(n)$;
- direct causality from y_j to y_i, $y_j \rightarrow y_i$ exists if Y_j is useful to predict $y_i(n)$;
- extended direct causality from y_j to y_i, $y_j \dot{\rightarrow} y_i$ exists if $\acute{Y}_j$ is useful to predict $y_i(n)$;
- causality from y_j to y_i, $y_j \Rightarrow y_i$ exists if a cascade of L direct causality relations occurs such that $y_j \rightarrow y_m \cdots \rightarrow y_i$;
- extended causality from y_j to y_i, $y_j \dot{\Rightarrow} y_i$ exists if a cascade of L extended direct causality relations occurs such that $y_j \dot{\rightarrow} y_m \cdots \dot{\rightarrow} y_i$.

While the definitions of direct causality and causality consider only lagged effects, instantaneous causality and extended causality definitions include instantaneous effects, i.e. effects from one series to another occurring within the same lag. In absence of instantaneous effects between all pairs of scalar processes, extended direct causality reduces to direct causality, and extended causality reduces to causality. Therefore, extended definitions we presented above, may be viewed as generalizations which combine instantaneous to lagged effects, traditionally studied for causality estimation [59],[Faes et al., 2011a].

To give a brief and intuitive summary of the above causality and coupling definitions, a graphical representation is reported in Fig. 2.3 for an example of network with 4 interacting processes.

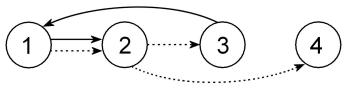

Figure 2.3: Schematic representation of a set of interactions. Nodes correspond to processes and connecting arrows depict direct causality relations. Lagged and instantaneous effects are depicted with solid and dashed arrows, respectively.

For this process, the observed connectivity relations are:

- direct causality occurs only when lagged effects are present: $1 \rightarrow 2$ and $3 \rightarrow 1$;
- extended direct causality follows from both lagged and instantaneous direct causality: $1 \dot{\rightarrow} 2$, $2 \dot{\rightarrow} 3$, $2 \dot{\rightarrow} 4$ and $3 \dot{\rightarrow} 1$;
- causality: $1 \Rightarrow 2$, $3 \Rightarrow 1$ and $3 \Rightarrow 2$;
- extended causality: $1 \dot{\Rightarrow} 2$, $1 \dot{\Rightarrow} 3$, $1 \dot{\Rightarrow} 4$, $2 \dot{\Rightarrow} 1$, $2 \dot{\Rightarrow} 3$, $2 \dot{\Rightarrow} 4$, $3 \dot{\Rightarrow} 1$, $3 \dot{\Rightarrow} 2$ and $3 \dot{\Rightarrow} 4$ (because of the several cascades of instantaneous and/or lagged effects);
- direct coupling: $1 \leftrightarrow 2$, $2 \leftrightarrow 3$, $2 \leftrightarrow 4$ and $3 \leftrightarrow 1$ (no common driving of two processes on a third one is observed);
- coupling: between all pairs of processes.

2.2.1 eMVAR modeling

The MVAR model described in 2.5 is a strictly causal model, accounting only for lagged effects. The model coefficients $\mathbf{A}(k)$ are defined only for positive lags ($k > 0$) and don't describe any zero-lag correlation among the observations. As a consequence, if zero-lag correlation exists among the processes, it becomes part of the correlation among the model inputs $\mathbf{U}$ and the input covariance matrix Σ results not diagonal, contradicting the assumptions of spectral factorization [60]. This may have bad consequences in the estimation of the causality measures described in section 2.1.3. To solve this issue, we propose an alternative approach to the strictly causal model (see [Erla et al., 2009] for details), named *extended multivariate autoregressive* (eMVAR) model.

Time domain

The multivariate process $\mathbf{Y}(n)$ can be described including instantaneous effects into the model [Erla et al., 2009]:

$$\mathbf{Y}(n) = \sum_{k=0}^{p} \mathbf{B}(k)\mathbf{Y}(n-k) + \mathbf{W}(n), \tag{2.18}$$

where $\mathbf{W}(n) = [w_1(n), \ldots, w_M(n)]^T$ is a vector of zero-mean uncorrelated white noise processes. Note that the lag variable k starts now from the value 0 and instantaneous effects from $y_j(n)$ to $y_i(n)$ are consequently modeled by the coefficients $b_{ij}(0)$ of the matrix $\mathbf{B}(0)$. Furthermore, in the eMVAR model, the absence of correlation among the noise inputs w_i is not an assumption: the covariance matrix $\Lambda = cov(\mathbf{W}(n))$ is guaranteed to be diagonal by the inclusion of the instantaneous effects.

The strictly causal model in Eq. 2.5 can be transformed into the extended model in Eq. 2.18 by left moving the term $\mathbf{B}(0)\mathbf{Y}(n)$ in 2.18 and multiplying both terms of the equation by $\mathbf{L} = [\mathbf{I} - \mathbf{B}(0)]^{-1}$, where $\mathbf{I}$ is the $M \times M$ identity matrix. In this way, the following relations are evidenced:

$$\mathbf{B}(k) = \mathbf{L}^{-1}\mathbf{A}(k) \quad \text{and} \quad \mathbf{W}(n) = \mathbf{L}^{-1}\mathbf{U}(n) \qquad (k = 1, \ldots, p). \tag{2.19}$$

Note that the two models reduce into the same in the absence of instantaneous effects; in fact, if the matrix $\mathbf{B}(0)$ has all zero elements, $\mathbf{L} = \mathbf{I}$ and the extended causal model reduces to the strictly causal model ($\mathbf{A}(k) = \mathbf{B}(k)$, $\mathbf{U}(n) = \mathbf{W}(n)$). On the contrary, in presence of instantaneous effects, $\mathbf{A}(k) \neq \mathbf{B}(k)$ at each lag k. So different causality patterns may be estimated depending on whether instantaneous effects are included or not in the MVAR model.

The presented extended multivariate autoregressive model gives the possibility to define the causality measures introduced in section 2.2 in terms of the off-diagonal elements $b_{ij}(k)$ of $\mathbf{B}(k)$. Here below is presented an updated list of the coupling and causality definitions [Faes et al., 2010a],[49]:

- instantaneous causality from y_j to y_i exists if $b_{ij}(k) \neq 0$;
- direct causality from y_j to y_i, $y_j \rightarrow y_i$ exists if $b_{ij}(k) \neq 0$ for at least one $k \geq 1$;
- extended direct causality from y_j to y_i, $y_j \dot{\rightarrow} y_i$ exists if $b_{ij}(k) \neq 0$ for at least one $k \geq 0$;
- causality from y_j to y_i, $y_j \Rightarrow y_i$ exists if $b_{m_s m_{s-1}}(k_s) \neq 0$ for a set of lags k_s with values in $(1, \ldots, p)$;
- extended causality from y_j to y_i, $y_j \dot{\Rightarrow} y_i$ exists if if $b_{m_s m_{s-1}}(k_s) \neq 0$ for a set of lags k_s with values in $(0, \ldots, p)$;
- direct coupling $y_j \leftrightarrow y_i$ exists if $b_{ij}(k) \neq 0$ and/or $b_{ji}(k) \neq 0$ for at least one $k = 0, \ldots, p$;
- coupling $y_j \Leftrightarrow y_i$ exists if $b_{m_s m_{s-1}}(k_s) \neq 0$ for a set of $s = 1, \ldots, L-1$ values, with $L \geq 2$ (either with $m_0 = j$, $m_{L-1} = i$ or with $m_0 = i$, $m_{L-1} = j$) and a set of lags k_s.

Frequency domain

Fourier transform of Eq. 2.18 gives the spectral representation of an eMVAR process:

$$\mathbf{Y}(f) = \mathbf{B}(f)\mathbf{Y}(f) + \mathbf{W}(f) = \mathbf{G}(f)\mathbf{W}(f), \tag{2.20}$$

where $\mathbf{Y}(f)$ and $\mathbf{W}(f)$ are the FTs of $\mathbf{Y}(n)$ and $\mathbf{W}(n)$ and the $M \times M$ coefficient matrix $\mathbf{B}(f)$ is defined in the frequency domain as:

$$\mathbf{B}(f) = \sum_{k=0}^{p} \mathbf{B}(k) e^{-j2\pi fkT}. \tag{2.21}$$

$\mathbf{G}(f)$ is called transfer matrix of the system and is defined as:

$$\mathbf{G}(f) = [\mathbf{I} - \mathbf{B}(f)]^{-1} = \bar{\mathbf{B}}(f)^{-1}. \tag{2.22}$$

For the extended causal model the spectral matrix and its inverse are defined as:

$$\mathbf{S}(f) = \mathbf{G}(f)\Lambda\mathbf{G}^H(f), \quad \mathbf{P}(f) = \bar{\mathbf{B}}^H(f)\Lambda^{-1}\bar{\mathbf{B}}(f). \tag{2.23}$$

It can be easily shown that the spectral matrix and its inverse in Eq. 2.23 are exactly the same than those in Eq. 2.10 [49]. Hence, the spectral representation for strictly causal MVAR and extended processes are equivalent. As a consequence, also the coupling and direct coupling measures are equivalent in the two representations, depending only on the elements of $\mathbf{S}(f)$ and $\mathbf{P}(f)$, as shown in Eq. 2.4.

A significant difference, in presence of instantaneous effects, is evident in evaluating causality. We want to stress that the original formulation of DC and gPDC fully holds only under the assumption of uncorrelation of the input processes (diagonality of Σ and Σ^{-1}). If this assumption is not fulfilled, the spectral factorizations in Eq. 2.12 do not hold anymore and the DC and gPDC may become unable to identify causality and direct causality in the frequency domain. On the contrary, in the eMVAR representation the covariance matrix Λ and its inverse are diagonal by construction. In this case the factorizations in Eq. 2.12 can be applied (with $\mathbf{B}(f)$ and $\mathbf{G}(f)$ in place of $\mathbf{A}(f)$ and $\mathbf{H}(f)$) both for coherence:

$$\Gamma_{ij}(f) = \frac{S_{ij}(f)}{\sqrt{S_{ii}(f)S_{jj}(f)}} = \sum_{m=1}^{M} \frac{\lambda_m G_{im}(f)}{\sqrt{S_{ii}(f)}} \frac{\lambda_m G^*_{jm}(f)}{\sqrt{S_{jj}(f)}} = \sum_{m=1}^{M} \xi_{im}(f)\xi^*_{jm}(f), \tag{2.24}$$

and for partial coherence:

$$\Pi_{ij}(f) = -\frac{P_{ij}(f)}{\sqrt{P_{ii}(f)P_{jj}(f)}} = -\sum_{m=1}^{M} \frac{\frac{1}{\lambda_m}\bar{B}_{mj}(f)}{\sqrt{P_{jj}(f)}} \frac{\frac{1}{\lambda_m}\bar{B}^*_{mi}(f)}{\sqrt{P_{ii}(f)}} = -\sum_{m=1}^{M} \chi_{mj}(f)\chi^*_{mi}(f), \tag{2.25}$$

where λ_i is the ith element of the diagonal covariance matrix $\Lambda = cov(\mathbf{W}(n))$. The last terms of Eq. 2.24 and 2.25 are the so called *extended directed coherence* (eDC) and *extended partial directed coherence* (ePDC) , defined as [Faes et al., 2010a],[61]:

$$\xi_{ij}(f) = \frac{\lambda_j G_{ij}(f)}{\sqrt{\sum_{m=1}^{M} \lambda_m^2 \left|G_{im}(f)\right|^2}} \quad \text{and} \quad \chi_{ij}(f) = \frac{\frac{1}{\lambda_i}\bar{B}_{ij}(f)}{\sqrt{\sum_{m=1}^{M} \frac{1}{\lambda_m^2} \left|\bar{B}_{mj}(f)\right|^2}}. \tag{2.26}$$

Eqs. 2.26 contain information of both the lagged ($k > 0$) and instantaneous ($k = 0$) information flow from y_j to y_i, being calculated from $\mathbf{B}(f)$. They measure extended causality and extended direct causality, respectively.
The normalization conditions of the strictly causal representation are respected also for this new approach. $|\xi_{ij}(f)|^2$ represents the normalized proportions of $S_{ii}(f)$ coming from y_j, while $|\chi_{ij}(f)|^2$ is the normalized proportions of $P_{jj}(f)$ sent to y_i.

Even if the multivariate process is modeled by the extended representation considering instantaneous effects, it is possible to obtain from the same model "lagged" causality. To this end, one has to exclude the coefficients with the information about zero-lag interactions as follows:

$$\tilde{\mathbf{B}}(f) = \bar{\mathbf{B}}(f) + \mathbf{B}(0) = \mathbf{I} - \sum_{k=1}^{p} \mathbf{B}(k) e^{-j2\pi fkT}, \quad \tilde{\mathbf{G}}(f) = \tilde{\mathbf{B}}(f)^{-1}. \tag{2.27}$$

Consequently, *instantaneous directed coherence* (iDC) and *instantaneous partial directed coherence* (iPDC) can be defined as:

$$\tilde{\gamma}_{ij}(f) = \frac{\lambda_j \tilde{G}_{ij}(f)}{\sqrt{\sum_{m=1}^{M} \lambda_m^2 \left|\tilde{G}_{im}(f)\right|^2}} \quad \text{and} \quad \tilde{\pi}_{ij}(f) = \frac{\frac{1}{\lambda_i} \tilde{B}_{ij}(f)}{\sqrt{\sum_{m=1}^{M} \frac{1}{\lambda_m^2} \left|\tilde{B}_{mj}(f)\right|^2}}. \tag{2.28}$$

iDC and iPDC are different from DC and gPDC given in Eq. 2.14 and 2.17, because the presence of instantaneous effects leads to different estimates of the coefficient matrix ($\mathbf{A}(k) \neq \mathbf{B}(k)$). Only in the absence of instantaneous effects $\mathbf{A}(k) = \mathbf{B}(k)$, and consequently DC, iDC and eDC are the same, as such as gPDC, iPDC, and ePDC.

To conclude this part, a summarizing table is proposed, including the main frequency-domain MVAR coupling and causality measures, and the new proposed measures based on the eMVAR model.

Table 2.1: Frequency-domain measures of coupling/causality between the processes y_i and y_j.

		MVAR	eMVAR
DIRECT			
Direct coupling	$\leftrightarrow$	PC $\Pi_{ij(f)}$	
Direct causality	$\rightarrow$	gPDC $\pi_{ij(f)}$	iPDC $\tilde{\pi}_{ij(f)}$
Extended direct causality	$\dot{\rightarrow}$		ePDC $\chi_{ij(f)}$
DIRECT+INDIRECT			
Coupling	$\Leftrightarrow$	COH $\Gamma_{ij(f)}$	
Causality	$\Rightarrow$	DC $\gamma_{ij(f)}$	iDC $\tilde{\gamma}_{ij(f)}$
Extended causality	$\dot{\Rightarrow}$		eDC $\xi_{ij(f)}$

2.3 Theoretical illustrative examples

In this section the various frequency-domain measures presented in sections 2.1.3 and 2.2.1 are studied for two MVAR processes with imposed connectivity patterns. This allows a better comprehension of the meaning of these measures and of the differences between them. In the first example only lagged interactions are considered, to discuss differences between coherence and partial coherence, and between DC and gPDC. In the second one instantaneous interactions are also considered. The simulations proposed here are taken from [Faes et al., 2011a].

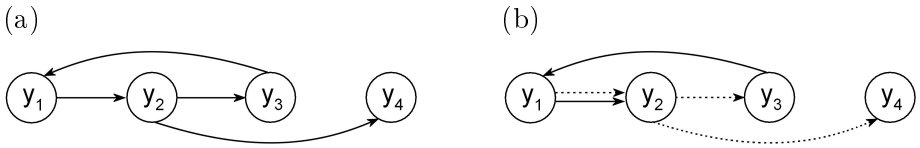

Figure 2.4: Examples of coupling/causality patterns considering (a) only lagged effects and (b) instantaneous+lagged effects. Solid arrows indicate lagged connections, while dashed lines are instantaneous effects.

2.3.1 Strictly causal interactions

Let consider the MVAR process of order $p = 2$, composed by $M = 4$ scalar processes, generated by the equations:

$$\begin{cases} y_1(n) = 2\rho_1 \cos(2\pi f_1) y_1(n-1) - \rho_1^2 y_1(n-2) + 0.7 y_3(n-2) + u_1(n) \\ y_2(n) = y_1(n-1) - 0.5 y_1(n-2) - \rho_2^2 y_2(n-2) + u_2(n) \\ y_3(n) = 0.5 y_2(n-1) + u_3(n) \\ y_4(n) = 0.5 y_2(n-1) + u_4(n) \end{cases} \tag{2.29}$$

The process innovations u_i are independent white noises of unit variance ($\Sigma = \mathbf{I}$). The diagonal elements of the coefficient matrix $\mathbf{A}(k)$ generate complex conjugate poles (with modulus $\rho_1 = \rho_2 = 0.8$ and phases $\pm\pi/4$, $\pm\pi/2$) for the processes y_1, y_2, determining autonomous oscillations at 0.125 and 0.25 Hz, respectively. The off-diagonal elements of $\mathbf{A}(k)$ determine direct causality and causality among the processes, and consequently direct coupling and coupling, according to the interaction diagram in Fig. 2.4a. Specifically, *direct causality* is set over the directions $y_1 \rightarrow y_2$ ($a_{21}(1) = 1$, $a_{21}(2) = -0.5$), $y_2 \rightarrow y_3$ ($a_{32}(1) = 0.5$), $y_2 \rightarrow y_4$ ($a_{42}(1) = 0.5$), and $y_3 \rightarrow y_1$ ($a_{13}(2) = 0.7$). The corresponding *causality* relations are $y_1 \Rightarrow y_2$, $y_2 \Rightarrow y_3$, $y_2 \Rightarrow y_4$, $y_3 \Rightarrow y_1$ (direct effects), and $y_1 \Rightarrow y_3$, $y_1 \Rightarrow y_4$, $y_2 \Rightarrow y_1$, $y_3 \Rightarrow y_2$, $y_3 \Rightarrow y_4$ (indirect effects).

The theoretical profiles of the spectral and cross-spectral density functions computed from the coefficients values (Eq. 2.10 and 2.4), are depicted in Fig. 2.5. The spectra of the four processes, reported as diagonal plots in Fig. 2.5a (black), exhibit clear peaks at the frequency of the two imposed oscillations: the peaks at 0.125 Hz and 0.25 Hz are dominant for y_1 and y_2, respectively, and appear also in the spectra

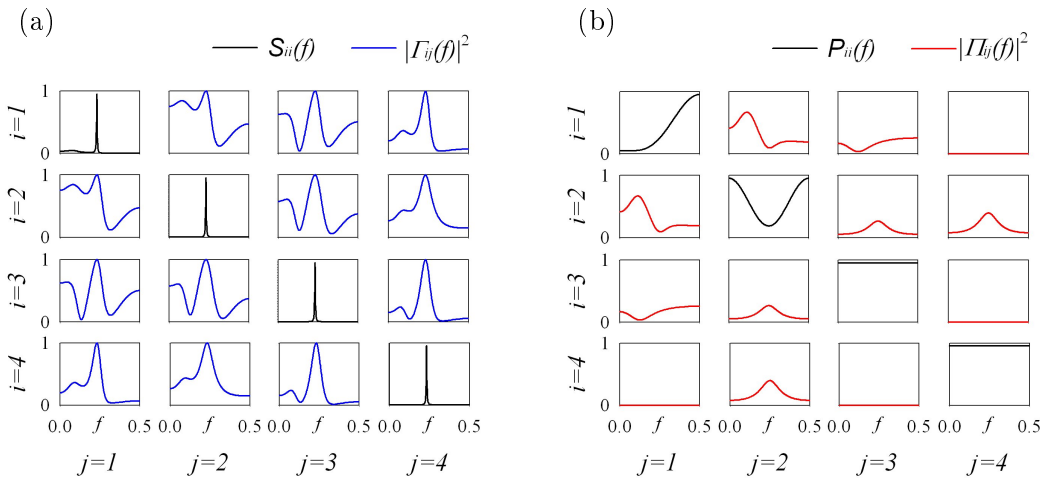

Figure 2.5: Spectral functions and frequency-domain coupling measures for the theoretical example (2.29). $S_{ii}(f)$: spectrum of the process y_i; $P_{ii}(f)$: inverse spectrum of y_i; $\Gamma_{ij}(f)$: coherence between y_j and y_i; $\Pi_{ij}(f)$: partial coherence between y_j and y_i.

of the remaining processes according to the imposed causal information transfer. The inverse spectra are also reported as diagonal plots in Fig. 2.5b (black). Off diagonal plots of Fig. 2.5a and Fig. 2.5b depict respectively the trends of the squared magnitudes of COH and PC. Note the symmetry of the two functions ($\Gamma_{ij}(f) = \Gamma^*_{ji}(f)$, $\Pi_{ij}(f) = \Pi^*_{ji}(f)$), reflecting the fact that they measure coupling and direct coupling but cannot account for directionality of the considered interaction. As expected, COH is non-zero for each pair of processes, thus measuring the full connectivity of the considered network. PC is clearly non-zero whenever a direct coupling relation exists ($y_1 \leftrightarrow y_2$, $y_2 \leftrightarrow y_3$, $y_2 \leftrightarrow y_4$, $y_3 \leftrightarrow y_1$), and is uniformly zero between y_1 and y_4 and between y_3 and y_4 where no direct coupling is present.

The trends of the causality measures (Eq. 2.14,2.17,2.26 and 2.28) computed from the coefficients values are depicted in Fig. 2.6. Since instantaneous causality is absent (all the imposed effects from one process to another are lagged), $\mathbf{B}(0) = 0$, $\mathbf{A}(k) = \mathbf{B}(k)$, and $\Sigma = \Lambda = \mathbf{I}$. Therefore, as expected, eDC is equivalent to DC and iDC, and also ePDC, iPDC and gPDC are equivalent functions.
Fig. 2.6a shows the ability of the DC function to distinguish causality relations. In fact, comparing its trends with that obtained for coherence, we observe easily that they are not symmetric and that relations from y_4 to the other nodes are absent. The same is noticed also for gPDC function (Fig. 2.6b). In fact squared gPDC trends are not symmetric and relations are absent, whenever their direction does not respect the imposed causality patterns.
As expected, DC is able to detect all causality relations: $y_1 \Rightarrow y_2$, $y_2 \Rightarrow y_3$, $y_2 \Rightarrow y_4$, $y_3 \Rightarrow y_1$ (that we know to be direct relations) and $y_1 \Rightarrow y_3$, $y_1 \Rightarrow y_4$, $y_2 \Rightarrow y_1$, $y_3 \Rightarrow y_2$ and $y_3 \Rightarrow y_4$ (indirect). Differently, squared gPDC reveals only direct causality relations: $y_1 \rightarrow y_2$, $y_2 \rightarrow y_3$, $y_2 \rightarrow y_4$, $y_3 \rightarrow y_1$.

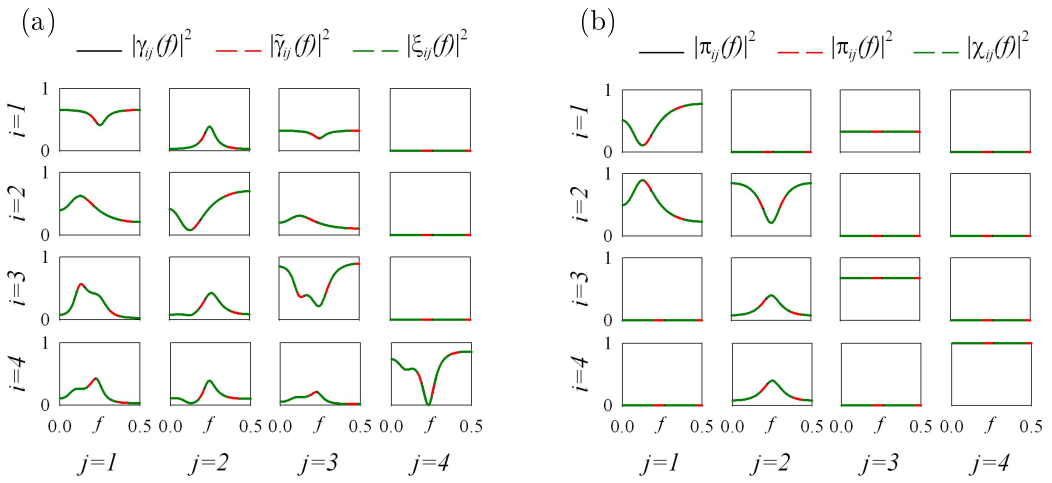

Figure 2.6: (a) Squared DC for the strictly causal model ($|\gamma_{ij}(f)|^2$) and for the extended model: iDC ($|\tilde{\gamma}_{ij}(f)|^2$) and eDC ($|\xi_{ij}(f)|^2$). (b) Squared gPDC for the strictly causal model ($|\pi_{ij}(f)|^2$) and for the extended model: iPDC ($|\tilde{\pi}_{ij}(f)|^2$) and ePDC ($|\chi_{ij}(f)|^2$).

Finally, it is interesting to stress the normalization conditions consequences of these two measures on their meaning. Squared DC, $\left|\gamma_{ij(f)}\right|^2$, measures causality strength from y_j to y_i as the normalized proportion of $S_{ii}(f)$ which is due to y_j. Hence, looking at each row i of the trends' matrix for squared DC it is possible to understand how much of $S_{ii}(f)$ is due to the other processes j. The absence of external contributions from y_4 on the power of y_1 is, for example, reflected by the null profile of $\left|\gamma_{14(f)}\right|^2$. At the same time, $\left|\gamma_{11(f)}\right|^2$ is not uniformly equal to 1, because of the contribution from y_2 and y_3 on y_1. A specular interpretation to that given for squared DC holds for squared gPDC. The difference is that now contributions are measured as outflows instead as inflows, are normalized to the structure sending the signal instead to that receiving the signal, and reflect the concept of direct causality instead that of causality. For example, the inverse spectrum of y_1 is decomposed into a contribution flowing out directly only towards y_2 and into a contribution coming from the same process, which describes the part of $P_{11}(f)$ which is not sent to any of the other processes.

2.3.2 Instantaneous and lagged interactions

Let now consider the MVAR process of order $p = 2$, composed by $M = 4$ scalar processes, generated by the equations:

$$\begin{cases} y_1(n) = 2\rho_1 \cos(2\pi f_1) y_1(n-1) - \rho_1^2 y_1(n-2) + 0.7 y_3(n-2) + w_1(n) \\ y_2(n) = y_1(n) - 0.5 y_1(n-2) - \rho_2^2 y_2(n-2) + w_2(n) \\ y_3(n) = 0.5 y_2(n) + w_3(n) \\ y_4(n) = 0.5 y_2(n) + w_4(n) \end{cases} \tag{2.30}$$

The process innovations w_i are independent white noises of unit variance ($\Lambda = \mathbf{I}$). The diagonal elements of the coefficient matrix $\mathbf{B}(k)$ generate complex conjugate

poles (with modulus $\rho_1 = \rho_2 = 0.8$ and phases $\pm\pi/4$, $\pm\pi/2$) for the processes y_1, y_2, determining autonomous oscillations at 0.125 and 0.25 Hz, respectively. The off-diagonal elements of $\mathbf{B}(k)$ determine the relations from one process to another, according to the interaction diagram in Fig. 2.4b. Specifically, the imposed causal effects are *exclusively instantaneous* from y_2 to y_3 and to y_4, ($b_{32}(0) = b_{42}(0) = 0.5$), *exclusively lagged* from y_3 to y_1 ($b_{13}(2) = 0.7$), and *mixed instantaneous and lagged* from y_1 to y_2 ($b_{21}(0) = 1$, $b_{21}(2) = -0.5$).

The theoretical profiles of the spectral and cross-spectral functions (Eq. 2.23 and 2.4), computed from the coefficients values, are depicted in Fig. 2.7.

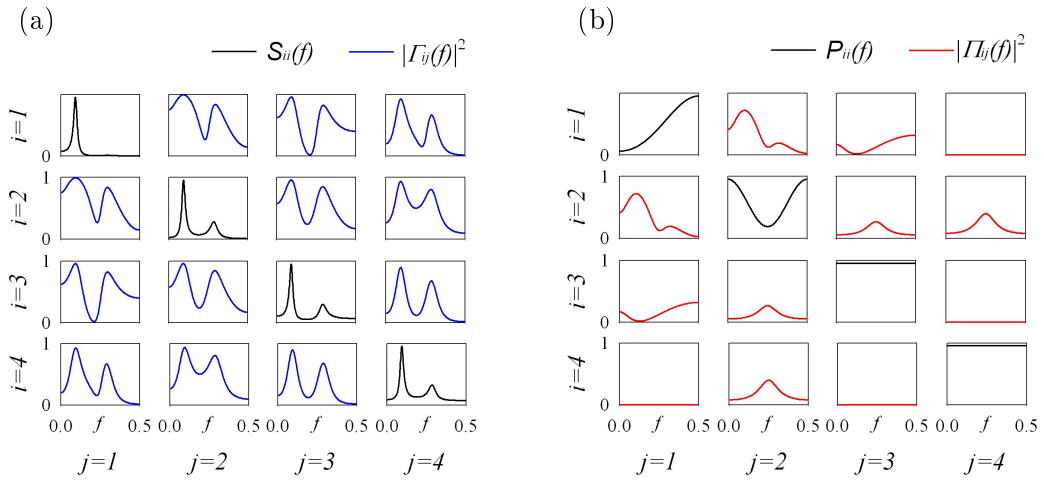

Figure 2.7: Spectral functions and frequency-domain coupling measures for the theoretical example (2.30). $S_{ii}(f)$: spectrum of the process y_i; $P_{ii}(f)$: inverse spectrum of y_i; $\Gamma_{ij}(f)$: coherence between y_j and y_i; $\Pi_{ij}(f)$: partial coherence between y_j and y_i.

Due to the equivalence of Eqs. 2.10 and 2.23, the profiles of spectra and inverse spectra, as well as of COH and PC, perfectly overlap when calculated either from the strictly causal or from the extended MVAR representation. The spectral representations closely reflect the time domain diagram in Fig. 2.4b. For instance, the squared PCs reported in Fig. 2.7b have a one-to-one correspondence with the extended MVAR diagram, as a nonzero PC is shown exactly when a direct coupling is present (i.e., $y_1 \leftrightarrow y_2$, $y_1 \leftrightarrow y_3$, $y_2 \leftrightarrow y_3$, and $y_2 \leftrightarrow y_4$).
The problems of using the strictly causal MVAR representation in the presence of instantaneous effects become severe when one aims at disentangling the coupling relations to measure causality in the frequency domain. Only the extended spectral causality profiles are correct while the strictly causal one may be strongly misleading. This is demonstrated in Fig. 2.8 and Fig. 2.9, depicting the frequency-domain evaluation of causality and direct causality for the considered theoretical example.
The pattern of causality relations imposed in Eq. 2.30 is not reflected by the DC measured from the strictly causal model. The squared DC profile (black solid curves) describes indeed many other causal effects besides the three correct ones (from $y_1 \Rightarrow y_2$, from $y_3 \Rightarrow y_1$ and from $y_3 \Rightarrow y_2$); precisely, lagged causality relations are indicated

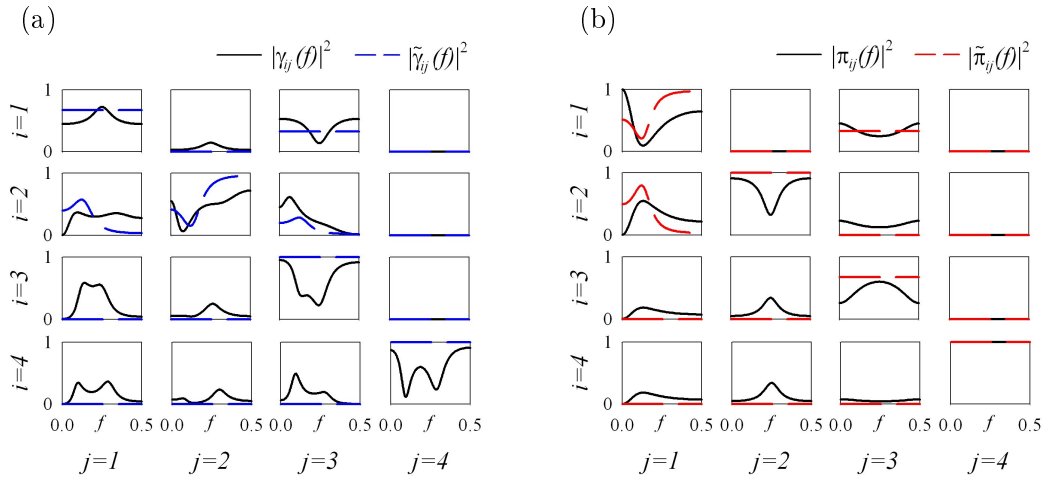

Figure 2.8: (a) Squared DC for the strictly causal model ($|\gamma_{ij}(f)|^2$) and iDC ($|\tilde{\gamma}_{ij}(f)|^2$). (b) Squared gPDC for the strictly causal model ($|\pi_{ij}(f)|^2$) and iPDC ($|\tilde{\pi}_{ij}(f)|^2$).

also from y_1 to y_3 and to y_4, from y_2 to y_1, to y_3 and to y_4 and from y_3 to y_4. These effects are actually due to instantaneous interactions, and thus should not be represented by the DC, as it is a measure of lagged causality only. The correct representation is given using the iDC: in this case, the nonzero iDC values are those measured over the three directions with imposed causality, while the squared iDC is zero over all other directions (blu dashed curves). The relations of causality emerging thanks to the instantaneous effects are detected by the eDC computed and plotted in Fig. 2.9a, which is able to measure also instantaneous effects in addition to the lagged ones. Thus, we see that a correct frequency-domain representation of causality and extended causality is given by the iDC and eDC functions derived from the extended MVAR representation of the considered process.

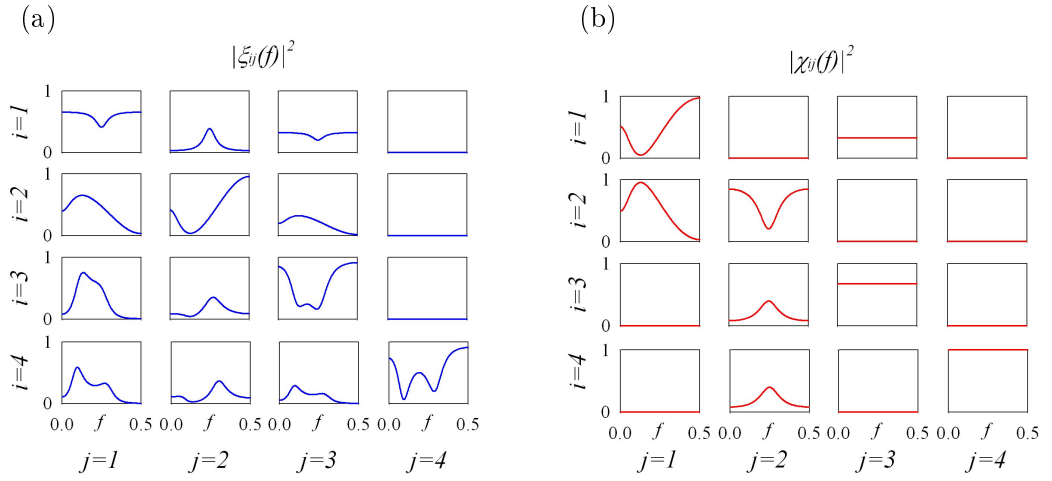

Figure 2.9: (a) Squared eDC ($|\xi_{ij}(f)|^2$) and (b) squared ePDC ($|\chi_{ij}(f)|^2$) for the theoretical example (2.30).

A similar situation occurs when direct causality and extended direct causality are studied. The iPDC correctly portrays (lagged) direct causality: $y_1 \rightarrow y_2$ and $y_3 \rightarrow y_1$, being zero over all other directions (red dashed curves in Fig. 2.7b); the ePDC portrays all extended causality relations: $y_1 \dot{\Rightarrow} y_2$ (mixed instantaneous and lagged effect), $y_3 \dot{\Rightarrow} y_1$ (lagged effect), $y_2 \dot{\Rightarrow} y_3$ and $y_2 \dot{\Rightarrow} y_4$ (instantaneous effects). On the contrary, utilization of the strictly causal MVAR representation leads to erroneous interpretation of lagged direct causality. Indeed, as seen in Fig. 2.7b (black solid curves), the gPDC interprets as lagged the instantaneous connections from y_2 to y_3 and from y_2 to y_4. Moreover, spurious causality effects are measured, as the gPDC is nonzero from y_1 to y_3, from y_1 to y_4, from y_3 to y_2 and from y_3 to y_4, even if no direct effects (neither lagged nor instantaneous) are imposed over these directions.

2.4 MVAR analysis in Practice

In this section some practical aspects are discussed, that are useful for the application of the previously presented theoretical concepts to the recorded signals.
Before starting the computation of the various functional connectivity measures, several issues have to be considered. First, the available set of neurophysiological time series has to be preprocessed and checked for the assumption of stationarity. After that, the proper data epoch has to be chosen: it has to be stationary and long enough to produce a reliable fit. Moreover, the optimal model order has to be found. Identification algorithms have to be then applied to the observed time series for providing estimates of the model coefficients. Finally, coupling/causality frequency-domain estimates can be obtained. These results can be associated to the activation detection results coming from the power analysis, for a full understanding of the brain networks under analysis. Finally, model validation and statistical significance of the results have to be considered.

2.4.1 Preprocessing

As a first step, recorded signals have to be preprocessed, making them suitable for the subsequent analysis. In fact, scalp signals like EEG and MEG can be seriously disturbed by various noise sources, e.g., powerline interference, muscle noise, eye movements or eye blinks, and cardiac signals [62]. These artifacts may strongly compromise signals interpretation and analysis. The first two disturbances can be handled by specific frequency band filters (usually notch band-pass filters for powerline interference and low-pass filters for muscle noise). Asking subjects to fixate a visual target may reduce voluntary eye movements (blinks and saccades) in cooperative subjects during brief recording sessions, but this approach does not eliminate involuntary eye movements and cannot be used when the subject is performing a task requiring eye movements. A possible solution is to detect signal segments with artifacts larger than an arbitrarily preset threshold and to exclude them from further analysis. This is one of the most commonly used method for dealing with artifacts in research settings, provided that the consequent amount of data lost after artifact rejection results acceptable. Many other methods for removing especially eye movements and blinks artifacts are available, e.g. regression in the time or frequency domain [63, 64] performed on parallel neurophysiological signals and electrooculographic (EOG) recordings, or methods based on principal component analysis (PCA) [65] and on blind source separation by independent component analysis (ICA) [62]. Each one of these approaches showed advantages and disadvantages [66]. Nowadays, the rejection of signal segments affected by artifacts, if possible, seems to be the less risky solution, when MVAR model based causality analysis has to be performed after preprocessing. In fact, clear results about the possible influence of the various correction algorithms on the causality estimates are not yet available. Usually, MVAR causality studies in neurosciences adopt only preprocessing techniques such as digital filtering and downsampling [8, 67, 68, 26, 69, 56]. However, a standard optimized procedure for preprocessing in EEG/MEG functional connectivity studies is not yet available and further investigations are required.

2.4.2 Stationarity

For a consistent estimation of the MVAR coefficients, each time series $y(n)$ has to be at least weakly stationary [70, 71]. Weak stationarity implies that the major characteristics of the stochastic process governing the time series do not change over time. In particular the following two conditions have to be fulfilled [70, 33]:

- mean stationarity: $E(y(n)) = \mu$ for all $n \in Z$;
- covariance stationarity: $cov(y(s), y(n)) = E[(y(n) - \mu)(y(s) - \mu)]$ depends only on the time displacement $n - s$ for all $s, n \in Z$. For $n = s$ this condition implies that the variance of the time series has to be constant over time.

These requests are easier to accomplish by analyzing short data epochs. Unfortunately, the selection of short signal segments does not solve completely the problem. In fact, the length of the window to analyze has to be chosen as a compromise between the methodological request of analyzing stationary signals, which prompts for the use of short time windows, and the necessity of reproducing a sufficient number of cycles for the slowest analyzed oscillation (e.g., the delta rhythm), which prompts for the use of long epochs. An operational approach to check the stationarity of the analyzed time series might be to test that no significant differences in mean and standard deviation occur between parts of the analyzed signal [72]. Usually we divide the signal into short epochs containing at least a complete oscillation of the slowest considered rhythm (e.g., 1 second length for delta rhythm) and check if the mean and the standard deviation values of each epoch are significantly different from those obtained in other epochs [Erla et al., 2011], following an approach similar to that presented in [73].

It is worth to mention some types of non-stationarity that may occur in the analyzed data, in particular:

- structural breaks: changes of (co)variance or mean at a certain point in the data;
- deterministic trends: a deterministic function of time enters the time series (e.g. linear or exponential trends).

Structural breaks are relevant for neural data, whose signals reflect spatio-temporal patterns of the electric and magnetic fields of the brain. It is well known that neural networks can exhibit complex behavior with nonlinear dynamics, e.g. changes of the signal system from one state to another [74], which is usually a clear case of a structural break. Another example is epilepsy, where the same brain area may suddenly switch from regular information processing into pathological abnormal excessive or synchronous neural activity in the brain [75]. Fortunately, structural breaks can often be found by visually inspecting the signals. Moreover, there are formal tests like the Chow- or Quandt-test to verify the absence of structural breaks [76, 77]. On the contrary, in the case of a deterministic trend, the time series can be transformed into a stationary series by subtracting the trend.

To conclude this paragraph, we remember that stationarity has to be checked also when time series are simulated imposing the MVAR model coefficients (e.g., simulations in Section 2.3). In this case, stationarity analysis turns into stability analysis of the process. A MVAR process is considered stable if all the Mp roots of the polynomial

$$det\left(\mathbf{I}+\sum_{k=1}^{p}\mathbf{A}(i)z^{-i}\right)_{z=e^{j2\pi fk}} \tag{2.31}$$

lie within the unit cycle [22]. In this context, stability of the MVAR model corresponds to stationarity of the series generated from such a model; thus it is sufficient to test for model stability to ensure that the underlying MVAR process is stationary.

2.4.3 Model Order Selection

Another critical issue of autoregressive modeling is the proper choice of the model order p. The estimation of the optimal p value is usually based on the evaluation of prediction error. The prediction error decreases or remain unchanged if the model order increases [22]. Hence, monitoring of the decrease in prediction error can be not enough to determine the optimal model order. A p value smaller than the true one results in larger estimated residual covariance matrix Σ than the true residual variances, since the additional terms omitted from the model would explain in part the signal matrix $\mathbf{Y}(n)$. On the other hand, once the value of p reaches the true order any further increase in p would lead to overfit the observed data [33]. To avoid overfitting, a degree of freedom correction has to be applied. Several criteria have been suggested to determine the correct model order. The most common is the Akaike information criterion [78]. Specifically, the optimal model order is selected as the value of p that minimizes the vector form of the AIC figure of merit:

$$AIC(p_i) = N \ln \det\left(\Sigma_{p_i}\right) + 2M^2 p_i, \tag{2.32}$$

where M is the number of data channels analyzed, N is the number of samples contained in each time series, and Σ_{p_i} is the estimate of the residual covariance matrix assuming a p_i model order. Note that the AIC function should be computed only for $p_i < 3\frac{\sqrt{N}}{M}$ [22].

2.4.4 Model identification and validation

Since the various frequency-domain functions measuring causality and coupling are estimated from the observed data, they are always an approximation of the the true unknown functions. The accuracy of the estimation process depends on factors like data length and type of coefficients identification method. There is a myriad of publications concerning linear model fitting (e.g., [79, 22, 60, 50, 33]). Nowadays a choice of a particular algorithm does not depend on calculation time anymore. However, certain algorithms may perform better when applied to certain types of data. In this section, some of the most commonly adopted approaches for identification from the recorded data of the MVAR models in Eqs. 2.5 and 2.18 are presented.

Strictly causal model (MVAR) identification

The several existing identification methods for the strictly causal MVAR model 2.5 are all based on the principle of minimizing the prediction error, i.e. the difference between actual and predicted data [22, 60, 33] (for a comparison of different estimators see [25]). One of the most commonly used approaches for estimating the MVAR coefficients $\mathbf{A}(k)$ from multichannel recordings in neurosciences studies is based on Vector Least Squares (VLS) model identification [80, 81]. First, the Eq. 2.5 is written in compact representation as:

$$\mathbf{Y} = \mathbf{A}\mathbf{Z} + \mathbf{U}, \tag{2.33}$$

where $\mathbf{A} = [\mathbf{A}(1), \ldots, \mathbf{A}(p)]$ is the $M \times pM$ matrix of the unknown coefficients, $\mathbf{Y} = [\mathbf{Y}(p+1), \ldots, \mathbf{Y}(N)]$ and $\mathbf{U} = [\mathbf{U}(p+1), \ldots, \mathbf{U}(N)]$ are $M \times (N-p)$ matrices, and $\mathbf{Z}$ is a $pM \times (N-p)$ matrix defined as:

$$\mathbf{Z} = \begin{bmatrix} \mathbf{Y}(p) & \cdots & \mathbf{Y}(N-1) \\ \vdots & \vdots & \vdots \\ \mathbf{Y}(1) & \cdots & \mathbf{Y}(N-p) \end{bmatrix}. \tag{2.34}$$

Given this representation, the method estimates the coefficient matrices through the well known least squares formula (minimizing the total squared residue over the data samples from $p+1$ to N):

$$\hat{\mathbf{A}} = \mathbf{Y}\mathbf{Z}^T \left(\mathbf{Z}\mathbf{Z}^T\right)^{-1}, \tag{2.35}$$

and the input process as the residual time series: $\hat{\mathbf{U}} = \hat{\mathbf{A}}\mathbf{Z} - \mathbf{Y}$. The VLS approach requires a priori model order selection, that is commonly performed via the multichannel AIC criterion, minimizing the Akaike figure of merit within a predefined range of orders (typically from 1 to 30).

Even though VLS is a very common approach for model identification, it suffers from a number of limitations (tendency to overestimation of the true model order, inability to discern missing terms, high noise sensitivity) that leave room for the development of more accurate MVAR identification methods [22, 82]. Here, we present an alternative approach for MVAR model identification, proposed in [Erla et al., 2009]. It is based on the recently proposed Vector Optimal Parameter Search (VOPS) algorithm [82]. It consists in a two step procedure:

1. Given an initial model order p_{max} the linearly independent candidates have to be selected from the M–channel candidate vectors arranged as p_{max} row blocks in the $p_{max}M \times (N - p_{max})$ matrix $\mathbf{Z}$ in 2.34. Independence of the candidates is evaluated by multivariate least squares analysis, and the q independent candidates are collected in a $qM \times (N - p_{max})$ matrix $\mathbf{Z}_1$, $q \leq p_{max}$.

2. The r most significant candidates have to be chosen among the subset of q independent candidates ($r \leq q$). To this aim, the observations $\mathbf{Y}$ are projected onto the set of independent candidates $\mathbf{Y} = \mathbf{A}_1\mathbf{Z}_1$, and the multivariate least squares solution is found as:

$$\hat{\mathbf{A}}_1 = \mathbf{Y}\mathbf{Z}_1^T \left(\mathbf{Z}_1\mathbf{Z}_1^T\right)^{-1} = \left[\hat{\mathbf{A}}_1(1) \ldots \hat{\mathbf{A}}_1(q)\right].$$

The independent candidates are then rearranged in descending order according to the values

$$C_k = \text{trace of } \frac{1}{(N - p_{max})} \left[\mathbf{A}_1(k)\mathbf{Z}_1(k)\right] \left[\mathbf{A}_1(k)\mathbf{Z}_1(k)\right]^T ,$$

where $\mathbf{Z}_1(k)$ is the k–th row of $\mathbf{Z}_1$, $k = 1, \ldots, q$.
The quantity $\nu_k = (C_k - C_{k+1}) / C_k$ is then plotted as a function of k, and the first maximum, ν_r, is used as criterion to select the number r of significant terms [82]. The output of this second step is a $rM \times (N - p_{max})$ matrix $\mathbf{Z}_2$ containing only the independent and significant candidates.

The multivariate least squares solution of the system $\mathbf{Y} = \mathbf{A}_2\mathbf{Z}_2$, given by

$$\hat{\mathbf{A}}_2 = \mathbf{Y}\mathbf{Z}_2^T \left(\mathbf{Z}_2\mathbf{Z}_2^T\right)^{-1} = \left[\hat{\mathbf{A}}_2(1) \ldots \hat{\mathbf{A}}_2(r)\right] ,$$

yields the r nonzero coefficients of $\hat{\mathbf{A}}$, while the remaining $p_{max} - r$ coefficients are set to zero.

In [Erla et al., 2009], using Monte Carlo simulations generated by different MVAR models, the proposed VOPS algorithm is compared with the traditional VLS identification method. The VOPS was proved to provide more accurate gPDC estimates than the VLS

- in presence of interactions with long delays and missing terms;
- for noisy multichannel time series.

The first result is ascribed to the fact that the AIC can provide only the maximum model order, and is not able to discern possible missing terms in the true MVAR model. Hence, the subsequent VLS estimation yields all parameters pertaining to the maximum model order, regardless of whether or not there are missing model terms. As a result, besides an overestimation of the true model order, a bias occurs in the accuracy of other pertinent parameters. On the contrary, the parameter search criterion of the VOPS algorithm makes it able to extract only the correct parameters despite initial overdetermined model order selection.
Also the second result has particular significance considering that the presence of measurement noise and of physiological noise due to unknown sources is unavoidable in neural connectivity analysis.

Extended causal model (eMVAR) identification

eMVAR model identification can be performed following this scheme:

1. estimation of $\mathbf{A}(k)$, $\mathbf{U}(n)$ and Σ for the strictly causal model in Eq. 2.5;
2. solution of Eq. 2.19, $\mathbf{U}(n) = \left[\mathbf{I} - \mathbf{B}(0)\right]^{-1} \mathbf{W}(n) = \mathbf{L}\mathbf{W}(n)$, to estimate $\mathbf{B}(0)$ and $\mathbf{W}(n)$;
3. estimation of the coefficients $\mathbf{B}(k) = \left[\mathbf{I} - \mathbf{B}(0)\right] \mathbf{A}(k)$.

The first step can be performed by means of the classic VLS approach or by the recently proposed VOPS approach (as presented above for strictly causal models). The second step is more problematic, requiring to extract the zero-lag relations from the covariance of the observed data, which is not directional. In other words, the same matrix $\mathbf{U}(n)$ can result from several combinations of $\mathbf{L}$ and $\mathbf{W}(n)$. To find a unique solution, more information is required than the covariance information alone. Two approaches are proposed: a priori imposition of the structure of instantaneous causation (first approach, eMVARprior) or assumption of non-gaussianity of the innovations (second approach, eMVARng). The first approach [Erla et al., 2009] sets the direction (but not the strength) of the instantaneous transfer paths. Notice that, mathematically, the matrix $\mathbf{L}$ results from the Cholesky decomposition [22] of the noise covariance matrix of the strictly causal model $\Sigma = \mathbf{L}\Lambda\mathbf{L}^T$ and is therefore a lower triangular matrix. Thus, $\mathbf{B}(0)$ becomes lower triangular with null diagonal. To fulfill this constraint in practical applications, the observed time series within the vector $\mathbf{Y}$ have to be ordered in a way such that instantaneous effects are allowed from y_j to y_i ($b_{ij}(0) \neq 0$ for each $j < i$) but not from y_i to y_j ($b_{ji}(0) = 0$ for each $j < i$). Therefore, the prior knowledge of the direction of instantaneous causal effects can be used to reorder the observed variables in such a way. On the contrary, if a priori knowledge of the instantaneous causality relations is not available, the second approach can help to overcome the problem [Faes et al., 2010a, Faes et al., 2011a]. It is based on the assumption of non-gaussianity for the independent processes $\mathbf{W}$ [59, 83]. The algorithm is composed by two steps:

1. independent component analysis (ICA) is performed on the estimated residuals $\mathbf{U}(n)$. The mixing matrix $\mathbf{M}$ is found. It represents an unordered and non-normalized version of $\mathbf{L}$;

2. an appropriate row-permutation followed by normalization is applied to $\mathbf{M}^{-1}$ to get an estimate of $\mathbf{L}^{-1}$, and thus of $\mathbf{B}(0)$.

It can be shown that, if the observed variables can be analyzed in a causal order, the row permutation at step 2 is unique, so that the solution of the algorithm is univocal (the model is identifiable).
The advantage of this second procedure with respect to the first one is that no a priori information are required for the identification. This can be very useful in real EEG/MEG data analysis, since the direction of the instantaneous effects between signals is not known. The drawback is that this approach introduces the additional model assumption of non-gaussian innovations (which has to be tested and, if not satisfied, forces the researcher to discard the specific signals' trial).

Model validation

After model identification, the suitability of the estimated model for describing the observed data has to be checked (validation), i.e. the model assumptions must be verified.

First, the residuals $\mathbf{U}(n)$ have to be:

- temporally uncorrelated (white): the stochastic variables $u_i(n-l)$ and $u_j(n-m)$ are independent for each $i, j = 1, \ldots, M$ and for each $m \neq l$;
- mutually independent: $u_i(n)$ and $u_j(n)$ are independent for each $i \neq j$.

Available tests are, for example, the Ljung-Box portmanteau test for whiteness (which checks for the overall significance of groups of residual correlations) [60, 84, 85], and the Spearmann's rho test or the Kendall's τ test for independence [60].
Note that whiteness of the extended residuals $\mathbf{W}$ always corresponds to whiteness of the strictly causal residuals $\mathbf{U}$, differing $\mathbf{W}$ and $\mathbf{U}$ only in the instantaneous structure. On the contrary, independence of $\mathbf{W}$ corresponds to independence of $\mathbf{U}$ only in absence of instantaneous effects. In fact, violation of the assumption of independence of the strictly causal residuals is the reason to introduce the extended model in place of the strictly causal one.
When the strictly causal residuals results not independent, the condition for identification of the instantaneous model have also to be verified. Depending on the approach chosen to identify the instantaneous model (as seen in Paragraph 2.4.4), the adequacy of the a priori imposed instantaneous structure or the non-gaussianity of the extended residuals $\mathbf{W}$ have to be checked. Non-gaussianity may be tested, e.g., by the Jarque-Bera test for non-normal distributions. See [60] for a review of all these statistical validation tests.

Implementation on simulations

The two model identification approaches presented above (Sec. 2.4.4) can be tested on practical realizations of the MVAR processes illustrated in Sec. 2.3 [Faes et al., 2011a]. Starting from the extended innovations $\mathbf{W}(n)$, the corresponding strictly causal innovations are estimated as $\mathbf{U}(n) = [\mathbf{I} - \mathbf{B}(0)]^{-1}\mathbf{W}(n)$, being imposed the model coefficients values $\mathbf{B}(0)$ (in accordance with Eqs. 2.29 and 2.30). After that, the calculated $\mathbf{U}(n)$ are used as an input for a strictly causal model. In this way, it is possible to generate realizations $\mathbf{Y}(n) = \{y_m(n)\}$ of Eqs. 2.29 and 2.30, with $m = 1, \ldots, M$ and $n = 1, \ldots, N$ ($M = 4$ and $N = 500$ in our example).
The innovations $w_m(n)$ were generated as independent gaussian white noises for testing the eMVARprior identification approach, and as independent non-gaussian white noises for testing the eMVARng approach. Non-gaussianity was achieved first generating $z_m(n)$ as independent gaussian white noises and then applying the nonlinear transformation $w_m(n) = sign(z_m(n))|z_m(n)|^q$, with q chosen in the range $[0.5, 0.8]$ or $[1.2, 2.0]$ to yield respectively a sub-gaussian or super-gaussian distribution for w_i [59].

For each of the two identification approaches, the analysis was performed in three different cases:

(a) absence of instantaneous effects (Eq. 2.29);

(b) presence of instantaneous effects (Eq. 2.30) with satisfied model assumptions;

(c) presence of instantaneous effects (Eq. 2.30) with non-satisfied model assumptions.

The first two cases were designed to test the ability of the two identification approaches to estimate frequency-domain causality when instantaneous effects are trivial and significant, respectively. In the third case the effects on the connectivity measures of wrong model assumptions are investigated. Wrong assumptions were simulated in the third case imposing

- an incorrect causal ordering for the observed series (i.e. any ordering different than the two correct orderings set in Eq. 2.30 for instantaneous causal effects: $[1, 2, 3, 4]$ and $[1, 2, 4, 3]$), for eMVARprior identification approach;
- a gaussian distribution for the extended innovations $\mathbf{W}$ for eMVARng identification approach.

Fig. 2.10 shows simulation results obtained for 100 realizations of the considered MVAR processes using the two identification approaches under the three conditions presented above.
The two top panel rows show representative trends of expected and estimated frequency-domain causality functions (one selected eDC and ePDC in Fig. 2.10.I, and one selected iDC and iPDC in Fig. 2.10.II). The third panel row shows the percentage of rejection of the four performed validation tests (whiteness and independence of $\mathbf{U}$ and $\mathbf{W}$ residuals and gaussianity of $\mathbf{W}$ residuals); the fourth panel row shows the distribution of the error, estimated as the mean absolute value of the difference between estimated and true causal coupling, computed for each measure (eDC, ePDC, iDC and iPDC) and averaged over the full frequency range.

When instantaneous effects are not present in the simulations (condition (a)), both eMVARprior and eMVARng identification approaches estimate correctly the imposed causal relations. In fact, theoretical and estimated measures appear almost overlapped and the error values are low. In this case, the assumptions of whiteness and independence of the residuals $\mathbf{U}$, and of non-gaussianity of the extended residuals for the eMVARng approach, were satisfied in almost all simulations.
In presence of significant instantaneous effects, the strictly causal residuals $\mathbf{U}$ are never independent, indicating the necessity of moving to the extended representation. When the model assumptions required for identification are satisfied (condition (b)), i.e. correct imposition of the direction of instantaneous effects for eMVARprior approach and presence of non-gaussian innovations for eMVARng approach, the estimation is successful. In fact, estimation errors are low.
On the contrary, the identification is unsuccessful when the model assumptions are not satisfied (condition (c)). The estimated frequency-domain causality measures deviate from the expected profiles and estimation errors result high.
In the case of eMVARprior identification (I), the imposed wrong direction for the instantaneous effects do not lead to unfulfillment of the validation tests (iW and g are near zero). This result is due to the fact that all the models estimated with different instantaneous causal orderings are equally admissible, in terms of description

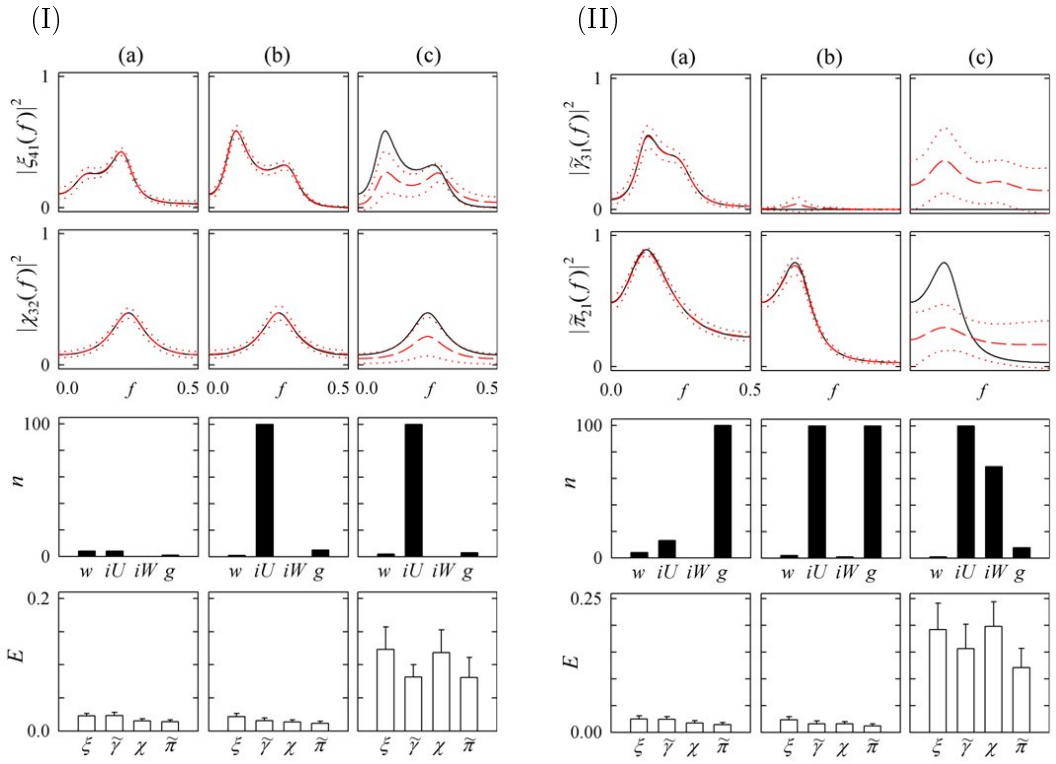

Figure 2.10: Results of the identification for 100 realizations of the process (a) in absence of instantaneous effects, (b) in presence of instantaneous effects with satisfied model assumptions, and (c) in presence of instantaneous effects with non-satisfied model assumptions. The adopted identification approach is (I) eMVARprior or (II) eMVARng. From top to bottom, panels show: representative squared causality functions (black solid: theoretical profile; red dashed±dotted: mean±std.dev. of estimated profiles); number of realizations n for which rejection of the hypothesis of whiteness (w), independence of strictly causal (iU) and extended (iW) residuals, and gaussianity of extended residuals (g) is attained; and full-frequency range average error E estimated (mean±std.dev.) for squared eDC (ξ), iDC ($\tilde{\gamma}$), ePDC (χ) and iPDC ($\tilde{\pi}$) functions.

of the data structure. Differently, in the case of eMVARng identification (II), the presence of gaussian innovations leads to failure of validation tests performed on the extended residuals (iW is high and g is very low).

2.4.5 Statistical significance

After the MVAR model based estimation of the coupling/causality measures of interest, it is necessary to determine a significance threshold for these measures strengths, in order to distinguish real connections from spurious ones. In fact, due to practical estimation problems, measures with values greater than zero might simply occur at some frequencies by chance, even in absence of a true interaction. This issue is commonly solved by means of statistical hypothesis testing procedures, based on:

- a null hypothesis H_0 of zero interaction, against which observations are tested (it has to be rejected only if an interaction exists, except for α% of all cases, where α is the type-I error);
- a distribution of the causality/coupling measures of interest, computed under the null hypothesis of absence of interaction (no-interactions distribution);
- a statistical test performing a comparison between the values of the causality/coupling measures computed from the original series and the no-interactions distribution. In practice, the upper limit of the confidence interval of the no-interactions distribution is set as significance threshold. This threshold is then compared at each frequency with the estimated measure.

From these preliminary observations it is easy to elicit that the key step for the statistical significance analysis is the evaluation of the no-interactions distribution. Analytical formulations, elegant and computationally efficient, are currently available for COH, DC, DTF, and PDC [54, 86]. Numerical methods, more general and free from approximations, estimate the significance level specifically for each coupling/causality measure. In the present work, we consider only numerical methods, since they often perform better in finite samples than analytical measures based on asymptotic considerations [87]. Many approaches are available, e.g the random permutation of the data [88, 89] or the leave one out method (LOOM) [25, 89]. In this work, we focus on procedures based on Fourier Transformed surrogate data generation [90, 91, 92, 93], which will be applied for statistical significance validation in the following application chapter (3).

Surrogate data analysis to test coupling and causality

After setting the null hypothesis against which observations are tested, a set of surrogate time series can be calculated, which share the properties of the original series, but lack of the investigated property (coupling/causality). Consequently, the no-interactions distribution is obtained as the distribution of the coupling/causality measure of interest calculated for the surrogate time series.
Depending on the coupling/causality measures of interest, different null hypotheses are defined:

- $H_0(1)$ = the observed series are a realization of a MVAR process with absence of coupling between y_i and y_j;
- $H_0(2)$ = absence of direct coupling between y_i and y_j;
- $H_0(3)$ = absence of causality from y_i to y_j;
- $H_0(4)$ = absence of direct causality from y_i to y_j.

According to these hypothesis, different surrogate data are defined. Here we briefly present the so called Fourier Transformed (FT) surrogates [90, 91, 92] and the Causal FT (CFT) surrogates [93],[Erla et al., 2011b].

Consider the $M \times N$ multivariate time series $\mathbf{Y}(n) = [y_1(n), \ldots, y_M(n)]^T$, with $n = 1 \ldots, N$. For each time series $y_m(n)$ $(m = 1, \ldots, M)$, a *FT surrogate* series $\bar{y}_m(n)$ can be calculated in the following way:

1. the discrete FT operator is applied: $Y_m(f) = \Im\{y_m(n)\} = A_m(f)e^{i\varphi_m(f)}$ for the discrete frequencies $f = k/(NT)$ $(k = 0, \ldots, N-1)$;
2. the Fourier phases $\varphi_m(f)$ are replaced by realizations of a random variable $\theta_m(f)$ uniformly distributed in the range $[0, 2\pi)$, while the Fourier amplitudes $A_m(f)$ are not changed;
3. the inverse FT is calculated: $\bar{y}_m(n) = \Im^{-1}\left\{A_m(f)e^{i\theta_m(f)}\right\}$.

The surrogate series $\bar{y}_m(n)$ preserve the power spectrum of the original series $y_m(n)$, but are fully uncoupled, being independent the random phases $\theta_m(f)$ [90]. Note that FT surrogates are consistent with all the null hypotheses above, as they destroy any type of coupling (direct, indirect, along forward and backward directions).

CTF surrogates are time series in which the causal coupling is destroyed only over some directions of interaction, while it is preserved over the other directions.
After identification of the MVAR model in Eq. 2.5 or 2.18, some of the model coefficients are forced to zero, depending on the frequency-domain coupling/causality measure under investigation:

- to test causality $y_i \Rightarrow y_j$, it is necessary to set to zero all the coefficients describing the direct dependencies originating from y_i ($a_{mi}(k) = 0$ for strictly causal model and $b_{mi}(k) = 0$ for the extended model, $m = 1, \ldots, M$, $m \neq i$, $k = 0, \ldots, p$) as well as the direct dependencies ending into y_j ($a_{jm}(k) = 0$ or $b_{jm}(k) = 0$,$m \neq j$) $\Longrightarrow$ CFTf surrogates [93]. These surrogates results consistent with $H_0(3)$ and $H_0(4)$ null hypotheses.
- to test direct causality $y_i \rightarrow y_j$, it is necessary to set to zero all coefficients describing the direct dependence from y_i to y_j ($a_{ji}(k) = 0$ or $b_{ji}(k) = 0$) $\Longrightarrow$ CFTd surrogates [93]. They are consistent only with $H_0(4)$.
- to test direct coupling $y_i \leftrightarrow y_j$, all coefficients describing the direct dependence $y_i \rightarrow y_j$ ($a_{ji}(k) = 0$ or $b_{ji}(k) = 0$) and $y_j \rightarrow y_i$ ($a_{ij}(k) = 0$ or $b_{ij}(k) = 0$) have to be set to zero. This latter solution, in which both backward and forward causal directions are destroyed (consistent with both $H_0(2)$ and $H_0(4)$ hypotesis), is proposed in [Erla et al., 2011b] and named CFTbf surrogates.

The reduced model, described by the new coefficients set, is iterated, using as inputs M independent white noise realizations.
The resulting series are $\hat{\mathbf{Y}}(n) = [\hat{y}_1(n), \ldots, \hat{y}_M(n)]^T$. The discrete FT operator is applied to the original series $Y_m(f) = \Im\{y_m(n)\} = A_m(f)e^{i\varphi_m(f)}$, as well as to the series derived from the reduced model $\hat{Y}_m(f) = \Im\{\hat{y}_m(n)\} = \hat{A}_m(f)e^{i\hat{\varphi}_m(f)}$. After that, the Fourier amplitudes of the original series and the Fourier phases of the series derived from the reduced model are set, respectively, as amplitudes and phase of the frequency-domain representation of the CTF surrogates $\tilde{Y}_m(f) = A_m(f)e^{i\hat{\varphi}_m(f)}$.

Finally, the inverse FT is calculated $\tilde{y}_m(n) = \Im^{-1}\left\{\tilde{Y}_m(f)\right\}$.
The CFT surrogate series $\tilde{y}_m(n)$ preserve the power spectrum of the original series $y_m(n)$, as well as the phase differences among time series in accordance with the models 2.5 or 2.18, where causality, direct causality or direct coupling from y_i to y_j is zero (depending on which zero-setting procedure has been followed).

After calculating the no-interactions distribution, given by the values of the coupling/causality measure of interest obtained from a certain number of surrogate data, a statistical test is performed to reject/accept the null hypothesis. To this aim, we usually adopt a nonparametric statistical test based on percentiles with 5% significance[1] [Erla et al., 2011a, Erla et al., 2011b, Papadelis et al., 2011a]. For each frequency, the coupling/causality measures of interest computed from the original series are compared with a significance threshold, calculated as the 95th percentile of the no-interactions distribution. When the threshold is exceeded, the null hypothesis is rejected. If, on the contrary, the value is below the threshold, the original series are interpreted as consistent with the considered null hypothesis.

2.4.6 Selection of the regions of interest

To complete the methodological framework given above, we discuss some possible approaches for the selection of the *regions of interest* (ROIs) , i.e., cortical or subcortical areas that are activated during the experimental paradigm (stimulation or task execution). By considering one representative signal for each selected ROI, it is possible to limit the number of time series analyzed in the following connectivity analysis. This is a non-trivial aspect, since EEG and MEG signals are recorded on the scalp surface by a high number of derivations (from 19 electrodes of the 10-20 EEG standard system to 256 sensors of the MEG apparatus). A scalp connectivity analysis considering all these signals makes no sense. In fact, besides the methodological limitations imposing to consider a low number of signals for MVAR modeling, it has to be considered that a joint analysis of all derivations behavior would give confusing results, with difficult interpretation. In addition, the information recorded on each location of the scalp is redundant in respect to that recorded from derivations located in its proximity. This is due to the fact that variations in time of the electric or magnetic field recorded on close electrodes may be due to the same brain source underlying them. Hence, there is no advantage in including in the MVAR model signals recorded from very close electrodes, containing the same information. The selection of one representative signal for each area is definitely to prefer.
Three main approaches were considered here for ROIs detection, based on:

- a priori selection of the areas involved by the experimental paradigm, based on neurophysiological or neuroanatomical previous knowledge;
- evaluation of the *event related fields* (ERFs) or *event related potentials* (ERPs) (depending on the analyzed data, MEG or EEG respectively);

[1] The percentile is used, since it is suitable either for normal or non-normal distributions of the connectivity measures (e.g., it is required by the non-normality of the coherence distribution [94]).

- calculation of a certain number of virtual signals by means of the available source imaging techniques.

The first approach is very common in neurosciences for scalp signal studies [95, 68, 96, 69]. It results intuitive, fast and requires neither assumptions on the signal generation nor signal elaborations before MVAR modeling. Anyway, it does not assure that the selected recordings are the most representative for the activated areas. For this reason, it is recommended to check these signals for activation before further analysis. As an example, in [Erla et al., 2011a, Erla et al., 2011b] a priori selection of the ROIs is applied, using the detection of band-specific power task-related changes as a test for activation (see Sec. 2.4.7).

A test for activation is not necessary when ERFs/ERPs approach for ROIs selection is adopted. In fact, the latter is based on the selection of the most activated areas for each specific stimulus/task. Consider that the simplest model for neural response to a certain stimulus or task assumes that a neurophysiological signal like EEG or MEG can be decomposed in two components: the first is invariant in latency and topography (and is only dependent on the specific stimulus or task), while the second is a noise component (containing spontaneous activity and other confounding oscillations) [97]. Because of the prevalence of the second component, it is very difficult to detect the first one from a single recording (trial). The evoked response can be obtained only by averaging the signal recorded immediately after the stimulus/task onset in many trials: $ERF_i(n) = \langle y_i(n) \rangle$, where $y_i(n)$ is the sample n of the signal recorded from the electrode i.
Even if the mean operator removes an important part of the information contained in the signal, many sensory and cognitive tasks can be characterized by highly consistent ERF/ERP waves. For example, averaging all the trials obtained in an EEG signal recording session from an occipital electrode (like Oz) in presence of visual stimulation, a significant event related potential can be observed around the latency of 100 ms. By mapping the distribution of the average activity at each latency, the topography of the neural response to the stimulus/task (activated areas) is obtained.

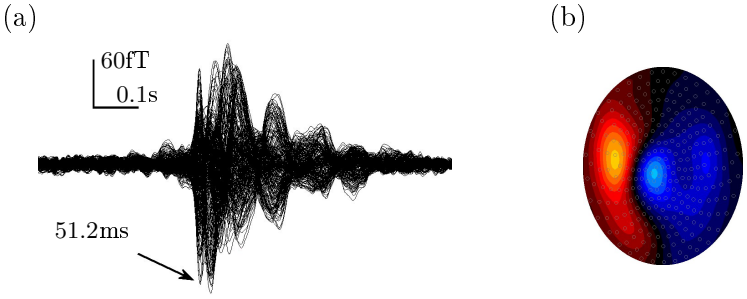

Figure 2.11: Example of ERF ROIs selection for a visuo-tactile task in a representative subject. (a) Grand-average signal, (b) ERF map for the first peak with latency 51.2ms, corresponding to the somatosensory ERF, color scaled in the range ±200fT.

The simpliest ERFs/ERPs approach for ROIs selection:

- calculates the grand-average signal for each channel to detect the latencies of the various ERFs/ERPs significantly related to the stimulus/task under analysis (e.g., see Fig. 2.11a);
- generates a ERF/ERP map for each detected latency to locate each component in space (e.g., see Fig. 2.11b).

A similar approach is presented in [Erla et al., 2010], based on spatially detection of the characteristic ERFs/ERPs of each involved task. Specifically, ERFs are estimated from the data recorded on the scalp. Then ERF variance is calculated on the signals recorded before the task onset (rest-ERF variance). Differently, task-ERF variance is computed considering the typical time intervals for the ERFs expected for each specific task (for example 70-150 ms after task onset for tasks involving visual cortex and 25-70 ms for haptic somatosensory cortex involvment, as in Fig. 2.12). Finally, for each considered latency interval, the channels with the highest increase in ERF variance moving from rest to task can be selected as ROIs.

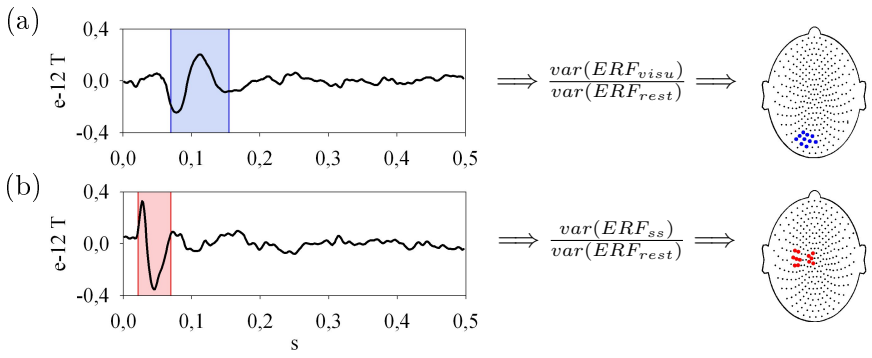

Figure 2.12: Event-Related Fields (ERFs) after stimulus, for visual (a) and somatosensory (b) brain areas in one representative subject. On the right, maps of the ten visual (blue) and somatosensory (red) channels with the higher increase in signal variance moving from rest to task (ROIs) for this participant. Adapted from [Erla et al., 2010].

It is worth to remember that the potential distribution on the scalp represents a modified copy of the real cortical distribution, because the anatomical structures interposed between scalp and cortex reduce its transmission. As a consequence, part of the spatial information on the actual distribution of the electrical activity is lost on the scalp level [43]. For this reason, when analyzing data on the scalp level, their low spatial resolution has always to be taken into account, in order to avoid risky interpretations of the results.
Nowadays, an improvement can be obtained by means of spatial enhancement algorithms, such as current source density calculations or deblurring [98, 99, 100, 18]. Furthermore, numerous approaches are available for the calculation of locations and "virtual signals" of the neural sources generating the scalp recorded configuration of signals (source imaging techniques). Scalp recordings do not directly indicate the location of the active neurons in the brain, due to the ambiguity of the underlying

static electromagnetic inverse problem [101]. This issue can be solved only by introducing a priori constraints on the generation of EEG and MEG signals. The more appropriate these assumptions are, the more trustable the source estimations. In recent years, several approaches have been developed based on different mathematical, biophysical, statistical, anatomical or functional constraints. They range from equivalent current dipole estimations, assuming a limited number of focal sources, to the calculation of many distributed sources (e.g., sLORETA, Minimum Norm Estimation, and Beamformers). Exaustive reviews on EEG/MEG source imaging, which explain in detail the formal implementation of the a priori constraints in the different algorithms are, for example, [101] and [102].
From the neuroscientific point of view, these approaches are very effective, allowing an accurate localization of the task-involved ROIs, often combined with MRI or other anatomical information. After that, spatially filtering the data, they calculate the virtual signals associated to each source, as shown for example in [Papadelis et al., 2011b].
It is important to remember that, besides the assumptions for the solution of the inverse problem, these methodologies require many analytical steps, such as the number and positioning of electrodes (including the reference electrode) and the determination of relevant time points or periods for source localization, which should be carefully considered and selected. In addition, the effects of these procedures on the signals should be carefully valued before further connectivity analysis, to check that no spurious functional connectivity patterns will be introduced while estimating the sources. In fact many studies tested the spatial accuracy of the various approaches in localizing the sources (e.g., [103]), but a rigorous demonstration of the influence of these processing methods on the calculated virtual signals' connectivity relations is not yet available.

2.4.7 Power spectral analysis

To conclude this methodological chapter, we discuss briefly power spectral analysis techniques, whose information can be associated to the functional connectivity analysis inside specific frequency bands, in order to give a larger comprehension of the brain mechanisms related to task execution.
As seen above, a complete framework for the frequency-domain analysis of a certain dataset can be obtained by calculating the MVAR model coefficients and extracting power content and connectivity measures at the same time. Starting from the MVAR model coefficient estimates, the so called spectral density matrix can be easily calculated by means of equation 2.10. It contains the auto-spectra of each considered signal on the diagonal.
The advantage of power MVAR model-based estimates over FT based approaches in real data analysis has been previously discussed [104, 105]. Autoregressive power analysis was demonstrated to be more effective than FT based analysis in evaluating the frequency content of short signals. In fact, AR analysis describes data trough the model coefficients, thus yielding a compact representation of the process. In addition, this approach gives the possibility to overcome both the traditional monovariate analysis focusing on a single signal, and the bivariate analysis limited to two signals only [68, 69]. Since neurophysiological data are a largely unknown mixture of

activities of the actual brain sources, a more comprehensive picture on the system behavior is obtained from multivariate analysis, where a set of signals are modeled together and analyzed simultaneously [106, 107].
A further advantage of MVAR power analysis is the possibility of using accurate methods for the selection of power content within each assigned frequency band, i.e., spectral decomposition techniques [108, 109]. For each pole of the MVAR transfer function, a peak of the power spectral density can be identified. To estimate the power associated to each peak, it is necessary to integrate the spectral density on an appropriate frequency window centered on the frequency peak. Spectral decomposition techniques allow to estimate the power and the corresponding frequency band-width for each peak, in such a way that the sum of the estimated powers between 0 Hz and Nyquist frequency is equal to the integral of the spectral density on the whole band. The residue integral theorem is applied, stating that the integral of a complex function (here the z-Transform of the spectral density) on a closed loop (in this case the unit cycle) is proportional to the sum of the residuals of the poles of the function. The number of poles in the unit cycle is equal to the model order p [22]. Moreover, if we normalize to the Nyquist frequency, the power spectral density is displayed in the frequency interval $[0, 1/2]$. So the residue integral is actually limited to the area of the unit cycle where values have positive imagery part. As a consequence, residuals to consider are relative to the poles with positive imagery part (their number is around $p/2$) (see [108] for details).

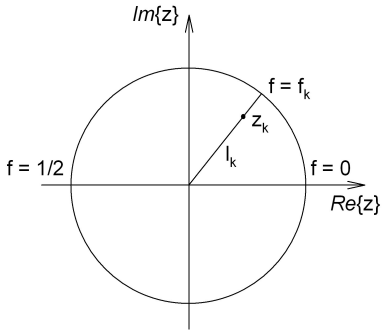

Figure 2.13: Generic pole of the complex spectral density $S_i(z)$, with correspondent power spectral density $S(f_k)$.

In the multivariate case [109] the same principle is adopted. Here the procedure is only complicated by the fact that, before power decomposition of the process y_i, its power spectral density has to be described as a sum of partial spectra:

$$S_{ii}(f) = \sum_{m=1}^{M} S_{i|m}(f) = \sum_{m=1}^{M} H_{im}(z)\sigma_m^2 H_{im}^*(z^{-1}) \text{ ,where } z = e^{j2\pi fT} \text{ ,} \qquad (2.36)$$

where $S_{i|m}(f)$ is the part of $S_{ii}(f)$ due to y_m. Then, each partial spectra can be decomposed (partial fraction expansion) in a sum of bell-shaped functions, centered around the frequency of k-th the pole, and has a sharpness related to the pole modulus (see for details [109]).

Besides the information on the frequency band-specific content, power spectral analysis is useful to detect neural activation. In fact, task-related changes in power are usually observed in correspondence of brain regions involved in a specific task. Examples can be found in [Erla et al., 2010, Erla et al., 2011a, Papadelis et al., 2011a] and will be discussed in the following chapter.

Chapter 3

Application: visuo-motor integration

The theoretical and methodological framework presented in the previous chapter can be applied to study the mechanisms underlying many cognitive processes. In this chapter we focus on the study of visuo-motor integration processes, i.e. processes in which motion is controlled with the perceived visual information, and of multisensory integration processes, i.e. processes in which the information perceived through different sensory modalities is coded, analyzed and matched. Specifically, a goal-directed grasping motor behavior is investigated through a visuo-motor matching protocol. The aim is to identify the involved brain areas and to distinguish the networks related to specific tasks from those due to integration, by analyzing EEG and MEG signals recorded from healthy subjects. This deeper knowledge of the "normal" brain functioning could be a starting point also for the future analysis of rehabilitation stages and procedures in pathological conditions [110, 111, 112].

3.1 Introduction

Let us consider an apparently simple everyday action, like goal directed grasping of a certain object. This is a highly complex brain procedure involving multimodal sensory and motor processes. In fact, in order to reach, grip and control an object, the brain is required to integrate the visual and haptic sensory information in input, and simultaneously control the motor system. To do this, specific cortical and sub-cortical regions are activated and communicate with each other. This scheme reflects the two principles governing the functional mechanisms of the human brain: specialization and connectivity, as discussed in Chapter 1.

Although the relevance of cross-systems integration processes is becoming increasingly clear, the mechanisms underlying them are much less understood. One of the most common hypotheses is that a huge number of neurons, organized in functionally specialized assemblies, communicate locally and on a long-range scale through synchronized firing patterns [113, 114, 17]. Following this idea, the so called *binding theory* was formulated [115]. It assumes that the integration of spatially distributed information into a coherent percept is based on transiently formed functional networks linking the various brain regions by phase-locked oscillatory activity. This theory was originally proposed to explain object recognition mechanisms, in which different features are processed at different spatially distributed brain locations and subsequently merged to form an object representation. Afterward, this model has been adopted for the interpretation of other particular aspects of perception, cognition and action, such as the integration between multimodal sensory inputs and motor control.

The most direct way to detect coherently oscillating neuronal groups in the brain is the analysis of synchronization of the recorded Local Field Potentials. However, this technique is invasive and provides only a partial view of the electrical activity of the brain, limited to the areas in which the needle electrodes are placed. Many studies demonstrated that the synchronized oscillatory activity of distant brain areas can be detected easily and in a non-invasive way by studying the correlation between neurophysiological signals recorded on the scalp upon the areas of interest (see, for example, [116, 17, 117, 113]). To analyze functional and effective connectivity by this approach, the recording modality is required to be highly temporal-resolved, such as MEG and EEG are [18, 118].

In the last years, many studies have been proposed in which functional connectivity was estimated from EEG/MEG signals by coherence analysis [36, 37, 38, 39, 40, 41, 42]. One of the main objectives of these studies was to identify the functional role of each different brain rhythm in inter-areas communication. In fact, each frequency band was hypothesized to contain distinct components reflecting specific functions. Usually the synchronization frequency is considered to be inversely proportional to the distance between the communicating brain areas. In [113, 119, 120] high frequency synchronization (γ band coherence) was associated to functional connectivity between close brain areas, while θ, α and β coherence was related to long-range

information flow. However, the different role of the various brain rhythms seems not to be solely dependent on the distance of the communicating regions. Task-specific synchronization was also considered. High frequency synchronization was believed to have an important role in high cognitive processes [121, 122], but also alpha large-scale synchrony was observed [123]. Moreover, long-range synchronization was detected at different frequency bands during motion [113]. Concerning visuo-motor and related multisensory integration processes, large-scale enhanced interregional synchronization was mainly found in α and β frequency ranges [69, 120, 119]. Nevertheless, controversial results on this topic are often encountered and a clear and complete picture is still missing.
Besides the role of different frequencies in brain communication, the task-involved areas and their connectivity pattern were also analyzed. In visuo-motor integration studies, precentral cortices (premotor and motor areas) and occipito-parietal regions (visual areas and parietal cortex) were mainly considered [124, 125, 112, 126, 127, 128, 129, 130].

The aim of this chapter is to verify and extend these findings. The theoretical methods presented in Ch. 2 for functional and effective connectivity (coupling and causality) analysis are tested on real data, to further discuss possible advantages and limitations and elucidate the neuronal mechanisms underlying visuo-motor integration. EEG results are partly tested by replicating the results of Classen [69]. Causality analysis is applied to extend these results. In addition to cortico-cortical connectivity analysis of the EEG signals, recorded by channels located around the motor/premotor area and the visual cortex, MEG signals are analyzed. A pilot study is performed, estimating the functional coupling at the source level using a beamformer technique to provide more accurated spatial information about the regions involved in the visuo-motor integration task and about their cortico-cortical coupling.
The analyzed continuous visuo-motor task requires the tracking of a visual target changing continuously in size by adapting the force of a pinch grip [Erla et al., 2011a, Erla et al., 2011b]. This task is a good example of functional cooperation between visual and motor areas, since it poses a demand on the brain to continuously analyze the visual signal showing the discrepancy between requested and actually generated force and to produce an adequate force accordingly.

3.2 The dataset

The dataset of this study has been recorded in the MEG Center of the Institute of Medical Psychology & Behavioral Neurobiology at the University of Tübingen (Germany).

3.2.1 Subjects and experimental setup

Twelve healthy volunteers participated in the study. They were right handed, according to the Edinburgh handedness inventory [131], with mean age 25.2 ± 2.2 years;

Figure 3.1: Experimental setup. The subject sits inside the magnetically shielded room with the helmet shaped dewar, with the EEG cap on the head. The screen in front of the subject displays the feedback and the fixation cross. The pinch grip is on the subject's right side.

six of them were females. All participants were free of known past or present neurological problems. The study was approved by the Medical Ethics Committee of the University of Tübingen. All subjects gave written informed consent prior to the experiment according to the Declaration of Helsinki.

During the experiment, the participants comfortably sat inside a light dimmed magnetically shielded room (MSR). Their right hand rested comfortably to reach a pinch grip device. Subjects were asked to gaze at a fixation cross displayed at the center of a screen (size: 1024×768 pixels; monitor frame rate: 60 Hz), placed about 60 cm in front of them. A projector (PLC-XP41, Sanyo), standing outside the MSR, projected images through a cut-away portal in the shield on the screen (see Fig. 3.1).

3.2.2 Experimental description

Participants accomplished four tasks in total.

1. In the continuous *visuo-motor task* (VM) , participants were asked to track a target stimulus varying sinusoidally in size (at a frequency of 0.3 Hz), by adapting the force exerted by their right hand thumb and forefinger on a force sensor pinch grip (Fig. 3.2a). The force of the isometric contraction was measured by an in-house built force transducer, which used strain gauges fixed on the upper and lower surfaces of a manipulandum. The difference between the requested and actually produced force was continuously measured and visualized on the screen as a white rectangle changing its size horizontally (Fig. 3.2b). Participants were instructed to align this rectangle as precisely as possible to the black stationary rectangle on the screen (adopted as reference). The visual feedback was projected at the center of the screen, with the extreme positions of the rectangle subtending a visual angle of 4^o.

2. In the *visual plus motor task* (V+M) , participants were asked to produce the same sinusoidal isometric activation as in the VM condition, but without the visual feedback about the produced force.

3. In the *visual task* (V) , participants watched the sinusoidally varying target stimulus and the stationary rectangle without performing the pinch grip task.

4. Finally, in the *motor task* (M) , participants were instructed to imagine a metronome with 1 s pulse and correspondingly press the pinch grip with half the amount of their maximum force, which was estimated as the average force exerted in the other tasks.

The task order was randomized between subjects. To record brain activity during stable performance and avoid learning effects across sessions, participants became familiar with the VM task in a separate session preceding EEG/MEG recording. Finally, to reduce the presence of artifacts in the recordings, participants were asked to refrain from blinking as much as possible.

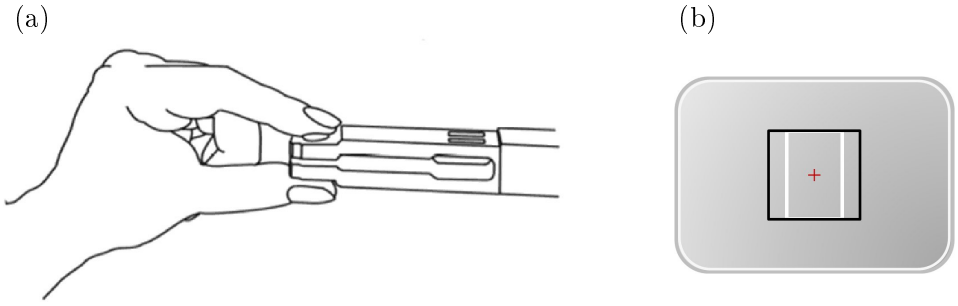

Figure 3.2: (a) The pinch grip with force transducer that measures the isometric contraction applied to the manipulandum. (b) The visual feedback about the requested (black rectangle) and the actual force produced by the subject (white rectangle). Adapted from [Erla et al., 2011a]

Each subject performed four blocks in total (Fig. 3.3a), corresponding to each type of task (V, M, V+M and of VM). Each block lasted 10 min and 30 s and comprised three trials of 3 min and 30 s, which were continuously recorded. In particular, each trial included 1 min of rest (baseline), 2 min of task (V, M, V+M or VM) and 30 s of pause. During baseline, participants stared at the fixation cross without performing any task. In the 30 s pause, participants were allowed to relax their eyes from fixation and, if necessary, to blink (Fig. 3.3b). The baseline time windows served as control condition for comparison with task execution and, together with the pause periods, helped to limit finger muscular fatigue during the following motor task execution. The experimental procedure for each block is depicted in Fig. 3.3a. Before each block and after the last block alertness and tiredness were assessed by means of a Visual Rating Scale (VRS). Subjects were asked to rate their current status of alertness (from extremely bad to extremely good) and tiredness (from none to extremely tired). Nevertheless no subject showed limited alertness and no one reported severe task-induced fatigue or tiredness during the experiment [Erla et al., 2011a].

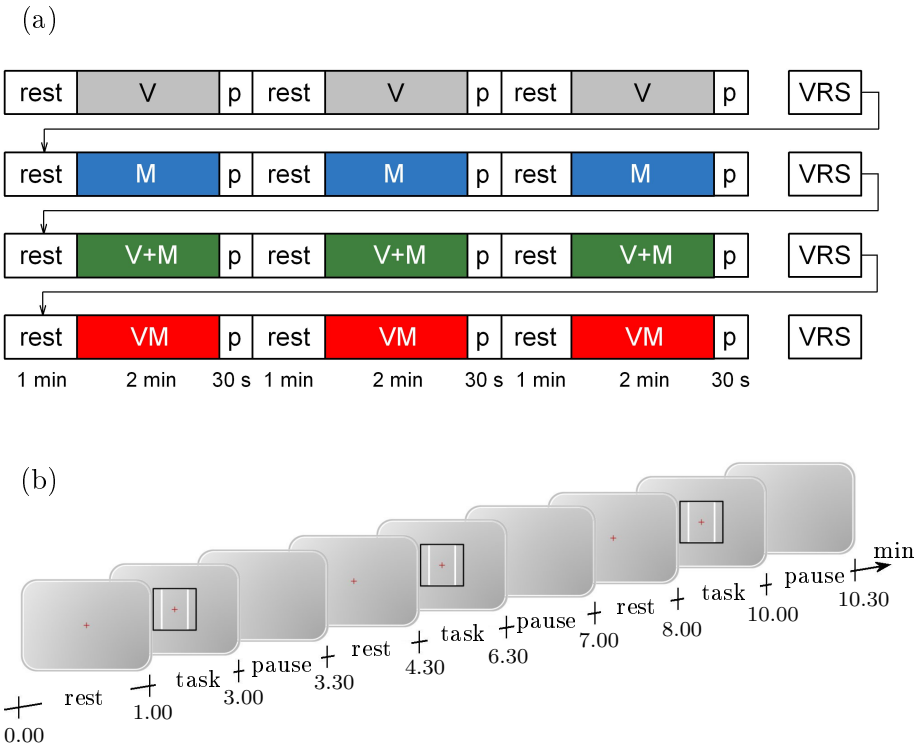

Figure 3.3: Schematic representation of the experimental procedure. (a) Each block of either V, M, V+M or VM, lasts 10min and 30s and consisted of three trials. Each trial starts with 1 min rest, followed by 2 min task and ends with 30 s pause, during which participants could relax their eyes. (b) Corresponding images presented on the screen. Adapted from [Erla et al., 2011a]

3.2.3 Data acquisition

Combined EEG/MEG was recorded while subjects performed the tasks.

EEG signals were acquired with 33 AgCl-cup electrodes, according to 10-20 standard electrode placement system plus additional intermediate positions in cortical areas of interest for the specific tasks (see Fig. 3.4). All electrodes were referenced to the earlobes common reference and grounded to Fpz. EEG activity was sampled at 586 Hz and band-passed at 0-200 Hz. Electrode impedances were kept below 5 kΩ [Erla et al., 2011a]. A bipolar signal was recorded at Fp1 and Fp2 locations (electrooculographic reference), in order to exclude trials contaminated with eye movements from further analysis.
Simultaneously, whole-head MEG recordings were acquired using a 275-channel axial gradiometer system (VSM MedTech Ltd). According to EEG, MEG data were sampled at 586 Hz and band-pass filtered at 0-200 Hz.

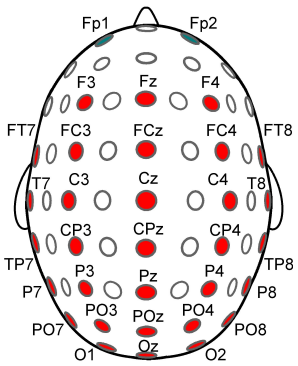

Figure 3.4: EEG montage. Fp1-Fp2 bipolar signal is adopted as EOG signal.

The signals recorded by the axial gradiometers were analyzed as synthetic third order gradiometers [132]. From every subject an anatomical MRI was obtained. To enable co-registration of MEG data with the anatomical brain scans, three coils were placed at the nasion and preauricular points prior to MEG data acquisition. The coils at the fiducial localizations served to continuously monitor the position of the subjects' head relative to the MEG sensors. After each acquisition, the coils were removed and at their locations were carefully placed radio-opaque washers for off-line co-registration of the recorded MEG data with the structural MR images obtained from each subject [Papadelis et al., 2011b].
Finally, bipolar electromyographic activity (EMG) was recorded from the muscle abductor pollicis brevis (APB) of the right hand, with the same sampling rate of the EEG/MEG.

Participants' performance was continuously recorded with the same sampling rate of the EEG. The correlation between the requested and performed grip force (Fig. 3.5a) was used as outcome index in each subject. A mean correlation across the three trials > 0.6 was set as threshold for subject inclusion in the analysis. Subjects generally showed high performances (0.74 ± 0.14) in the VM task. Only one subject presented low performance (mean correlation < 0.6) and was therefore excluded from further analysis [Erla et al., 2011a].

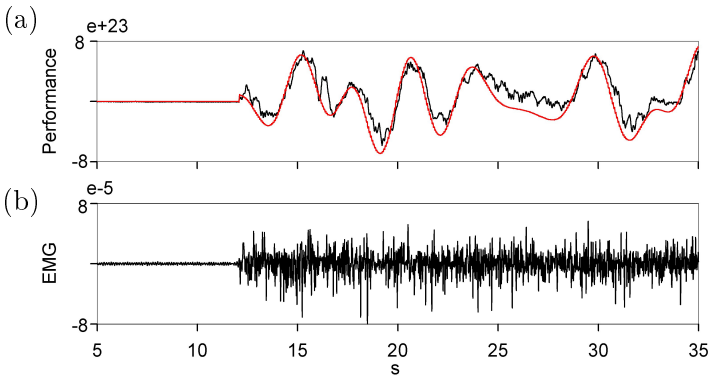

Figure 3.5: (a) Example of 30 seconds performance in one representative subject. Requested (red line) and the produced force (black line) are displayed. The first part of the signal was recorded during rest. Then the screen switched from the fixation cross to the VM task and the subject began to press the pinch grip. This was detected also by the EMG co-registered signal (b).

3.3 EEG data analysis

3.3.1 Preprocessing

EEG signals were FFT band-pass filtered (3-45 Hz) to remove power supply noise and extract information within the frequency bands of interest, and down-sampled from 586 to 146 Hz to reduce redundancy. After that, the mean value was removed from the signals.
The preprocessed EEG signals were visually inspected to identify possible artifacts and one subject was excluded from further analysis due to the excessive presence of signal artifacts.
For each subject and trial, EEG windows of 10 s length (from 3 s to 13 s before and after task onset) were selected for the analysis both in rest and in task conditions (V, M, V+M, VM). The window length was chosen as a compromise between the methodological request of analyzing stationary signals, which prompts for the use of short time windows, and the necessity of reproducing a sufficient number of cycles for the slower analyzed oscillation (here, the alpha rhythm), which prompts for the use of longer epochs.

3.3.2 ROIs selection

As depicted in Sec. 2.4.6, after preprocessing the data, a selection of the region of interest (ROIs) is suggested. Differently from what presented in [Erla et al., 2010], where an ERFs based approach is adopted, in this analysis the involved areas were a priori selected on the basis of prior neurophysiological knowledge, and tested for activation before to proceed with the connectivity analysis (Sec. 3.3.4).
According to previous findings (see Sec. 3.1), four cortical regions were considered as crucial for the execution of the proposed visuo-motor task: left central cortex (motor area contra-lateral to the moving right hand), right central cortex (motor area ipsi-lateral to the movement), parietal cortex and occipital cortex (visual area). From each of the four ROIs, three signals were collected as shown in Fig. 3.6.

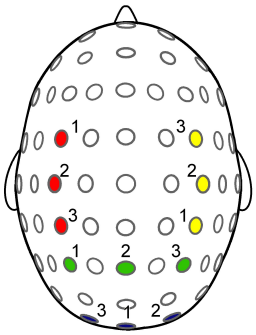

Figure 3.6: Selected channels. Three electrodes were considered for each area of interest: left motor (red), right motor (yellow), parietal (green) and visual cortex (blue). Each number (1, 2 or 3) indicates a combination of channels used for eMVAR identification.

In the following paragraphs, the eMVAR analysis performed for each subject, task (rest, V, M, V+M, VM), and trial of this dataset will be discussed. Since the connectivity between time series representing the same cortical area does not constitute a matter of interest and has not much sense at the scalp level, we decided to con-

sider in the model a single signal from each area of interest. Three combinations of electrodes were defined (keeping the distance between the four electrodes as large as possible, see Fig. 3.6) and eMVAR identification was executed for each one of them. Hence, for each subject, task, and trial, three eMVAR models were generated and, consequently, three sets of frequency-domain measures were obtained. We assumed that these three measures were all equally representative for the activation and connectivity of the ROIs' network in that subject and task [Erla et al., 2011b][1].

3.3.3 eMVAR model construction and validation

For each subject, experimental condition, trial, and electrodes-combination, the preprocessed signals were allocated into the data matrix $\mathbf{Y} = y_m(n)$ ($n = 1, \ldots, 1460$ samples and $m = 1, \ldots, 4$ derivations) to be described by an extended multivariate autoregressive model (Eq. 2.18). The optimal model order was estimated for each set of 4 signals through the Akaike information criterion presented in Sec. 2.4.3, imposing $p_{max} = 20$. It resulted on average $\bar{p} = 8.3 \pm 1.5$. Finally, the coefficient estimation was performed through the second approach for extended causal model identification presented in Sec. 2.4.4.

After model identification, the suitability of the estimated model for describing the observed data was checked. Specifically, the model assumptions of non-gaussianity and independence of the extended residuals were verified (Sec. 2.4.4).
The extended residuals $\mathbf{W}$ resulted non-gaussian in 83% of the analyzed models. Moreover, the estimated residuals $\mathbf{U}$ resulted never independent, while the extended residuals $\mathbf{W}$ were independent in 78% of the considered models. This is an important observation, which justifies the adoption of the extended model for the description of the data. In fact, violation of the assumption of independence of the strictly causal residuals is the reason to introduce the extended model in place of the strictly causal model. Only the sets of 4 signals satisfying simultaneously the assumptions of non-gaussianity and independence of the extended residuals were considered for the following analysis (in total, 77% of the sets).

Furthermore, the assumption of whiteness of the residuals was also tested. Since $\mathbf{W}$ and $\mathbf{U}$ differ only in the instantaneous structure, whiteness test gives the same result in both cases. In the 71% of the considered cases, whiteness of both residuals $\mathbf{U}$ and extended residuals $\mathbf{W}$ is verified. Whiteness is not observed in every case because, for a few of our EEG datasets, Akaike information criterion dropped monotonically with increasing model order. This is not related to the adopted model (strictly causal or extended) and corresponds to a behaviour observed in many previous studies (e.g., [8, 133, 134]). Taking into account these studies, we considered for the subsequent analysis also the sets which did not satisfy the whiteness assumption, even if part of the correlation structure of these data may be not well represented by the model.

[1] A simpler spectral and coherence analysis performed on a network of ten channels (considering prefrontal, motor, somatosensory, parietal and visual cortices) is presented in [Erla et al., 2011a].

3.3.4 Activation analysis

Activation was tested, in the selected signals, by detecting band-specific changes in the power related to the task.
After calculating the eMVAR model coefficients, the spectral matrix $\mathbf{S}(f)$ was determined according to Eq. 2.10, for each subject, experimental condition, trial, and electrodes-combination. The diagonal elements of $\mathbf{S}(f)$, $S_{ii}(f)$, represent the power spectral densities of each modeled signal y_i. In order to obtain objective and accurate power estimates, spectral decomposition was applied to each spectrum S_{ii}. This yielded the partial spectra $S_{ii|k}(f)$ related to the k poles of the processes, and corresponding to specific frequency bands (Sec. 2.4.7).
In Fig. 3.7 an example of spectral decomposition is shown for a representative subject (signal recorded in rest condition, first trial, P3 electrode). The model order is set to $p = 8$ and four poles are identified corresponding to four peaks at the frequencies $f_1 = 0.4$ Hz, $f_2 = 10.1$ Hz, $f_3 = 20.2$ Hz, and $f_4 = 32.6$ Hz. The spectral density S_{P3} is decomposed in the partial spectra $S_{P3|1}(1f)$, $S_{P3|2}(f)$, $S_{P3|3}(f)$, and $S_{P3|4}(f)$. The corresponding power estimates, measured as the areas subtended by each partial spectrum, result $P_1 = 14.0$, $P_2 = 2.8$, $P_3 = 0.5$, and $P_4 = 0.2$ μV^2/Hz. The overall power is $P = 17.6$ μV^2/Hz, which is well estimated by the sum of all the partial spectral powers.

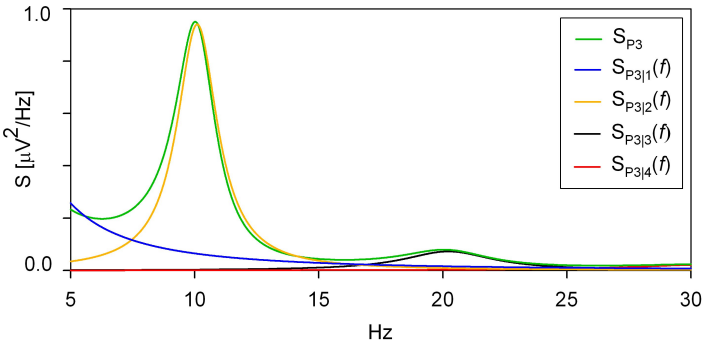

Figure 3.7: Example of spectral decomposition. Representative subject during rest, trial 1, electrode P3.

In this study we focused on alpha and beta frequency bands. In this way, long-range (alpha band) and medium-range (beta band) interactions are considered, avoiding short-range interactions that are difficult to distinguish from volume conductor effects at the scalp level. We decided to carefully consider this important aspect, even if the use of the extended MVAR model should deal with the volume conductor issue, being able to identify instantaneous relations between the involved areas. In addition, previous findings in visuo-motor integration research showed interregional synchronization mainly in α and β frequency ranges [69, 120, 119], justifying our restriction. Therefore, spectral power decomposition of each S_{ii} yielded the partial spectra $S_{ii}(\alpha)$ and $S_{ii}(\beta)$ related to the poles of the processes with frequency inside the alpha (8-13 Hz) and beta (13-30 Hz) frequency bands, respectively. The areas underlying the partial spectra were taken as measures of spectral power, P_α and P_β, within the two bands.

For each subject and experimental condition (R, V, M, V+M, and VM), single representative power values for each channel were obtained as average values across the three trials ($\bar{P}_\alpha$ and $\bar{P}_\beta$). Spectral power analysis aimed to characterize the activation of different cortical areas in response to the different tasks. Spectral power contents were thus compared between rest and task conditions to identify areas related to each control condition or to the visuo-motor integration processes. The statistical analysis was performed separately in each frequency band, after grouping results on the basis of the ROI they belong to (i.e., left central: FC3, C3, CP3; right central: FC4, C4, CP4; parietal: P3, Pz, P4 and occipital: O1, Oz, O2). For each assigned ROI, Kruskal-Wallis nonparametric one-way Analysis of Variance (ANOVA) was performed to assess the significance of differences due to stimulus-type (R, V, M, V+M, VM). When ANOVA indicated the presence of significant differences ($p < 0.05$), post-hoc multiple paired Wilcoxon tests were performed to assess the significance of the differences between rest (R) and task conditions (V, M, V+M, VM), as well as between each pair of task conditions. Correction for multiple comparisons was performed according to Holm's method [135].

Results

Fig. 3.8 depicts the results of the application of spectral analysis in a representative subject. The power spectral densities of four signals, recorded in proximity of the left motor cortex (channel C3 in panel a), of the right motor cortex (channel C4 in panel b), of the parietal cortex (channel Pz in panel c), and of the visual cortex (channel O2 in panel d), are displayed. The power spectral density of the EEG recorded above the left motor cortex (panel a) shows a major power decrease during tasks involving motion (M, V+M, VM vs R condition), while no significant changes are noticed during the pure visual (V) condition. Results for the right motor cortex (panel b) are similar, even if the power decrease induced by the M task is lower than the power decrease due to the combined tasks (V+M and VM). An opposite behavior is observed in the EEG representing the parietal cortex and the visual cortex (panels c and d), where power decrease is detected during tasks involving vision (V, V+M, VM vs R condition), but not during the pure motor (M) condition. In the parietal area, the power decrease due to the pure V task results lower than the decrease induced by the combined tasks. These results hold both in alpha and beta frequency bands.

Fig. 3.9 summarizes the results of spectral analysis in the overall subject population in terms power contents in alpha and beta frequency bands. Average values across subjects are shown for each condition (R, V, M, V+M, VM) and cortical region of interest. Power changes showed a similar tendency in the central areas, while their behavior was different in the parietal and occipital regions. The left central area was analyzed separately, since it is representative of the left motor cortex (contralateral with the motor task). In both frequency bands, the power content in this area decreased significantly during M, V+M and VM, as compared to R and V. This result suggested that the left motor regions activated only in presence of right hand motion. In the right central area, the difference between R and M was not significant

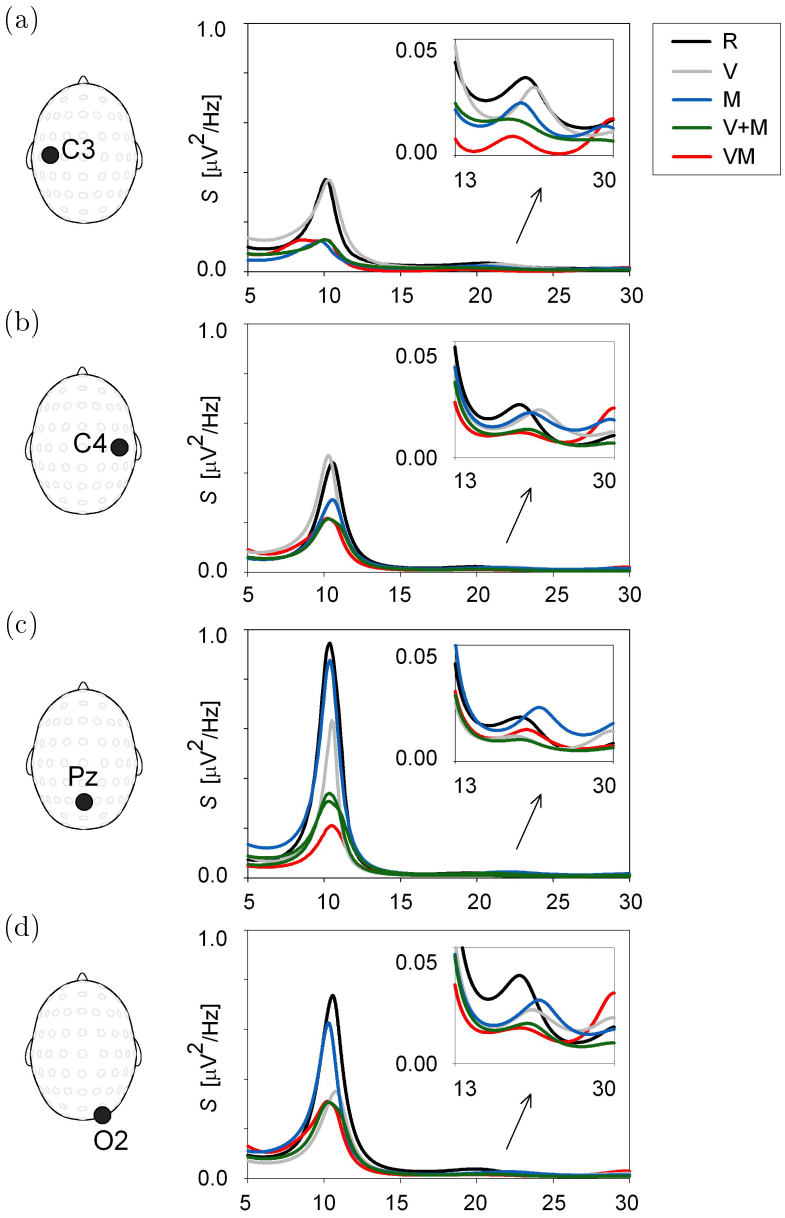

Figure 3.8: Application of spectral analysis in a representative subject for (a) one channel representing the left motor cortex (C3), (b) one channel representing the right motor cortex (C4), (c) one channel representing the parietal cortex (Pz), and (d) one channel located above the visual cortex (O2). Results are shown for R, V, M, V+M and VM, following the color code in the legend (top-right). On the left, schematization of electrodes positions.

in the alpha band, suggesting weaker ipsi-lateral activation. Parietal regions showed a significant power decrease during tasks involving a visual component (V, V+M and VM) vs R condition. M could not be distinguished from R, and showed significantly higher power than V (in the alpha band), V+M and VM (in both alpha and beta bands). Moreover, a power decrease was noticed during V+M and VM conditions as compared to V. The decrease was significant only in the alpha band during V+M, and in both frequency bands during VM. In the occipital area, a significantly lower power value in both alpha and beta bands was found for tasks involving a visual component (V, V+M, VM) vs R and M conditions. The only significant difference in power content between the two visuo-motor conditions (with and without feedback) was found in the beta band, where a significantly lower power was observed for the VM vs V condition (and not for V+M vs V) in the parietal area.

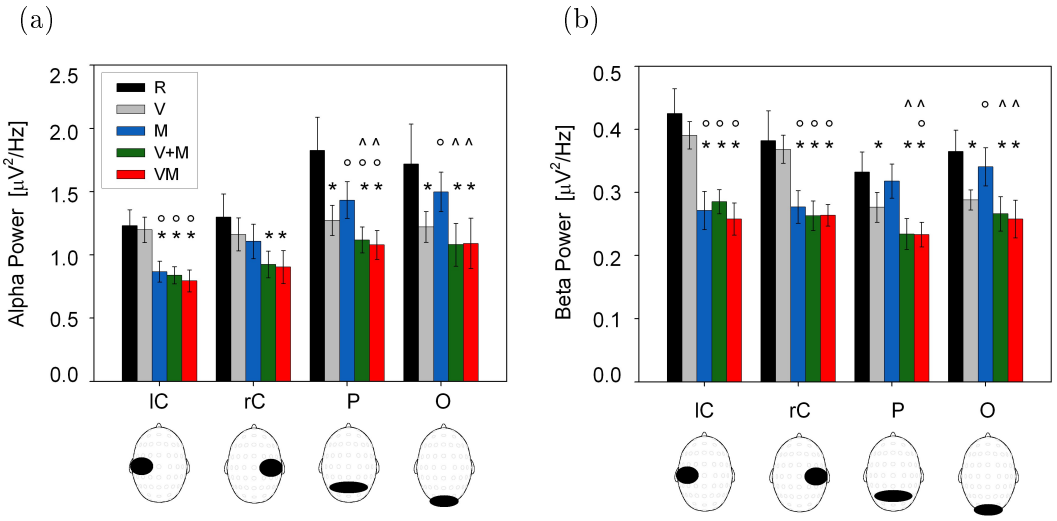

Figure 3.9: Spectral power values in alpha (a) and beta (b) frequency bands in the overall population. Data are expressed as mean ± standard error across subjects, for each experimental condition (R, V, M, V+M, VM, color coded as reported in the legend) and cortical area (lC: left central, rC: right central, P: parietal, O: occipital). Regions locations are indicated as black blobs in the scalp maps, displayed below the plots. Paired multiple tests: $*$ significant vs R; o significant vs V; $\wedge$ significant vs M.

3.3.5 Connectivity analysis

Starting from the estimated eMVAR coefficients, various frequency-domain measures of coupling and causality were calculated as described in Sec. 2.1.3 and 2.2.1. Connectivity analysis was divided into two steps:

1. the theoretical framework proposed in Ch. 2 was applied to rest and VM conditions, to test the proposed methods on real data and discuss possible advantages and limitations;

2. after selecting the more suitable frequency-domain connectivity measures, the global paradigm was studied, to further elucidate the neuronal mechanisms underlying visuo-motor integration.

First study

In the first study, linear coupling and causality were estimated between each pair of signals and the information content of the different adopted measures was compared. For each subject, experimental condition, trial, and electrodes-combination, all the frequency-domain connectivity measures summarized in Tab. 2.1 were computed. Specifically, we considered estimates of:

- direct+indirect coupling (COH) and causality (DC, iDC, eDC);
- direct coupling (PC) and causality (gPDC, iPDC, ePDC).

As discussed above, sets of 4 signals (one for each ROI) were considered in the eMVAR modeling. Therefore, a 4×4 matrix of functions was obtained for each connectivity measure, with each matrix element corresponding to a different connection or causal direction (for an example, see Figs. 3.11 and 3.12). After that, a corresponding 4×4 matrix of significance thresholds was determined for each function. The comparison between each connectivity measure and its significance threshold is useful to avoid false coupling detections in presence of independent oscillations occurring at nearby frequencies [92]. The threshold was case-by-case calculated as the 95th percentile of the no-interactions distribution (i.e., the distribution of the coupling/causality measures of interest obtained from 100 surrogate data). For each connectivity measure a procedure based on surrogate data generation was adopted (see Sec. 2.4.5):

- COH: FT surrogates;
- PC: CFTbf surrogates;
- DC, iDC, and eDC: CFTf surrogates;
- gPDC, iPDC, and ePDC: CFTd surrogates.

For each element of the 4×4 matrix and for each frequency, the connectivity measure of interest, computed from the original series, was compared with the threshold. Specifically, an average value of the measure and of its significance threshold was calculated in alpha (8-13 Hz) and beta (13-30 Hz) frequency bands. If the average threshold was exceeded by the average connectivity, the estimated coupling/causality was considered significant. If, on the contrary, the average connectivity value was below the average threshold, coupling/causality on that connection was considered not significant for that frequency band. Taking the band-average value is a common approach [136, 32], and is mathematically justified by the fact that several oscillations may be present in the analyzed band and the overall connectivity of these should be properly accounted by the chosen measure.
The statistical analysis of the results was divided in two parts, one for measures of direct+indirect connectivity (COH, DC, iDC, eDC) and one for measures of direct coupling and causality (PC, gPDC, iPDC, ePDC). The rationale of this separation stands in the fact that, while the absolute values of the measures in the first group have a meaningful physical interpretation in terms of amount of power transferred

from one process to another, direct measures are hardly useful in quantitative terms. In fact, their magnitude quantifies the information flow through the inverse spectral matrix elements, which do not find easy interpretation in terms of power spectral density, as seen in Sec. 2.1.3. As a consequence, two different approaches were adopted to analyze the results.

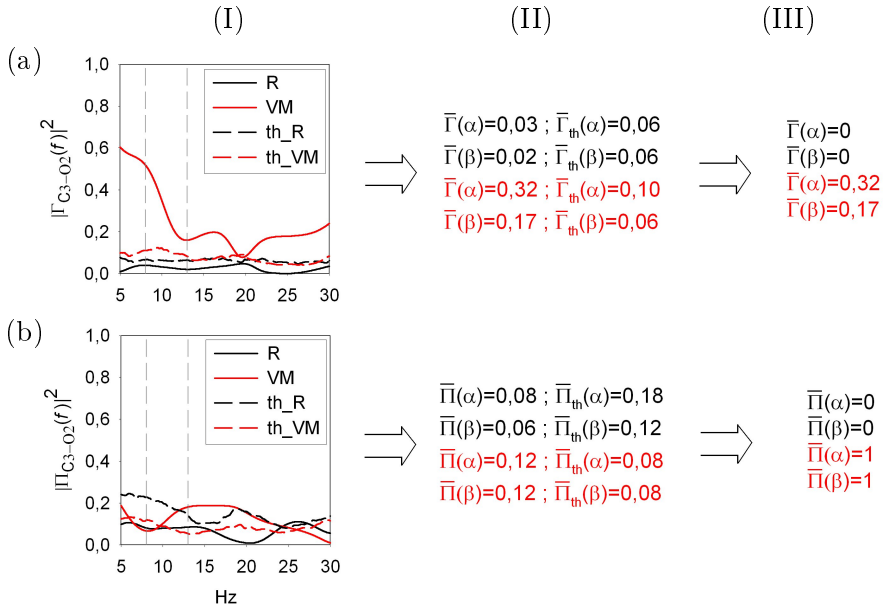

Figure 3.10: (I.a) Squared COH ($|\Gamma_{C3-O2}(f)|^2$) and (I.b) squared PC ($|\Pi_{C3-O2}(f)|^2$) for a subject during R (black solid lines) and VM (red solid lines), connection C3-O2. Dashed lines are the corresponding significance thresholds. Dashed gray lines indicates α and β frequency bands' limits. (II) Average values of the measures and of their thresholds within α and β are displayed. (III) Application of the thresholds: while for the measure of direct+indirect coupling (COH) the values exceeding the threshold are considered as meaningful coupling values, for the measure of direct coupling (PC) a binary response is adopted. In this example, increased coupling and direct coupling are observed due to task execution.

Measures of direct+indirect connectivity: for each subject, experimental condition, trial, electrodes-combination, and for each specific connection (element of the 4×4 connectivity functions matrix), the representative value for the degree of coupling/causality in each frequency band was considered equal to the average measure values inside the band, when the threshold was exceeded, while was imposed to zero, when lower than the threshold (e.g., Fig. 3.10a). After that, for each given connection and frequency band, a paired Wilcoxon test was performed between R and VM conditions to evidence possible changes in connectivity due to task execution.

Measures of direct connectivity: for each subject, experimental condition, trial, electrodes-combination, and for each specific connection, the representative value of the measure in each frequency band was considered equal to one, when the threshold was exceeded, while was imposed to zero, when not significant (e.g., Fig. 3.10b). This corresponds to counting the significant connections,

regardless of the absolute value of the connectivity measure. After that, for each given connection and frequency band, the proportion of significant connectivity patterns found in rest and task was compared. A Chi squared Pearson test was performed between R and VM conditions to evidence possible changes in connectivity due to task execution.

To illustrate the overall connectivity analysis, the results obtained for a sample subject (VM condition, trial 1, electrodes-combination 2) are presented in Figs. 3.10, 3.11 and 3.12.

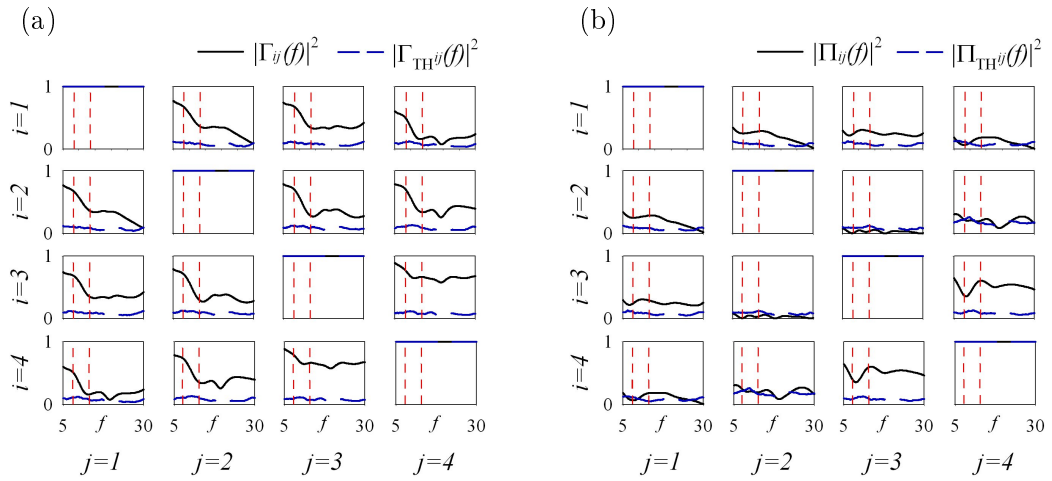

Figure 3.11: (a) Squared COH ($|\Gamma_{ij}(f)|^2$) and (b) squared PC ($|\Pi_{ij}(f)|^2$) for a representative subject during VM (solid black lines). Dashed blue lines represents the 95th percentile of the distribution of COH and PC over 100 surrogate series (significance threshold). Dashed red lines at 8 and 13 Hz indicate the borders of the α and β frequency bands. $i, j = 1, \ldots, 4$ indicates respectively channels C3, C4, Pz and O2.

Fig. 3.11 depicts the results of the application of frequency-domain coupling analysis. The coherence functions (panel a) and partial coherence functions (panel b) are displayed for each pair of signals. The computed thresholds for significance are also shown (dashed blue lines). Both 4×4 matrices are symmetric, reflecting the fact that COH and PC are measures of coupling and do not contain information on the direction of the interactions. The coherence is significant for each connection and its value is related to the amount of power transferred from one process to another. The partial coherence results not significant (in both alpha and beta frequency bands) between channels 2 and 3 (C4-Pz connection) and between 2 and 4 (C4-O2 connection), indicating that, in this subject and condition, the interaction between these areas is not direct.
In Fig. 3.12 the results of the frequency-domain causality analysis are shown. The 4×4 matrices are clearly non-symmetric, giving different results for the different directions. On the left are displayed direct+indirect causality measures, while on the right are displayed direct causality measures. The former elicit the directions of the connectivity patterns found from COH analysis (Fig. 3.11a), while the latter show

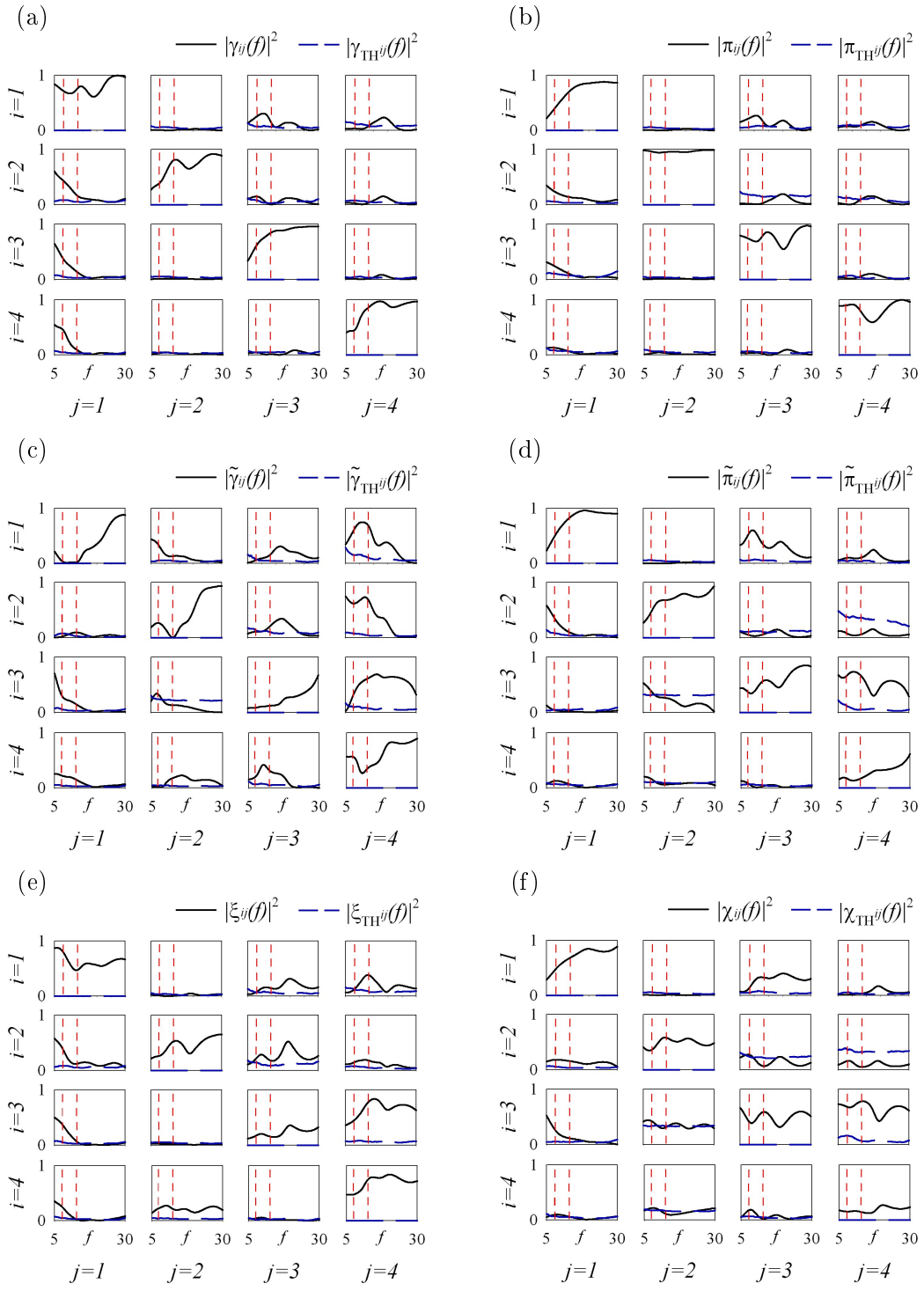

Figure 3.12: (a) Squared DC ($|\gamma_{ij}(f)|^2$), (b) gPDC ($|\pi_{ij}(f)|^2$), (c) iDC ($|\tilde{\gamma}_{ij}(f)|^2$), (d) iPDC ($|\tilde{\pi}_{ij}(f)|^2$), (e) eDC ($|\xi_{ij}(f)|^2$), and (f) ePDC ($|\chi_{ij}(f)|^2$), for a representative subject during VM (solid black lines). Dashed blue lines represents the 95th percentile of the distribution of surrogate data (significance threshold). Dashed red lines at 8 and 13 Hz indicates the borders of the α and β frequency bands. $i, j = 1, \ldots, 4$ indicates respectively channels C3, C4, Pz and O2.

the directions of each connection found in PC analysis (Fig. 3.11a). As an example, the non-significant connections observed in PC are not significant, over both directions, also in all the direct causality measures.
The presence of non negligible zero-lag interactions among the considered EEG signals was documented by the results of the validation tests. In fact, in this subject and condition, residuals $\mathbf{U}$ for the strictly causal model result non independent, while all the extended residuals $\mathbf{W}$ are independent. In addition, extended residuals result non-gaussian ($p = 1,8 \cdot 10^{-12}$), satisfying the eMVAR model assumptions.
The results obtained from the strictly causal model (panels a and b) can be compared with the corresponding outcomes of the extended causal model (panels c,e and d,f). In general, the dominant lagged connectivity direction is from back to front; DC, gPDC, iDC and iPDC appear indeed higher in the directions from y_j to y_i than from y_i to y_j, with $j > i$. In particular, connections from visual to left motor cortices are evident, due to the effect of the visual feedback, driving the movements of the subject. Strictly causal and extended measures show similar connectivity patterns. However, extended causality measures (panels c and d) seem to highlight the information flow better than the correspondent strictly causal measures (panels a and b), as documented by their higher values in almost all the connections that are significant compared to the threshold. As a consequence, extended measures seem better descriptors of the expected neurophysiological behavior than the strictly causal functions. Finally, the usefulness to model instantaneous effects can be deduced looking, for example, at the results for the direct connection C3↔Pz ($1 \leftrightarrow 3$ in the plots). While gPDC (panel b) shows significant direct causality both on C3→Pz and Pz→C3, at least in alpha frequency band, the extended model indicates connection Pz→C3 as lagged, but does not indicate any significant connection over the opposite direction C3→Pz (panel d). The link C3→Pz is observed again in ePDC (panel f), suggesting this relation as instantaneous. Therefore, we may interpret the lagged effect C3→Pz in panel b as a spurious result in the strictly causal analysis. [Erla et al., 2011b]

Population results

Figs. 3.13 and 3.14 schematize the results of coupling and causality analysis in terms of task-related connectivity changes in the overall population of subjects for alpha and beta bands, respectively. Only connections showing statistically significant changes between rest and VM task are displayed, to evidence the activation patterns of the network subserving the execution of the task and compare results that can be obtained using the different measures presented in Ch. 2. For simplicity, the channel located in the middle of the each ROI is visualized as representative for the three derivations belonging to the area. In the following, left central area will be indicated as lC, right central area as rC, parietal area as P and occipital area as O.
Coupling measures are presented in the first column, while causality measures in the second (measures obtained from the strictly causal model) and in the last two columns (measures obtained from the extended model). COH and PC reveal the presence of significant task-related changes in coupling between each pair of ROIs,

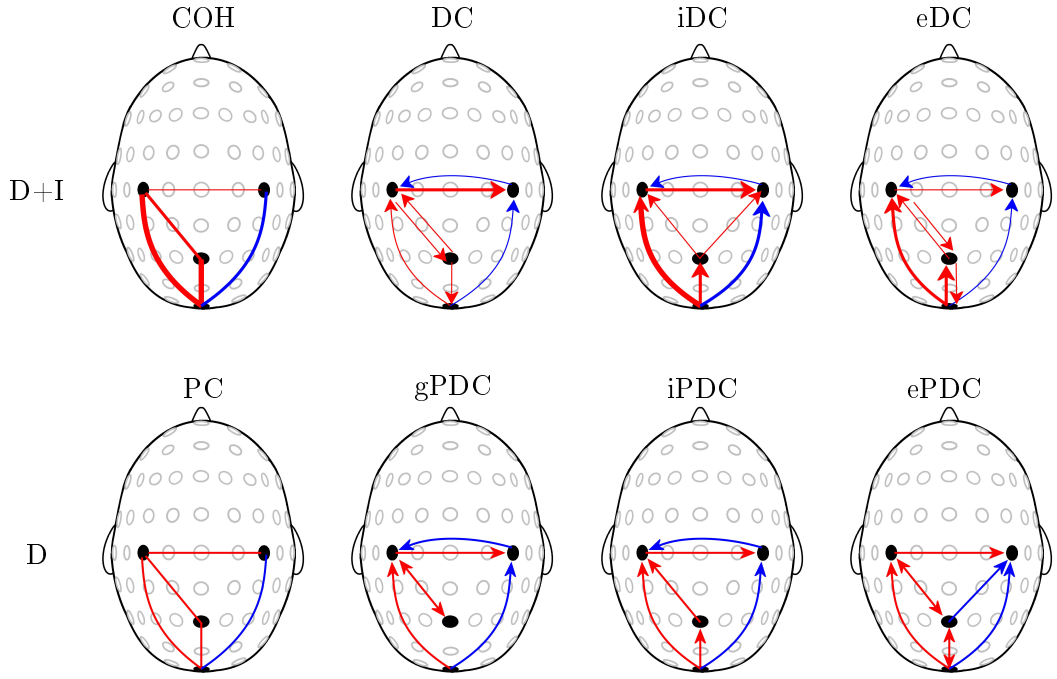

Figure 3.13: Cortico-cortical connectivity changes in the α frequency band during VM in the overall population of subjects. Lines indicate significant changes in the connectivity measure's value from rest to task condition (blue: significant decrease; red: significant increase). Coupling measures are presented in the first column, strictly causal measures in the second column, while measures obtained from the extended model are depicted in the last two columns. First row contains the direct+indirect measures (D+I), while direct measures are presented in second row (D). For simplicity, the channel located in the middle of each ROI was displayed as representative for the three derivations belonging to the area (C3 represents here the three left motor channels, C4 the right motor area, Pz the parietal and Oz the occipital). In the first row, lines are thin when the difference between average task and rest values is < 0.1, medium for differences larger than 0.1 but lower than 0.3, and tick for differences > 0.3. Adapted from [Erla et al., 2011b].

but they cannot elucidate the directions of the detected relations. This aspect is clarified by the causality analysis, in which the significance of the changes is valued for each connection and direction.
The first row contains the direct+indirect measures, while direct measures are presented in the second row. As explained above, the absolute value of direct+indirect measures can be interpreted in terms of amount of power transferred from one process to another, normalized in respect to the total inflow entering the "arrival-ROI". Hence, for each direct+indirect measure, the average value across subjects, trials and electrodes-combinations was calculated in rest and VM conditions for each connection and direction ($\overline{|\Gamma_{ij}|^2}_R$, $\overline{|\Gamma_{ij}|^2}_{VM}$, $\overline{|\gamma_{ij}|^2}_R$, $\overline{|\gamma_{ij}|^2}_{VM}$, $\overline{|\tilde{\gamma}_{ij}|^2}_R$, $\overline{|\tilde{\gamma}_{ij}|^2}_{VM}$, $\overline{|\xi_{ij}|^2}_R$, $\overline{|\xi_{ij}|^2}_{VM}$, for both alpha and beta frequency bands). The difference between average values in rest and task was displayed, when changes due to the task resulted significant, through the thickness of the lines (see first row in Fig. 3.13 and 3.14). In this way, looking at each region on the map, it is possible to understand how much of its

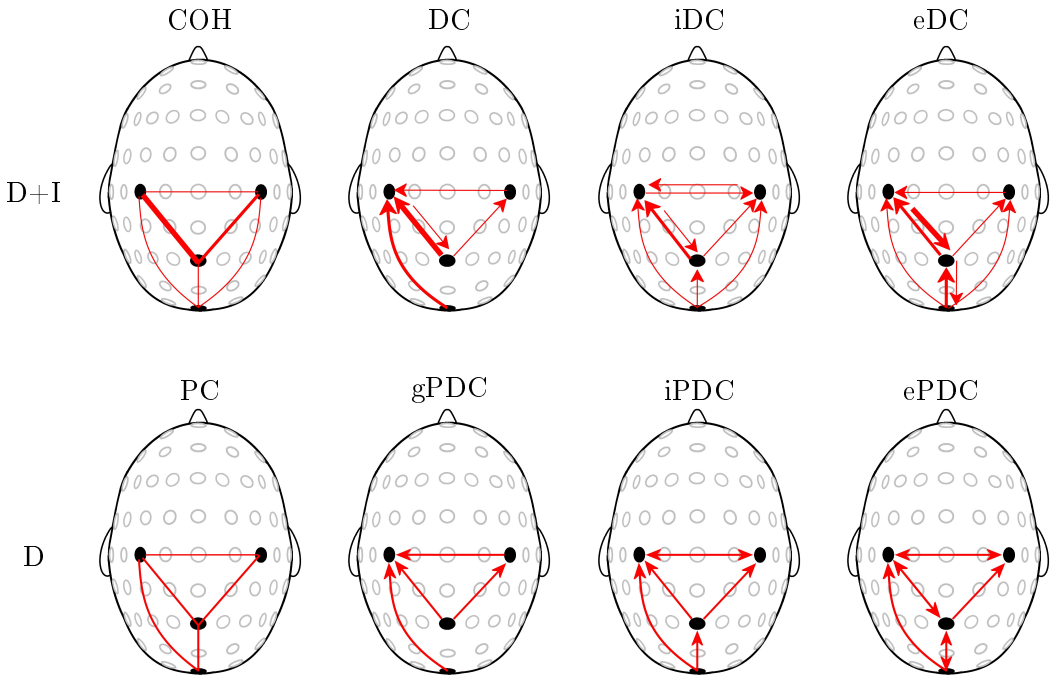

Figure 3.14: Cortico-cortical connectivity changes in the β frequency band during VM in the overall population of subjects. See the legend of Fig. 3.13 for details.

power is coming from the other regions. As a drawback, direct+indirect measures cannot distinguish between direct and indirect causal effects. This information can be extracted from the direct measures, which detect only direct relations. Anyway, the latter cannot completely substitute the direct+indirect measures. In fact, their quantitative interpretation is difficult, being them related to the inverse spectral matrix elements and not to the power. This is the reason why a binary statistics was applied to these measures. When, for example, a certain connection (and direction) was not significant (in respect to the surrogate data threshold) during rest and became significant in VM, this was interpreted as increase in connectivity for that connection (and direction). As a consequence, maps (second row in Fig. 3.13 and 3.14) show only connections with significant task-related changes, with a fixed arrow thickness.
Finally, differences evidenced in the results of the strictly causal measures (DC and gPDC) and of the extended measures (iDC, iPDC, eDC and ePDC) have to be discussed, to compare the effects of the two modeling approaches (MVAR and eMVAR, respectively). Lagged measures (i.e., DC vs iDC, or gPDC vs iPDC) are mostly in accordance to each other. In the alpha frequency band, task-related changes in the direct connections between motor cortices and between visual and motor cortices are similarly interpreted. Also in the beta frequency band many results agree. Anyway, some crucial differences arise. First of all, connection O→P appears significant only using iDC and iPDC estimators, while it is not present using DC and gPDC, in both frequency bands. This is a very important point, since the connection between

visual and parietal cortical regions is expected, being the parietal area considered as crucial for early sensorimotor transformations underlying action (especially for the visual control of hand action) [137, 138]. Moreover, in the alpha band, the causality increase over the opposite-direction, P→O, can be interpreted from the strictly causal measures as lagged and indirect (being significant for the DC). However, the information coming from eDC and ePDC measures (compared with that of iDC and iPDC) suggests that the instantaneous effects play a role in the increase of causal coupling over the P→O direction. This may be considered as an explanation for the relation P→O detected from DC but not from iDC, which, in this sense, results wrongly interpreted by the strictly causal model. The same argument can be applied to the increase in direct causality detected for the connection lC→P in the alpha band. In fact, both DC and gPDC indicate a significant increase, which is not detected from iDC and iPDC, but is detected by eDC and ePDC, again suggesting a contribution of instantaneous correlations. Finally, in beta band, iDC and iPDC show significant increase on the connection lC→rC, which is not significant in the strictly causal model, probably as a consequence of the spurious reorganization of the causal relations on different connections.

Second study

In the second study, linear coupling and causality were estimated by eMVAR model based measures, which were shown to be suitable to describe the variations of connectivity due to task execution and to detect important connections that are not evident from strictly causal analysis. The global paradigm was studied to further elucidate the neuronal mechanisms underlying visuo-motor integration.
The statistical analysis described for the first study (considering R and VM conditions) was here identically replicated for the signals recorded during V, M, and V+M tasks. Specifically, for each given connection and frequency band, iDC and eDC estimates obtained for each rest (R_V, R_M, R_{V+M} and R_{VM}) and task (V, M, V+M, VM) condition were compared through a a paired Wilcoxon test, to evidence possible changes in connectivity due to tasks execution. For iPDC and ePDC measures, Chi squared Pearson tests were performed between rest and task conditions. In addition, the results obtained for the various rest conditions (R_V, R_M, R_{V+M} and R_{VM}) were checked to be indistinguishable to each other (i.e., in statistical terms, to belong to the same distribution) by means of the same tests.
Connectivity maps were generated for each measure, condition and frequency band. They show only connections with statistically significant changes between rest and task. This allows to evidence the peculiar activation patterns of the network subserving the execution of the pure tasks (V, M) and of the combined tasks (V+M and VM), as well as disentangle the integration mechanisms.

Fig. 3.15 and 3.16 depict the results of the lagged measures (iDC and iPDC, respectively) in terms of task-related changes in the connectivity patterns. In the alpha frequency band (first row in the figures), lagged causality values significantly decrease or remain unchanged between the brain areas that are not involved in the pure tasks (V and M). In fact, during the pure visual condition V, a significant decrease of direct

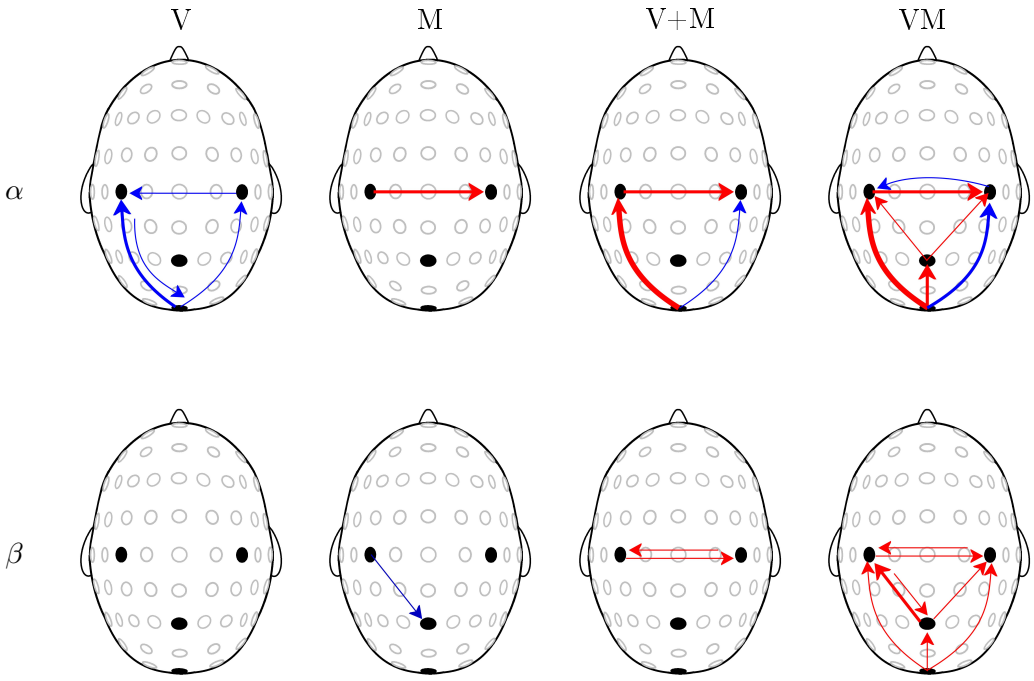

Figure 3.15: Cortico-cortical iDC changes in α (first row) and β frequency bands (second row) in the overall population. Lines indicate significant changes in iDC values between rest and task (blue: significant decrease; red: significant increase). Pure visual task (V) is presented in the first column, pure motor (M) in the second column, visuo-motor tasks in the last two columns (V+M and VM). For simplicity, the channel located in the middle of the each ROI was displayed as representative for the three derivations belonging to the area (C3 represents here the three left motor channels, C4 the right motor area, Pz the parietal and Oz the occipital). Lines are thin when the difference between average task and rest values is < 0.1, medium for differences larger than 0.1 but lower than 0.3, and thick for differences > 0.3. Adapted from [Erla et al., 2011b].

lagged causality is observed between the visual cortex regions and the motor cortex regions. Moreover, indirect lagged causality decreases from the right motor cortex to the left motor cortex. During the pure motor condition M, a significant increase of lagged causality (Fig. 3.15) and lagged direct causality (3.16) is observed, in the alpha frequency band, from the left central to right central areas i.e., between signals recorded from the motor cortices. No significant changes are observed between motor and visual cortices and, in the beta band, the relation from left motor to parietal areas shows a significant decrease.
During the visuo-motor tasks (V+M and VM) an involvement of all regions was observed. In fact, the relation between left and right motor areas, observed in the alpha frequency band during M, is also present in V+M and VM, and the significant decrease of causality in O→rC, observed during the pure visual task, is present also in the composed tasks. Moreover, a strong causality increase from visual to motor cortex is documented in the alpha band by a remarkable increase of the iDC (Fig. 3.15). Conversely, this connectivity relation was not significant during the execution of the pure tasks.

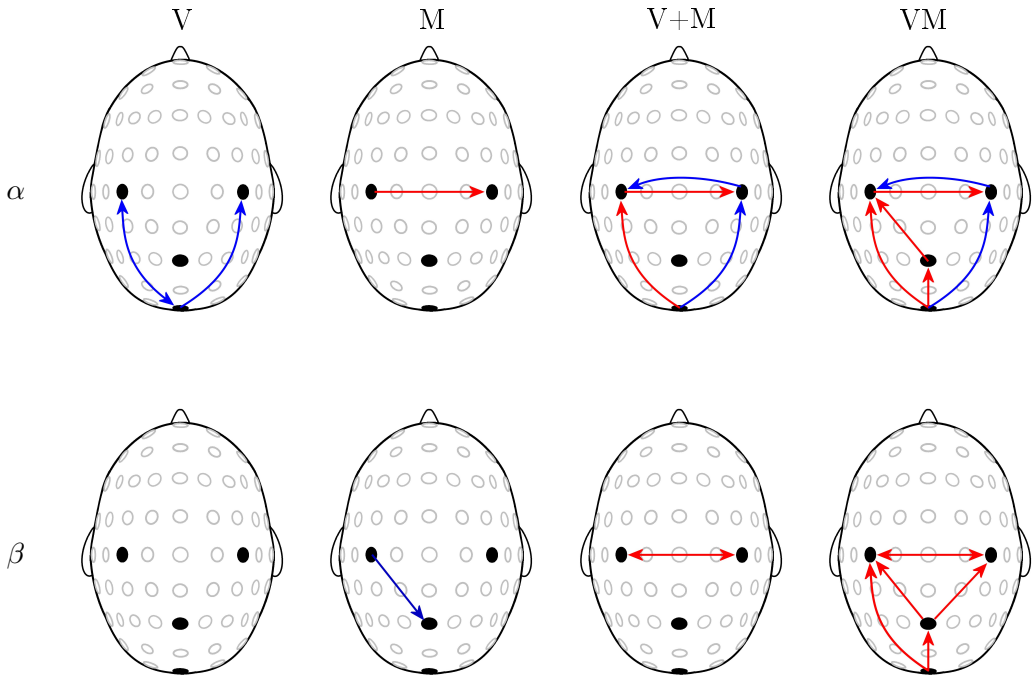

Figure 3.16: Cortico-cortical iPDC changes in α (first row) and β frequency bands (second row) in the overall population of subjects. See the legend of Fig. 3.15 for details.

The inter-regional connectivity patterns generated by the two visuo-motor tasks (with or without feedback), in the alpha band, show few differences. Specifically, the relations O→P and P→lC have increased causality in VM, but not in V+M. This result has to be ascribed to the visual feedback effect. Moreover, iDC increases weakly also in P→rC, probably as a consequence of the inability of this measure to distinguish between direct and indirect relations. As regards the beta frequency band, a significant increase of connectivity (mainly from back to front) in the brain network is observed only during the execution of the visuo-motor task with feedback (VM), while few significant changes are noticed in V+M. In fact, besides the activation of direct causal relations between the two motor areas, only during VM a significant increase is observed in the connectivity from the visual region to the motor areas (direct for left motor area and indirect for right motor) and the parietal area, and from the parietal to both central regions.
Finally, it is worth noticing that, while in alpha frequency band the activated network (significant increase in causality relations) is mainly located in the left part of the brain, i.e., contra-lateral to the motor task, and the right patterns are suppressed, in beta band the whole connectivity network is activated (mainly from back to front) without distinction between the two hemispheres.

Fig. 3.17 and 3.18 summarize the significant task-related changes in causality results for the extended measures (eDC and ePDC, respectively). The main differences observed between lagged and extended measures are related to the connections P→O,

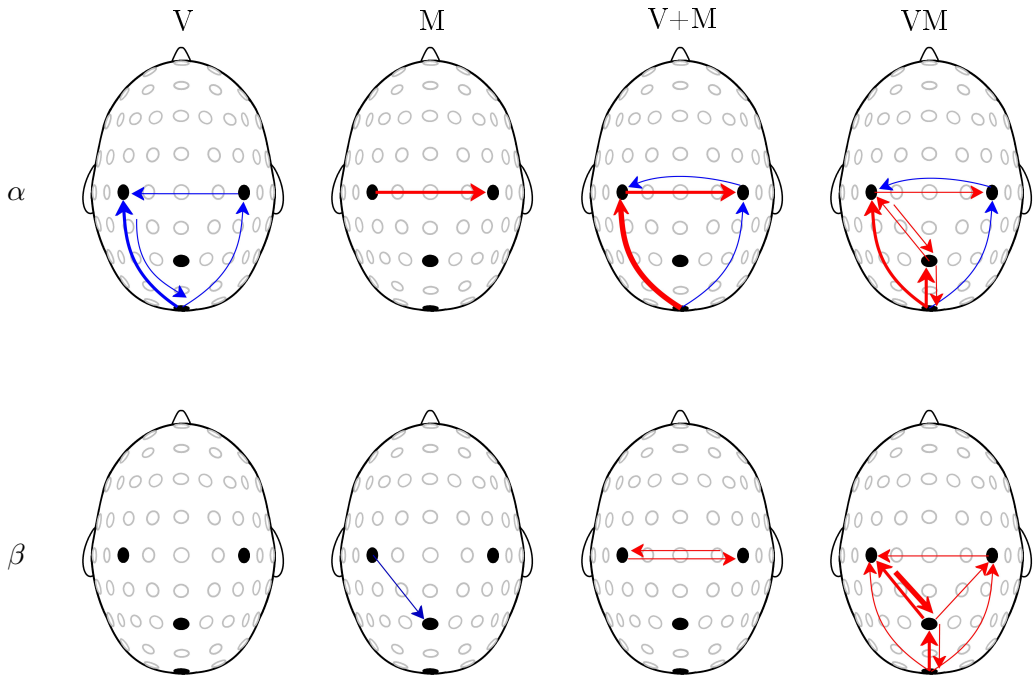

Figure 3.17: Cortico-cortical eDC changes in α (first row) and β frequency bands (second row) in the overall population of subjects. See the legend of Fig. 3.15 for details.

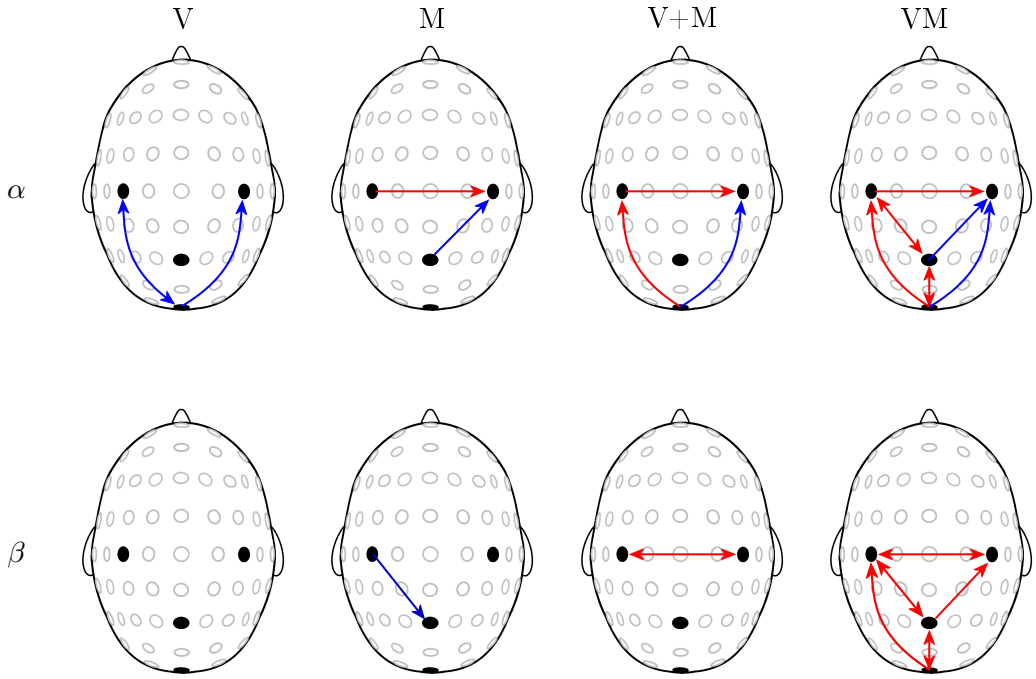

Figure 3.18: Cortico-cortical ePDC changes in α (first row) and β frequency bands (second row) in the overall population of subjects. See the legend of Fig. 3.15 for details.

lC→P and P→rC. In fact, during VM, a significant increase in extended direct causality is observed from parietal to occipital areas. This is present in both ePDC and eDC, but was absent in iPDC and iDC. This difference can be ascribed to instantaneous effects. Similarly, the significant decrease of ePDC from the parietal to the right central regions in alpha band, suppressing the significance of the indirect increase of causality on the same connection (not significant eDC changes), can be ascribed to a confounding influence of instantaneous effects on the detection of lagged causality. This is also the case of the increase of ePDC from the left motor area to the parietal in the beta band. In the latter case, the instantaneous effect seems to "overlap" the lagged indirect effect detected by iDC. All these results are presented in [Erla et al., 2011b].

3.3.6 Discussion

The binding theory assumes that the integration of spatially distributed information into a coherent percept is based on transiently formed functional networks linking the various brain regions by phase-locked oscillatory activity [115]. This model is adopted for the interpretation of many particular aspects of perception, cognition and action, such as the integration between multimodal sensory inputs and motor control. Starting from the fact that the cooperation between brain regions, involved in the processing of a task, may be elicited by studying the features of the signals recorded from them, this study aimed to:

- apply multivariate spectral analysis on multichannel EEGs recorded during a visuo-motor force-tracking paradigm, to compare the behavior of different frequency-domain connectivity measures;
- investigate the visuo-motor integration processes related to this task.

The experimental paradigm, applied in healthy subjects, involved the execution of two tasks demanding visuo-motor integration (VM, V+M), as well as pure-visual (V) and pure-motor (M) performances used as control conditions. The comparative analysis allowed to elicit specific mechanisms involved in integration processes.

First of all, multivariate power spectral analysis was applied in order to evidence changes in the rhythmic oscillations of EEG signals due to region activation, according to a paradigm which associates power decrease with area activation [139].
While executing the pure-visual task, subjects showed a significantly decreased power (i.e., task-induced activation) in both alpha and beta frequency bands in the parietal and occipital cortical regions, but not in the central areas. On the contrary, the execution of the pure-motor task induced activation of the left central region only, in the alpha frequency band, and of both central regions (left and right) in the beta band, suggesting stronger contra-lateral and weaker ipsi-lateral activation of the motor cortex. Finally, the execution of a combined task (V+M or VM) determined activation of both central and posterior brain areas.
The presence or absence of a visual feedback determined differences between power values only in the beta frequency band, suggesting the role of beta rhythm in the

feedback-mediated matching of motor performance and visual information. Moreover, differences due to the presence of visual feedback were observed only in the parietal area, suggesting the involvement of this brain region in visuo-motor integration. This is in accordance with previous studies conduced in both monkeys and humans by single cell activity, TMS and neuroimaging techniques [127, 126, 140, 137, 112]. They evidenced the crucial role of the parietal region in visuo-motor integration and precision grasping tasks.
From a methodological point of view, the proposed approach, based on parametric multivariate spectral analysis instead of classical non-parametric (Fourier transform-based) spectral analysis, provides a compact and complete description of the signal dynamics in terms of model parameters [22]. This method was combined here with a supplementary procedure for power spectral decomposition. The algorithm for spectral decomposition allowed precise and objective determination of the power associated to each oscillatory component of the spectrum [109].
Overall, these results indicated the suitability of spectral decomposition to measure band-specific power contents, reflecting neuronal network activation during task performance engaging different brain regions. Activation was related to power decrease, confirming what found in [Erla et al., 2010, Erla et al., 2011a].

After studying activation of the brain ROIs, strictly causal and extended multivariate autoregressive model-based analyses were performed on rest and VM conditions, to test the proposed methods on real data and discuss possible advantages and limitations of the different coupling and causality measures. Specifically, we considered estimates of direct+indirect coupling (COH), direct+indirect causality (DC, iDC, eDC), direct coupling (PC) and direct causality (gPDC, iPDC, ePDC). Alpha and beta frequency bands were considered, to focus on long-range (alpha) and medium-range (beta) interactions [119], and on the basis of previous findings in visuo-motor integration research, showing interregional synchronization mainly in these frequency ranges [69, 120, 119].
First, the considered connectivity measures were separated into two main groups: direct+indirect and direct measures. While the former give information about the strength of each relation (in terms of amount of power transferred from one process to another) but are not able to distinguish between direct and indirect relations, direct measures elicit the structure of the investigated network but do not have easy interpretation in quantitative terms (since they quantify the information flow through the inverse spectral matrix elements). Therefore, both groups of estimates have to be considered and the connectivity patterns have to be interpreted considering both the strength of the connectivity and the direct/non-direct nature of the interaction. Coherence and partial coherence revealed the presence of significant changes in coupling between the cortical ROIs, due to task execution. To detect the forward and backward components of the revealed couplings, causality analysis was performed. Lagged causality measures obtained from the MVAR coefficients (DC and gPDC) were compared with that calculated from eMVAR coefficients (iDC and iPDC). Even if a general agreement was observed for the two groups of measures, suggesting a prevalent information flow from back to front areas and task-related changes both

in alpha and beta frequency bands, some important differences were shown. Indeed, significant causality increase was detected from the visual to the parietal areas in both frequency bands during the visuo-motor task only by adopting the extended model based measures. This causal relation is considered to be essential in visuo-motor integration processes. In fact, the posterior parietal cortex corresponds to the major terminal of the so called dorsal stream, projecting from the primary visual cortex [141]. This path has been recently demonstrated to be involved in eye movements, visually guided reaching and manipulation of objects and is believed to have an important role in transforming visual inputs into skilled motor actions [138, 142]. Moreover, the dorsal stream is considered to be part of a complex network of visuo-motor modules interconnected with other cortical and subcortical structures devoted to sensorimotor control [142]. Specifically, visual information is believed to reach the premotor areas via the parietal cortex [130, 128, 129, 138]. This compex network was detected in our data only thanks to the application of eMVAR based measures. In fact, while the causality from parietal to motor areas was revealed from both strictly causal and extended measures, the visual to parietal connection was significant only performing the extended analysis (Fig. 3.13 and 3.14).
The utilization of the extended MVAR model allowed also to distinguish lagged effects from instantaneous relations. As a consequence, some misleading task-related changes resulting from the strictly causal model could be recognized and ascribed to the presence of non negligible instantaneous relations between the recorded signals. As an example, the increase of causality indicated as lagged by DC and gPDC on the connection lC→P in the alpha frequency band was not significant in iDC and iPDC and was significant in eDC and ePDC. This suggests a misleading role of instantaneous causality on the detection of lagged causality when the traditional strictly causal model is applied.
Overall, these results showed that modeling the data with an approach that considers also instantaneous effects may lead to the detection of important connections, which are not detected from the strictly causal measures. Moreover, it allows a better comprehension of the causal relations between different cortical areas. In fact, eMVAR approach gives the possibility to distinguish between instantaneous and lagged effects, being the former probably related to volume conductor effects. The validation tests showed in Par. 3.3.3 are an additional reason to prefer eMVAR modeling to MVAR modeling, being the assumption of the latter not satisfied in real EEG datasets. In fact, the presence of non negligible zero-lag interactions among the considered EEG signals was documented by the non-independence of the residuals $\mathbf{U}$ for the strictly causal model. Differently, the assumptions of eMVAR modeling are accomplished for the selected signals, as extended residuals $\mathbf{W}$ are independent and non-gaussian. These conclusions demonstrate the suitability of the new proposed approach for real data applications and for the description of neurophysiological data and cognitive processes.

Finally, extended causality analysis was performed on the global paradigm, to further elucidate the neuronal mechanisms underlying visuo-motor integration. Task-induced modifications of the network connecting the activated brain areas were studied, ac-

cording to a paradigm which associated increase of interregional causality estimates with enhanced cooperation processes among the analyzed areas.
In the alpha frequency band, during the control conditions V and M, lagged causality values significantly decreased or remained unchanged between the brain areas that were not involved in the pure tasks. Connectivity decrease has been suggested as a potential strategy to minimize the influence of a distracting stimulus and to maintain performance quality by controlling the relative weight of information sources and/or focusing attention [69]. During the composed tasks (V+M and VM), our analysis revealed a connectivity pattern consistent with a combination of the activation patterns observed in the two control conditions (V and M), which suggested the role of alpha synchronization in enforcing the specific functional network surrounding the cortical areas involved in task execution. These results confirmed what found in [Erla et al., 2011a] by coherence analysis for a network of ten ROIs. Moreover, alpha connectivity from visual to motor cortex increased while performing the visuo-motor tasks (V+M and VM conditions), but not during V and M. This result underlined a tendency towards an enhanced driving role of the visual cortex over the motor cortex during tasks simultaneously involving both areas, according to mechanisms consistent with a visuo-motor integration process [15, 69, 129]. Furthermore, our results showed, in the alpha band, a stronger activation of the left side network of the brain (contra-lateral to the motor task), suggesting a different behavior of the two hemispheres due to the lateralization of the motor task. An important difference was found between V+M and VM conditions, i.e., an increased causality from the occipital to the parietal regions and from the parietal to the left motor areas, during VM. This suggests an enforcement of the connectivity network between visual and motor cortices due to the presence of the visual feedback and underlines the role of the parietal area in the visuo-motor integration process [137, 112, 130, 128], which was noticed also from the power analysis. The difference between V+M and VM tasks was even more evident in the beta band. While no substantial connectivity changes in respect to rest were observed in the V+M condition and no significant connectivity was found between visual and motor areas, confirming the results reported by [69], several connections showed a causality increase during the VM condition, which suggests a strong relation between feedback effects and beta connectivity increase. Summarizing, the different functional role of the two considered frequency bands was revealed by: (i) the absence of left-right connectivity pattern differences in the beta band, and (ii) the different impact of visual feedback on the network. These results provide novel quantitative information in the still open issue of the role potentially played by the different frequency bands [69, 120, 113].

A limitation of MVAR and eMVAR-based scalp signals analysis was the necessity to consider a low number of signals (ROIs) for a good fit of the data through the model. In fact, considering large numbers of derivations recorded in close positions on the scalp as an input for the same model, very often lead to unfulfillment of the model assumptions. This could be ascribed to the fact that signals recorded in close locations contain redundant information, because of the volume conductor effect. As a consequence, scalp connectivity analysis shows low spatial accuracy.

A promising solution seems to be the application of source imaging techniques to the recorded data, allowing the accurate detection of the location and of the time variations of the sources' activities generating the recordings. In the following paragraph a pilot study is presented applied to the MEG signals acquired in this study. Even if source imaging approaches are recommended before connectivity analysis whenever high number of recording channels are available at the scalp level to avoid the spatial redundancy issue, more accurate analysis is required to understand possible effects of the adopted source imaging techniques on the various estimated connectivity relations.

3.4 MEG data analysis

3.4.1 MEG source activity estimation

After filtering the recorded MEG signals (band-pass filtering between 0 and 70 Hz, notch-filtering to remove 50 Hz line noise) and subtracting the mean value, they were visually inspected for possible artifacts, and data from two subjects (the same we excluded from EEG analysis) were excluded from further analysis, due to strong artifact contamination.
Source activity was estimated using the *Synthetic Aperture Magnetometry* (SAM) [143, 132], a well-established spatial filtering tomographic scanning technique based on the nonlinear constrained minimum-variance beamformer. The activity related to the execution of the task was identified by sequentially applying the beamformer to a number of locations placed on a regular grid spanning the whole brain and volumetric SAM images were obtained. Specifically, power estimates were computed for the 30 s window preceding (rest) and for the 30 s following (task) the VM task onset. Source power difference was calculated between VM and rest for each 2 mm^3 volume element, and pseudo-t statistical parametric images were generated from this difference [132]. A multiple local-sphere model served as head model.
Each subject's MRI was spatially normalized into the Montreal Neurological Institute (MNI) template space using SPM5 (*http://www.fil.ion.ucl.ac.uk/spm/*); the resulting normalization parameters were applied to the volumetric SAM images, wich were overlaid on the individual participant's structural MRI. Hence, all volumetric images resulted in the same coordinate space and could be used for a group statistical analysis by means of Statistical nonParametric Mapping (SnPM). For details, see [Papadelis et al., 2011a].
Thirteen spatial regions of interest (ROI) were identified by scanning the group analysis volumetric images. The ROI locations were then compared with the probabilistic cytoarchitectonic maps (PCM) [144] by superimposing the group analysis volumetric image on the PCMs using the "Anatomy Toolbox" software [145].

Fig. 3.19a shows the significant decreases of source activity power during VM compared to rest, as revealed by group volumetric statistical analysis ($p < 0.05$). As for EEG analysis, source power decrease in low frequencies (i.e., alpha band) was related to increased neural activation [139]. Active sources were observed (see Fig. 3.19b):

- within the calcarine sulcus (cytoarchitectonic BA17, representing V1);
- in the left and right inferior occipital gyri and occipital convexities (BA18 and hOC5, representing most likely V2 and V5, respectively);
- around the rostral part of the left inferior frontal sulcus (BA45, BA46 and BA10, referred as rostral IFG);
- in the middle portion of the right IFG (BA45);
- in the left precentral sulcus and in the left postcentral sulcus (BA4a and BA3b, representing M1 and the primary somatosensory area SI, respectively);

- around the right precentral sulcus (BA4a, representing M1);
- around the left parietal opercular region (OP4 subdivision, most likely representing activation within the secondary somatosensory cortex SII);
- bilaterally, within the superior parietal lobe (SPL), corresponding to cytoarchitectonic area BA7 (SPL7a).

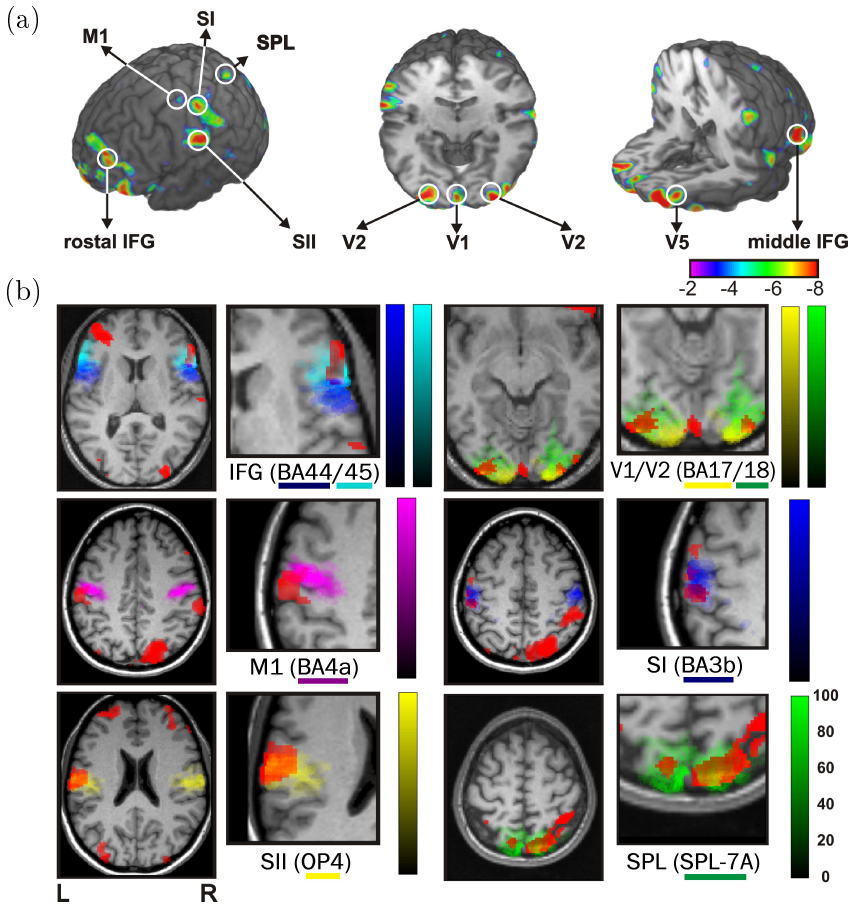

Figure 3.19: Source localization results. (a) Group-level data showing significant decrease in source power for VM vs R. Units are pseudo-t values superimposed onto a 3D structural representation of a single subject brain normalized to the MNI space. The maximum of each ROI is marked and labeled. (b) Comparison of source localization results to cytoarchitectonic areas. Only areas with significance of $p < 0.05$ are shown (red). Significant voxels are over-plotted on a single subject MRI and the PCMs are displayed for BA44/45, BA17/18, BA4a, BA3b, OP4, and SPL7A. The different colored scales show the cytoarchitectonic probability for each map.

For each subject's ROI, the source activity time course was estimated from -30 to 30 s with respect to the stimulus onset using the individual's VM condition covariance matrices [143].

3.4.2 Virtual Sensors' Time Courses Analysis

The time-courses were bandpass filtered (2-45 Hz), downsampled to 293 Hz and normalized (zero-mean). Ten second stationary segments were then selected for each subject, trial and condition (R, V, M, VM).
Signals were stored in a $M \times N$ matrix $\mathbf{Y} = [y_m(n)]$, with $m = 1, \ldots, 13$ ROIs and $n = 1, \ldots, 2930$ samples. This matrix was described by a multivariate autoregressive (MVAR) model (Eq. 2.5). Coefficients were estimated, with fixed order $p = 8$, by standard vector least squares identification (Par. 2.4.4).
For sake of simplicity, in this pilot study we focused on alpha frequency band, which was demonstrated to be crucial for visuo-motor integration processes in the previous studies (Sec. 3.3). The spectral matrix $\mathbf{S}(f)$ was obtained as in Eq. 2.10. Multivariate spectral decomposition (Par. 2.4.7) was applied to find the partial spectrum related to the pole of the process pertaining to alpha frequency band. The area underlying this partial spectrum was then taken as a measure of the power within the band, $\bar{P}_\alpha$.
The off-diagonal elements of $\mathbf{S}(f)$ were used to measure the linear coupling between each pair of signals y_i and y_j through the squared coherence function in Eq. 2.4. The average alpha coherence was also computed.
The significance of the coupling between the considered series was assessed by setting a threshold level in the coherence function, using FT surrogates (Par. 2.4.5), at the 95th percentile of the coherence distribution for the 100 generated surrogate series. The average coherence in the alpha frequency band was then compared to the threshold averaged in the same band, and set to zero if lower than the average threshold.
For both power and coherence, the average value across the three trials was estimated for each subject and condition. Wilcoxon paired T-test were performed to assess the significance of the difference between rest and task conditions (V, M and VM) both for spectra and coherence. The significance level was set to $p < 0.05$.

Results

In Fig. 3.20 the grand average spectral densities and the statistical results are shown for three representative source activities (left V2, left IFG and left M1) during R, V, M, and VM conditions. The spectral analysis at the source level confirms what found for the EEG coregistered signals. In fact:

- during the execution of the pure visual task, the alpha power significantly decreased, with respect to rest, only in the visual area (left V2);
- during M, alpha power significantly decreased only in the left motor area (left M1);
- during the visuo-motor task VM, a significant decrease was found in all the considered regions (left V2, M1, and IFG).

Similar results were obtained for the other considered brain sources. In fact, all visual regions showed the same behavior of left V2, right motor cortex showed weaker but similar activation than left motor, while parietal and IFG sources had lower

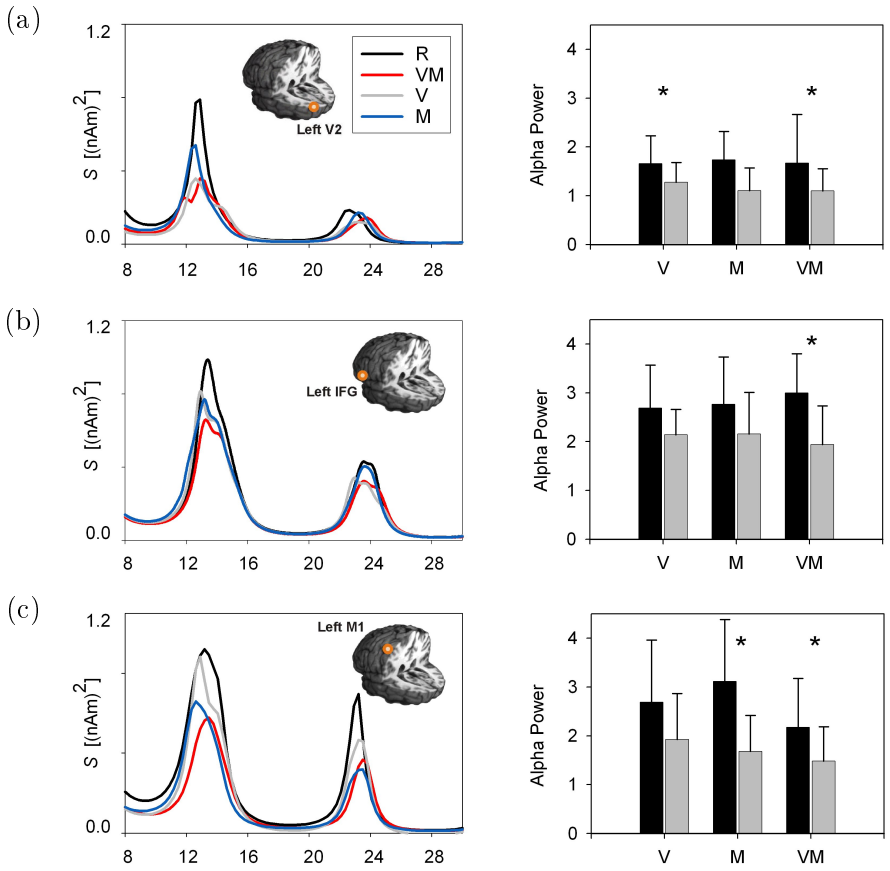

Figure 3.20: Alpha power group analysis in three representative sources: (a) left V2, (b) left IFG, and (c) left M1. (left) Grand average spectral density, (right) corresponding alpha power results (mean $\pm$ standard deviation) for the different conditions. $*$ significant ($p < 0.05$) vs R. In the histograms, black is adopted for rest condition R, while gray for the task conditions (V, M and VM).

alpha power with respect to rest only during the VM task. Finally, SI and SII were activated in every condition.

In Fig. 3.21 the grand average coherence functions and statistics are shown for two representative pairs of brain source activities (connections left IFG - left V2 and left M1 - left IFG) during R, V, M, and VM conditions. Significant increase of coherence, with respect to rest condition, on this connections was found only during the VM task, evidencing the crucial role of the left IFG area in visuo-motor integration.
Fig. 3.22 schematizes the results of coupling analysis in terms of task-related connectivity changes in the overall population of subjects for the alpha frequency band. During the pure visual task, a significant increase in alpha coherence was observed within the visual areas. In fact, the coupling values between left V5 and left V2, and between left V2 and right V1 significantly increased. A weak connectivity activation was found also between left V2 and the primary somatosensory area. Simultaneously, connections between right SPL7a and left M1 and between rigth V1 and right IFG

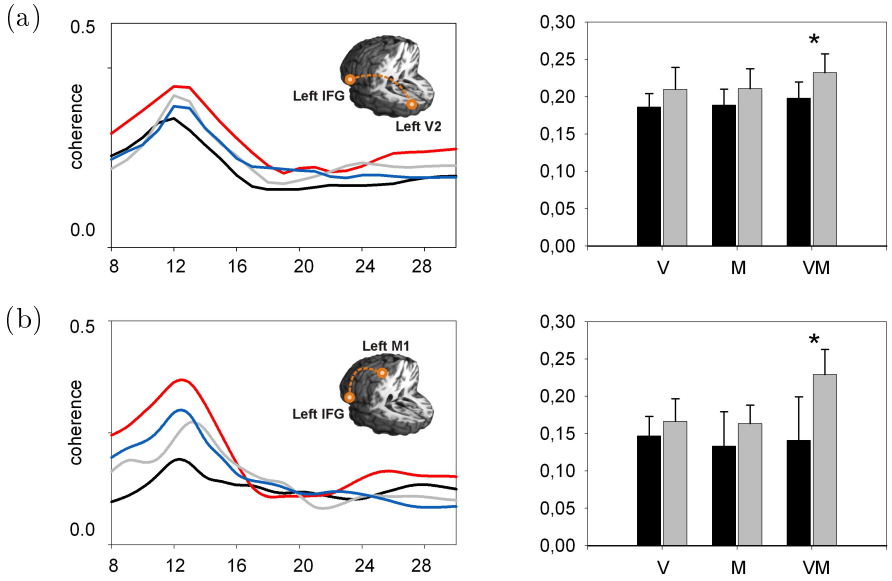

Figure 3.21: Alpha coherence group analysis for the connections (a) left V2 - left IFG and (b) left IFG - left M1. (left) Grand average coherence, (right) mean alpha coherence across subjects $\pm$ standard deviation for the different conditions (color coded as in Fig. 3.20). $*$ significant ($p < 0.05$) vs R.

were suppressed. The execution of a pure motor task induced increased connectivity on the connections left IFG-right SPL7a, left SII-right IFG and left M1-left SI. Strong significant task-related decreases of coupling were revealed in the posterior regions. For example, the connections between the visual sources and the left parietal area and between visual and left SII showed significantly decreased coherence. During VM task, a very different connectivity pattern was observed. Coherence increased in many connections. It is worth noticing the crucial role of the activated network involving the parietal and the IFG sources. In fact, the visual areas were strongly connected with parietal and IFG regions and these latter were then coupled with the left motor cortex. Moreover, both visual and motor areas showed an increased coherence with left SII.

3.4.3 Discussion

The aim of this pilot study, merging source imaging techniques with MVAR model-based coupling analysis, was to demonstrate the suitability of the methodological framework presented in chapter 2 for the connectivity analysis of MEG source activities. For simplicity, we focused on alpha frequency band and on a reduced paradigm, involving two control conditions (V and M) and the visuo-motor integration task (VM). Power and coherence analyses were performed in order to highlight the patterns of activation of the network involving the localized brain sources and to compare the results obtained at the source level with that obtained from the scalp EEG recordings (Sec. 3.3).

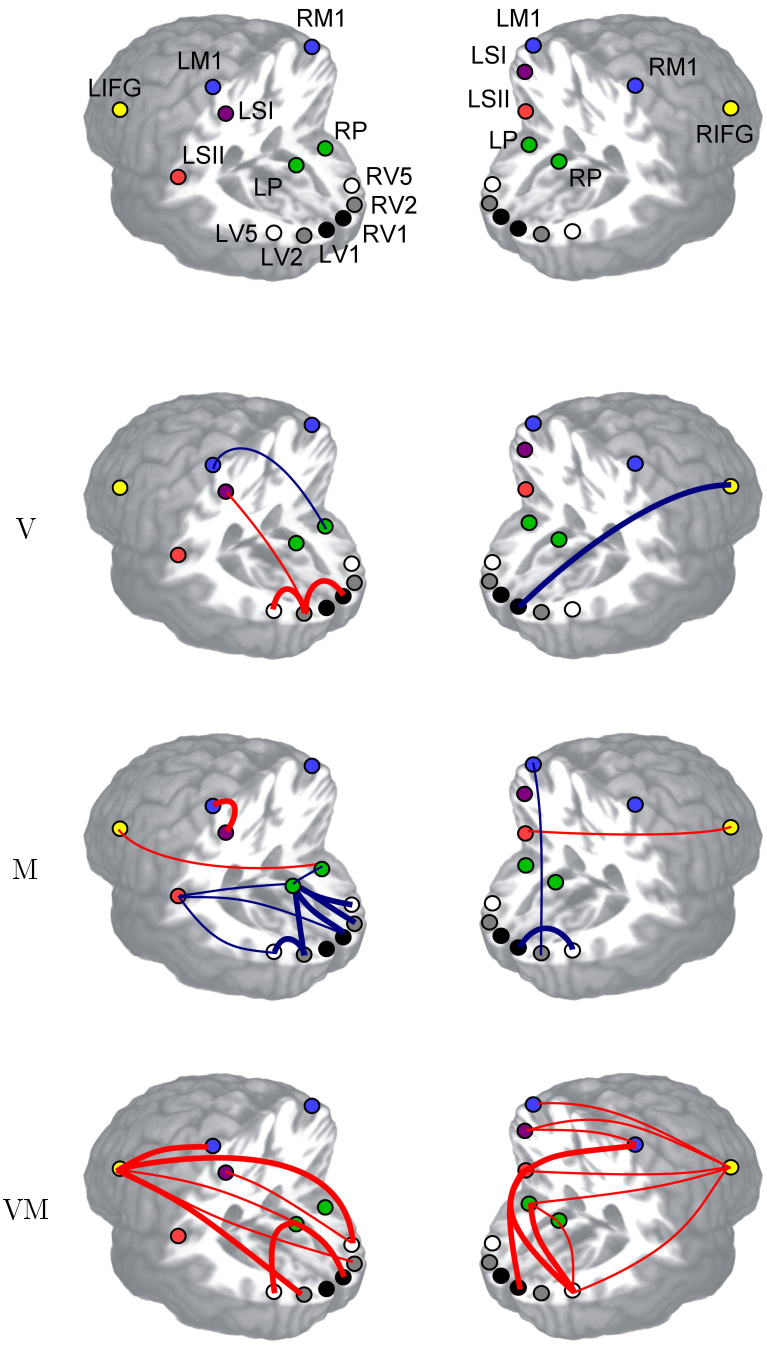

Figure 3.22: Task-induced coupling changes in α frequency band during a pure visual (V), a pure motor (M), and a combined visuo-motor task (VM), in the overall population of subjects. Lines indicate significant changes in coherence value from rest to task condition (blue: significant decrease; red: significant increase). Thin lines indicate differences between average task and rest values < 0.1 and tick lines differences > 0.1. To display the significant connections in a comprehensive way, the left and right sides of the brain are shown in the first and second column, respectively. In the fist row a figure legend is shown, indicating the considered ROIs. Adapted from [Papadelis et al., 2011a].

Active sources were localized in the early visual processing areas (V2 and V5), in the posterior parietal cortex, in the hand-related M1, in SI, in the parietal opercular region most likely representing SII, and in two distinct prefrontal regions, one more posterior in the caudal IFG, located between BA44 and BA45, and a separate one located around the most anterior portion of the inferior frontal sulcus (IFS). These brain regions composed a brain network that is similar to the one frequently reported during hand-object interaction tasks using low-temporal resolution whole-brain mapping techniques such as positron emission tomography (PET) or functional magnetic resonance imaging (fMRI) [146, 147] and confirmed also what found in [124, 125, 128, 129, 130].
The power decrease of the magnetic brain activity was examined in the alpha range. Our results are in accordance with previous studies using similar visuo-motor tasks, showing widespread power decrease in channels overlying occipital and central brain regions mainly in the alpha band [69] and associating alpha power decrease with cortical activation [139].
Coherence analysis confirmed what found in the EEG study in Sec. 3.3, concerning the role of the parietal regions in visuo-motor integration processes [138, 142]. In fact, also at the source level, a strong VM-related connectivity increase was shown between visual and parietal areas. The analysis of the source signals showed an additional, important functional link between the motor and visual cortex through the IFG. This coherent oscillatory activity was specific to the VM task and did not occur in the control tasks. Activation of IFG was expected, since it has already been reported in many neuroimaging studies, associated with object grasping and control precision-grip tasks [138, 147], mainly contra-lateral to the operating hand [148]. Even if the activation in the right IFG (ipsi-lateral to the operating hand) is not frequently reported in the literature, it is in agreement with recent fMRI studies, examining the cortical activity in controlling small isometric forces applied between the fingertips [147]. Interestingly, evidence for a similar functional connection has been found previously in an online visuo-motor task that bears several similarities with the present VM task, albeit the visual stimulus was biological (imitative task) rather than abstract as in the present experiment [149]. The authors found cortico-muscular coupling in the theta and gamma bands between the rostral IFG and the hand muscles involved in the task. In the present study we showed that such relation can be also detected in terms of coupling between the rostral IFG and M1.
As in the EEG study, the brain activities in motor or motor-related regions were bilateral. The occurrence of bilateral activation agrees well with previous findings showing that many motor regions are activated bilaterally during uni-manual motor tasks [150].
During V, a strong activation of the visual areas was reported, while coupling within and with other brain areas was suppressed or did not significantly change. During M, the network involving the motor and motor-related areas was active, while visual cortex networks were suppressed. This is in perfect agreement with what found in the EEG scalp analysis [Erla et al., 2011a, Erla et al., 2011b].
We conclude that, thanks to source imaging techniques a higher spatial resolution connectivity analysis can be performed. Our results at the scalp level and at the

source level are mainly in accordance, as both showed the suitability of the proposed methodological framework for brain connectivity analysis on real data, confirming various previous findings and allowing a robust neurophysiological analysis, in which also directionality of the interactions is considered.
We remark that coherence analysis is not able to distinguish between direct and indirect connectivity relations, and that this additional information can be provided by partial coherence analysis. Furthermore, no information about the directionality of the information flow is provided from this study. This aspect requires causality analysis, which can be evaluated by eMVAR model based frequency-domain causality measures (as shown in Ch. 2). As a future development, the extension of the pilot study presented here, will deal with all these aspects, aiming to provide a comprehensive analysis of coupling and causality for MEG sources, as already done for scalp EEG.

Chapter 4

Conclusions

Many everyday actions are the result of complex brain processes involving multimodal analysis of different sensory inputs and motor processes. To perform these tasks, different specialized brain regions activate and communicate with each other. Since the synchronization of neural firings plays a crucial role in determining connections between different brain regions, the study of brain connectivity requires recording techniques sensitive to coherently oscillating neuronal groups, such as EEG and MEG. Moreover, methods suitable to elicit connectivity information from these data are also needed. This task is complicated by a number of factors which include noise, non-stationarities, redundant information and confounding effects (e.g., volume conductor).

In this thesis we presented a set of mathematical tools, based on multivariate linear time series analysis, developed to quantify functional and effective connectivity from neurophysiological recordings like EEG and MEG. To provide reliable connectivity estimates, we considered many practical signal processing issues, such as the reduction of the amount of artifacts, the development of stationarity tests, and the selection of the optimal regions of interest and window-length to be analyzed. Moreover, we considered another crucial issue arising particularly when signals analysis is performed at the scalp level, i.e., the presence of interactions occurring within a time scale shorter than the sampling interval of the recorded EEG/MEG signals. These interactions, denoted as instantaneous effects, incorporate volume conductor effects, as well as any other interaction occurring at a higher temporal resolution than that of the sampled EEG/MEG signals. This aspect is disregarded by the traditional connectivity analysis approaches, even if it is likely to have a big impact on estimation of the connectivity network. We dealt with this issue proposing an extended multivariate autoregressive (eMVAR) model in which instantaneous effects are combined with the traditionally studied lagged effects. The usefulness of this representation was demonstrated both from a theoretical point of view and a practical point of view. In fact, we showed by simulated data that a model considering also instantaneous effects allows to correctly recognize known connectivity patterns, while, on the contrary, traditional approaches often yield spurious results. The need for introducing

the eMVAR model was confirmed by the application to real EEG/MEG data, as documented by the presence of residual correlations not described by the traditional MVAR model, indicating that zero-lag effects were far from negligible. In addition, utilization of the new approach in this application allowed us to detect and quantify the strength of important connections involved in the task-related transiently formed functional networks due to visuo-motor integration processes, which resulted not significant when the traditional approach was implemented. In particular, the functional path connecting visual and left motor cortices through the parietal regions was evidenced during the execution of tasks requiring visuo-motor integration. Moreover, the directionality of the information flow, mainly from back to front, was more fairly detected. These results confirmed some aspects evidenced in other more invasive studies, based for example on intra-cranical recordings or PET examinations.

Overall, we developed a robust methodological framework for the study of connectivity in brain processes. We demonstrated the efficacy of this new approach in the study of neurophysiological signals recorded during the execution of a visuo-motor task, both at the scalp level and at the spatially more accurate sources level. This suggests promising potentialities of eMVAR connectivity analysis for the study of many cognitive brain processes.

As a possible limitation, we remark that the connectivity measures proposed in this thesis were based on a linear model of the dynamics and dynamical interactions of the observed multivariate processes. Therefore, the proposed approach would not be able to detect and quantify nonlinear dynamics or couplings between different rhythms; when present, these complex interactions should be studied by means of nonlinear time series analysis approaches [22, 23, 20, 24, 151],[Faes et al., 2010b]. Nevertheless, we note that nonlinear approaches have been often shown to provide similar information than that yielded by linear methods in the analysis of neurophysiological signals [152, 153]; for instance, we have recently shown that the complexity of brain dynamics does not differ significantly when linear and nonlinear prediction methods are applied to EEG photic stimulation protocols [Erla et al., 2010, Erla et al., 2011]). In addition, the linear representation maintain the advantage of being strictly connected with the frequency-domain representation of multichannel data, so that brain activity and connectivity can be described specifically for each single rhythm (in this thesis we have shown different connectivity patterns for alpha and beta rhythms during visuo-motor integration). On the contrary, in quantifying higher order correlations within the data nonlinear techniques loose the ability to provide information about specific rhythms. Therefore, linear and nonlinear analyses may be considered as complementary approaches, and a future development would be to integrate the framework proposed here with tools for nonlinear connectivity analysis, to achieve a more comprehensive picture of brain interactions.

Summary

In order to accomplish even the most simple everyday action, different specialized brain regions activate and communicate with each other. Brain communication is hypothesized to be related to the synchronization of neural firings in different cerebral regions, and may therefore be detected and quantified exploiting recording techniques sensitive to coherently oscillating neuronal groups, like EEG and MEG. The concept of brain connectivity, which encompasses different aspects such as statistical dependencies (*functional connectivity*) and causal interactions (*effective connectivity*) between EEG/MEG signals recorded in spatially separated cortical locations, has become central for the investigation of the neurophysiological processes typically engaged in cognitive and perceptive processing. In the context of time series analysis, functional and effective connectivity can be investigated respectively in terms of coupling, i.e., the presence of interactions, and of causality, i.e., the presence of driver-response relationships, between two simultaneously collected neurophysiological time series. In the linear signal processing framework, connectivity is often formalized in the context of a multivariate autoregressive (MVAR) representation of the available time series, which allows to derive time- and frequency-domain pictures respectively by the model coefficients and by their spectral representation.
The present thesis aimed to introduce and validate an unified framework for frequency-domain evaluation of brain connectivity during visuo-motor integration processes, extending the traditional MVAR approach to improve the estimation of coupling and causality between signals recorded from the involved cortical regions.
In the first part of this work, we provided a common methodological framework for the computation of known frequency-domain connectivity measures based on linear time series analysis for the application to neurophysiological recordings. Within this framework, we discussed the theoretical interpretation of measures of coupling (coherence and partial coherence) and causality (directed coherence and partial directed coherence) in multivariate time series. We showed that:

- each measure has a different interpretation, reflecting the specific time-domain definitions of indirect+direct and direct coupling or causality (see 2.1);
- coherence and partial coherence are symmetric measures, from which we cannot infer the directionality of the information flow. However, they can be decomposed into factors eliciting directionality (i.e., directed coherence and partial

directed coherence);

- the squared modulus of the directed coherence measures the amount of power of the output signal which is received from the input signal, normalized to all incoming contributions. Differently, the partial directed coherence measures the fraction of inverse power of the input signal which is sent to the output signal, normalized to all outgoing contributions.

The picture emerging from these observations provides suggestions for the utilization of the various connectivity measures in the analysis of MV processes. First, measures of causality should be preferred to measures of coupling, as the information provided by the latter is not directional and, at least theoretically, is conveyed also by the former. Second, both DC and PDC should be considered as causality measures because they complement each other in terms of advantages and drawbacks: DC measures causality in meaningful physical terms as power contributions, but cannot separate direct effects from indirect ones; PDC determines the correct interaction structure in terms of direct causal effects, but its absolute values lack of straightforward interpretability, being related to the inverse spectral matrix elements.

In the second part of this work, we emphasized the necessity to extend the MVAR modeling approach, traditionally used to assess frequency-domain causality, whenever the time resolution of the recordings is lower than the time scale of the influences occurring in the observed multivariate process. In fact, in such a case, the interpretation of the lagged effects may change considerably if instantaneous effects are not included in the model. If, for example, the neurophysiological signals have a sampling frequency in the order of 100 Hz, influences faster than 10 ms (e.g., volume conductor effects) cannot be modeled by traditional MVAR analysis and this can induce worse or spurious connectivity results about the lagged effects. We showed that the traditional directed coherence and partial directed coherence (DC and gPDC) computed from the strictly causal model may lead to misleading connectivity patterns when instantaneous correlations are not trivial. On the contrary, the correct interpretation is obtained re-defining the same functions starting from the coefficients of the extended model (iDC and iPDC). Moreover, we introduced novel frequency-domain measures of causality and direct causality (eDC and ePDC), combining both lagged and instantaneous causality from one signal to another.

In the third part of this work, we discussed the most important steps to be considered for the application of MVAR and eMVAR model based analysis and we proposed improvements for some specific adopted algorithms. We treated methods for the preprocessing and for the assessment of the stationarity of the recorded neurophysiological time series. Moreover, the available identification algorithms for the estimation of the model coefficients were discussed and new robust approaches were proposed both for strictly causal model and for extended model coefficients estimation. Model validation techniques were also investigated. Finally, new methods for the assessment of the statistical significance of the various frequency-domain causality measures were discussed (globally denoted as CFT surrogate data based approaches), in addition to the most common FT surrogate based approaches for

coupling significance estimation.

This methodological framework was first validated on simulated data, and then applied to real EEG and MEG recordings. Validation allowed to test the proposed approaches and to discuss possible advantages and limitations. The subsequent application was devoted to investigate a visuo-motor force-tracking experimental paradigm, which evoked visual perception, motor action, and visuo-motor performance, attempting to reproduce mechanisms involved into basic everyday actions like grasping. EEG data were analyzed at the scalp level. After ROIs selection, activation analysis was performed by parametric multivariate spectral analysis combined with a supplementary procedure for power spectral decomposition. Connectivity analysis was divided into two steps. First, we estimated all the presented coupling and causality measures (COH, PC, DC, gPDC, iDC, iPDC, eDC and ePDC) from the data recorded during rest and during the execution of the visuo-motor task, to test the proposed methods and discuss possible advantages and limitations. We showed that:

- both direct+indirect and direct estimates have to be considered for a full comprehension of the involved connectivity patterns, since they contain information on the strength and the on the direct/non-direct nature of the interactions, respectively;

- modeling the data with an approach that considers instantaneous effects may lead to the detection of important connections, which are not detected using the strictly causal measures. Moreover, it allows a better comprehension of the causal relations between different cortical areas, distinguishing between instantaneous and lagged effects;

- the choice of eMVAR modeling in place of MVAR modeling is additionally justified by the results of the validation tests applied on this dataset, being the assumption of the latter not satisfied (the presence of non negligible zero-lag interactions among the considered EEG signals was documented by the fact that the strictly causal residuals were non-independent).

eMVAR model based analysis was then applied to the global paradigm, involving rest and visuo-motor conditions, plus three control conditions (i.e., pure visual, pure motor and visuo-motor without visual feedback) to further elucidate the neuronal mechanisms underlying visuo-motor integration. We evidenced that:

- the alpha frequency band plays an important role in enforcing the specific functional network surrounding the cortical areas involved in pure tasks execution;

- in the alpha band, there is a tendency towards an enhanced driving role of the visual cortex on the motor cortex during tasks simultaneously involving both areas, according to mechanisms consistent with a visuo-motor integration process;

- the activation of the left side network of the brain (contra-lateral to the motor task) is stronger, suggesting a different behavior in the alpha band of the two hemispheres due to the lateralization of the motor task;
- the connectivity network between visual and motor cortices in the alpha band is enforced in presence of the visual feedback, because of the involvement of the parietal area connecting the occipital and central regions;
- in the beta frequency band, task-related connectivity changes are strongly connected to the presence of the visual feedback;
- connectivity changes in the beta frequency band are bilateral.

These results partly replicated previous findings on visuo-motor integration processes. In addition, they provided novel quantitative information in the still open issue about the role potentially played by the different frequency bands, and extended previous findings by introducing directionality information (causality), thus complementing the more traditional coupling analysis.
Despite the demonstrated suitability of the proposed eMVAR approach for EEG connectivity analysis, some of the issues related to the difficulty of dealing with scalp signals still remain. In fact, we came up with problems in the identification of the extended model at increasing the number of channels involved in the analysis (i.e., the validation tests were not fulfilled), which we ascribed to the presence of redundant information. This issue poses some constraints on the spatial accuracy of the resulting connectivity estimates. A promising solution to these issues seems to be the application of source imaging techniques. Therefore, we performed a pilot study, merging source imaging techniques with MVAR model-based coupling analysis. Alpha power results confirmed what found for EEG signals, i.e., power decrease in the involved areas associated with activation. A strong visuo-motor related connectivity increase was shown between visual and parietal areas also at the source level, confirming EEG results. In addition, the adoption of source localization evidenced the functional link between the motor and visual cortex through the inferior frontal gyrus area, reported in many neuroimaging studies and associated with object grasping and control precision-grip tasks.

Overall, we developed a robust methodological framework for the study of connectivity in brain processes. We demonstrated the efficacy of this new approach in the study of neurophysiological signals recorded during the execution of a visuo-motor task, both at the scalp level and at the spatially more accurate sources level. This suggests promising potentialities of eMVAR connectivity analysis for the study of many cognitive brain processes.

Own References

[Erla et al., 2009] Erla, S., Faes, L. & Nollo, G. (2009). Proceedings of the 4th International IEEE EMBS Conference on Neural Engineering 1, 734–737.

[Erla et al., 2010] Erla, S., Faes, L. & Nollo, G. (2010). Methods of Information in Medicine 49, 496–500.

[Erla et al., 2011a] Erla, S., Faes, L., Nollo, G., Arfeller, C., Braun, C. & Papadelis, C. (2011a). Biomedical Signal Processing and Control in press, 2011.

[Erla et al., 2011b] Erla, S., Faes, L., Nollo, G., Arfeller, C., Braun, C. & Papadelis, C. (2011b). Improving evaluation of functional causality network during visuomotor taks by MVAR model with istantaneous interaction. In preparation.

[Erla et al., 2009] Erla, S., Faes, L., Tranquillini, E., Orrico, D. & Nollo, G. (2009). International Journal of Bioelectromagnetism 11, 74–79.

[Erla et al., 2011] Erla, S., Faes, L., Tranquillini, E., Orrico, D. & Nollo, G. (2011). Medical Engineering & Physics 33, 504–512.

[Erla et al., 2010] Erla, S., Papadelis, C., Faes, L., Braun, C. & Nollo, G. (2010). IFMBE Proceedings: XII Mediterranean Conference on Medical and Biological Engineering and Computing 29, 73–76.

[Faes et al., 2011a] Faes, L., Erla, S. & Nollo, G. (2011a). A framework for assessing frequency domain causality in multivariate linear processes with instantaneous interactions. In preparation.

[Faes et al., 2011b] Faes, L., Erla, S. & Nollo, G. (2011b). Measuring connectivity in linear multivariate processes: Definitions and interpretation. Submitted to Computational and Mathematical Methods in Medicine (Special Issue: Methodological Advances in Brain Connectivity).

[Faes et al., 2010a] Faes, L., Erla, S., Tranquillini, E., Orrico, D. & Nollo, G. (2010a). Proceedings of the 32nd Annual International Conference of the IEEE EMBS 1, 1699–1702.

[Faes et al., 2010b] Faes, L., Nollo, G., Erla, S., Papadelis, C., Braun, C. & Porta, A. (2010b). Proceedings of the 32nd Annual International Conference of the IEEE EMBS 1, 102–105.

[Papadelis et al., 2011a] Papadelis, C., Arfeller, C., Erla, S., Nollo, G. & Braun, C. (2011a). Inferior frontal gyrus functionally couples visual and motor cortex in sensorimotor control. Submitted to Plos.

[Papadelis et al., 2011b] Papadelis, C., Arfeller, C., Erla, S., Nollo, G., Cattaneo, L. & Braun, C. (2011b). In Conference Abstract: HBM Conference.

References

[1] K. J. Friston, "Functional and effective connectivity in neuroimaging: A synthesis," *Hum. Brain Mapp.*, vol. 2, no. 1-2, pp. 56–78, 1994.

[2] L. Lee, L. M. Harrison, and A. Mechelli, "A report of the functional connectivity workshop, Düsseldorf 2002," *NeuroImage*, vol. 19, pp. 457–465, June 2003.

[3] J. Driver and T. Noesselt, "Multisensory interplay reveals crossmodal influences on "sensory-specific" brain regions, neural responses, and judgments," *Neuron*, vol. 57, pp. 11–23, January 2008.

[4] C. Buechel and K. Friston, "Modulation of connectivity in visual pathways by attention: cortical interactions evaluated with structural equation modelling and fMRI," *Cereb Cortex*, vol. 7, pp. 768–778, Dec. 1997.

[5] A. Urbano, C. Babiloni, P. Onorati, and F. Babiloni, "Dynamic functional coupling of high resolution EEG potentials related to unilateral internally triggered one-digit movements," *Electroencephalography and Clinical Neurophysiology*, vol. 106, no. 6, pp. 477–487, 1998.

[6] A. Gevins, B. Cutillo, S. Bressler, N. Morgan, R. White, J. Illes, and D. Greer, "Event-related covariances during a bimanual visuomotor task. II. Preparation and feedback," *Electroencephalogr Clin Neurophysiol*, vol. 74, no. 2, pp. 147–160, 1989.

[7] M. Taniguchi, A. Kato, N. Fujita, M. Hirata, H. Tanaka, T. Kihara, H. Ninomiya, N. Hirabuki, H. Nakamura, S. E. Robinson, D. Cheyne, and T. Yoshimine, "Movement-related desynchronization of the cerebral cortex studied with spatially filtered magnetoencephalography," *NeuroImage*, vol. 12, no. 3, pp. 298–306, 2000.

[8] A. Brovelli, M. Ding, A. Ledberg, Y. Chen, R. Nakamura, and S. L. Bressler, "Beta oscillations in a large-scale sensorimotor cortical network: Directional influences revealed by Granger causality," *PNAS*, vol. 101, pp. 9849–9854, June 2004.

[9] A. A. Fingelkurts, A. A. Fingelkurts, and S. Kähkönen, "Functional connectivity in the brain - is it an elusive concept?," *Neuroscience and Biobehavioral Reviews*, vol. 28, no. 8, pp. 827–836, 2005.

[10] A. van Ooyen, "Competition in the development of nerve connections: a review of models. source," *Network*, vol. 12, pp. R1–R47, Feb 2001.

[11] K. J. Friston, C. D. Frith, P. F. Liddle, and R. S. J. Frackowiak, "Functional connectivity: The Principal-Component Analysis of large (PET) data sets," *J Cereb Blood Flow Metab*, vol. 13, pp. 5–14, 1993.

[12] K. J. Friston, C. D. Frith, and R. S. J. Frackowiak, "Time-dependent changes in effective connectivity measured with PET," *Human Brain Mapping*, vol. 1, no. 1, pp. 69–79, 1993.

[13] B. Horwitz, "The elusive concept of brain connectivity," *Neuroimage*, vol. 19, pp. 466–470, 2003.

[14] W. Singer, "Neuronal synchrony: A versatile code for the definition of relations?," *Neuron*, vol. 24, pp. 49–65, 1999.

[15] D. Senkowski, T. R. Schneider, J. J. Foxe, and A. K. Engel, "Crossmodal binding through neural coherence: implications for multisensory processing," *Trends in Neurosciences*, vol. 31, no. 8, pp. 401–409, 2008.

[16] G. Buzsáki and A. Draguhn, "Neuronal oscillations in cortical networks," *Science*, vol. 304, pp. 1926–1929, Jun 2004.

[17] P. Fries, "A mechanism for cognitive dynamics: neuronal communication through neuronal coherence," *Trends in Cognitive Sciences*, vol. 9, no. 10, pp. 474–480, 2005.

[18] P. L. Nunez and R. Srinivasan, *Electric Fields of the Brain, the Neurophysics of EEG*, pp. 1–166. Oxford University Press, second ed., 2006.

[19] A. Galka, *Topics in Nonlinear Time Series Analysis with Implications for EEG Analysis*. World Scientific, Singapore, 2000.

[20] E. Pereda, R. Q. Quiroga, and J. Bhattacharya, "Nonlinear multivariate analysis of neurophysiological signals," *Prog Neurobiol*, vol. 77, no. 1-2, pp. 1–37, 2005.

[21] C. J. Stam, "Nonlinear dynamical analysis of EEG and MEG: review of an emerging field," *Clin Neurophysiol*, vol. 116, pp. 2266–2301, Oct 2005.

[22] S. Kay, *Modern Spectral Estimation: Theory and Applications*. Prentice Hall, Englewood Cliffs, New Jersey, 1988.

[23] B. Gourévitch, R. Bouquin-Jeannès, and G. Faucon, "Linear and nonlinear causality between signals: methods, examples and neurophysiological applications," *Biological Cybernetics*, vol. 95, pp. 349–369, 2006.

[24] L. Faes, G. Nollo, and K. Chon, "Assessment of granger causality by nonlinear model identification: application to short–term cardiovascular variability," *Annals of Biomedical Engineering*, vol. 36, no. 3, pp. 381–395, 2008.

[25] A. Schloegl, "A comparison of multivariate autoregressive estimators," *Signal Processing*, vol. 86, pp. 2426–2429, 2006.

[26] L. Astolfi, F. Cincotti, D. Mattia, M. G. Marciani, L. A. Baccalá, F. de Vico Fallani, S. Salinari, M. Ursino, M. Zavaglia, L. Ding, J. C. Edgar, G. A. Miller, B. He, and F. Babiloni, "Comparison of different cortical connectivity estimators for high-resolution EEG recordings," *Human Brain Mapping*, vol. 28, pp. 143–157, 2007.

[27] E. Visani, G. Varotto, S. Binelli, L. Fratello, S. Franceschetti, G. Avanzini, and F. Panzica, "Photosensitive epilepsy: Spectral and coherence analyses of EEG using 14 hz intermittent photic stimulation," *Clinical Neurophysiology*, vol. 121, pp. 318–324, 2010.

[28] Kaminski, *Multichannel Data Analysis in Biomedical Research*, vol. 1 of *Understanding Complex Systems*. Handbook of Brain Connectivity, 2007.

[29] J. Sato, D. Takahashi, S. Arcuri, K. Sameshima, P. Morettin, and L. Baccalá, "Frequency domain connectivity identification: An application of partial directed coherence in fMRI," *Human Brain Mapping*, vol. 30, no. 2, pp. 452–461, 2009.

[30] L. Astolfi, F. Cincotti, D. Mattia, F. D. V. Fallani, S. Salinari, M. Ursino, M. Zavaglia, M. Marciani, and F. Babiloni, "Estimation of the cortical connectivity patterns during the intention of limb movements," *IEEE Eng Med Biol Mag*, vol. 25, pp. 32–38, 2006.

[31] L. Faes and G. Nollo, "Assessing frequency domain causality in cardiovascular time series with instantaneous interactions," *Methods Inf Med.*, vol. 49, no. 5, pp. 453–457, 2010.

[32] M. G. Knyazeva and G. M. Innocenti, "EEG coherence studies in the normal brain and after early-onset cortical pathologies," *Brain Research Reviews*, vol. 36, pp. 119–128, 2001.

[33] M. Priestly, *Spectral analysis and time series*. Academic Press, London, 1981.

[34] J. S. Bendat and A. G. Piersol, *Random Data: Analysis and Measurement Procedures*. John Wiley & Sons, New York, 1986.

[35] D. Walter, "Coherence as a measure of relationship between EEG records," *Electroencephalogr Clin Neurophysiol*, vol. 24, no. 3, pp. 282–292, 1968.

[36] H. Petsche and S. Etlinger, *EEG and thinking. Power and coherence analysis of cognitive processes*. Verlag der Oesterreichischen Akademie der Wissenschaften, 1998.

[37] C. Babiloni, G. Frisoni, F. Vecchio, M. Pievani, C. Geroldi, C. D. Carli, R. Ferri, F. Vernieri, R. Lizio, and P. Rossini, "Global functional coupling of resting EEG rhythms is related to white-matter lesions along the cholinergic tracts in subjects with amnesic mild cognitive impairment," *J Alzheimers Dis*, vol. 19, no. 3, pp. 859–871, 2010.

[38] O. Kislova and M. Rusalova, "EEG coherence in humans: relationship with success in recognizing emotions in the voice," *Neuroscience and Behavioral Physiology*, vol. 39, pp. 545–552, 2009.

[39] J. A. Frederick, D. L. Timmermann, H. L. Russel, and J. F. Lubar, "EEG coherence effects of audio-visual stimulation (AVS) at dominant and twice dominant alpha frequency," *Journal of Neurotherapy*, vol. 8, no. 4, pp. 25–42, 2004.

[40] R. B. Govindan, J. Raethjen, K. Arning, F. Kopper, and G. Deuschl, "Time delay and partial coherence analyses to identify cortical connectivities," *Biological Cybernetics*, vol. 94, pp. 262–275, 2006.

[41] F. Andres and C. Gerloff, "Coherence of sequential movements and motor learning," *J Clin Neurophysiol*, vol. 16, no. 6, pp. 520–527, 1999.

[42] J.-M. Schoffelen, R. Oostenveld, and P. Fries, "Imaging the human motor system's beta-band synchronization during isometric contraction," *NeuroImage*, vol. 41, no. 2, pp. 437–447, 2008.

[43] P. L. Nunez, R. Srinivasan, A. F. Westdorp, R. S. Wijesinghe, D. M. Tucker, R. B. Silberstein, and P. J. Cadusch, "EEG coherency I: statistics, reference electrode, volume conduction, laplacians, cortical imaging, and interpretation at multiple scales," *Electroencephhalography and Clinical Neurophysiology*, vol. 103, pp. 499–515, 1997.

[44] P. L. Nunez, R. B. Silberstein, Z. Shi, M. R. Carpenter, R. Srinivasan, D. M. Tucker, S. M. Doran, P. J. Cadusch, and R. S. Wijesinghe, "EEG coherency II: experimental comparisons of multiple measures," *Clinical Neurophysiology*, vol. 110, pp. 469–486, 1999.

[45] C. W. J. Granger, "Investigating causal relations by econometric models and cross–spectral methods," *Econometrica*, vol. 37, no. 3, pp. 424–438, 1969.

[46] M. Ding, Y. Chen, and S. L. Bressler, *Granger causality: Basic theory and application to neuroscience*, ch. 17, pp. 437–460. Handbook of Time Series Analysis, Wiley-VCH Verlag, 2006.

[47] C. W. J. Granger, "Testing for causality: a personal viewpoint," *J Econ Dynamics Control*, vol. 2, pp. 329–352, 1980.

[48] Y. Chen, S. L. Bressler, and M. Ding, "Frequency decomposition of conditional granger causality and application to multivariate neural field potential data," *Journal of Neuroscience Methods*, vol. 150, pp. 228–237, 2006.

[49] L. Faes and G. Nollo, *Multivariate Frequency Domain Analysis of Causal Interactions in Physiological Time Series*, ch. 21, pp. 403–428. Biomedical Engineering Trends in Electronics, Communications and Software, A.N. Laskovski, 2011.

[50] S. L. Marple, *Digital spectral analysis: with applications.* Prentice-Hall Signal Processing Series, Upper Saddle River, NJ, USA: Simon and Schuster, New Jersey, 1987.

[51] P. J. Franaszczuk and K. J. Blinowska, "Linear model of brain electrical activity-EEG as a superposition of damped oscillatory modes," *Biological Cybernetics*, vol. 53, pp. 19–25, 1985.

[52] L. A. Baccalá and K. Sameshima, "Partial directed coherence: a new concept in neural structure determination," *Biol Cybern*, vol. 84, pp. 463–474, 2001.

[53] L. A. Baccalá, K. Sameshima, G. Ballester, A. C. D. Valle, and C. Timo-Iaria, "Studying the interaction between brain structures via directed coherence and Granger causality," *Applied Signal Processing*, vol. 5, no. 1, pp. 40–48, 1988.

[54] M. Eichler, "On the evaluation of information flow in multivariate systems by the directed transfer function," *Biol Cybern*, vol. 94, pp. 469–482, 2006.

[55] M. Kaminski and K. Blinowska, "A new method of the description of the information-flow in the brain structures," *Biological Cybernetics*, vol. 65, no. 3, pp. 203–210., 1991.

[56] M. Kaminski, K. J. Blinowska, and W. Szelenberger, "Topographic analysis of coherence and propagation of EEG activity during sleep and wakefulness," *Electroencephalography and clinical Neurophysiology*, vol. 102, pp. 216–227, 1997.

[57] L. A. Baccalá and K. Sameshima, "Generalized partial directed coherence," in *15th IEEE International Conference on Digital Signal Processing*, pp. 163–166, 2007.

[58] L. Astolfi, F. Cincotti, D. Mattia, M. Marciani, L. A. Baccalá, F. de Vico Fallani, S. Salinari, M. Ursino, and M. Z. F. Babiloni, "Assessing cortical functional connectivity by partial directed coherence: Simulations and application to real data," *IEEE Transactions Biomed Eng*, vol. 53, no. 9, pp. 1802–1812, 2006.

[59] A. Hyvarinen, S. Shimizu, and P. Hoyer, "Causal modelling combining instantaneous and lagged effects: an identifiable model based on non–gaussianity," *Proceedings of the 25th International Conference on Machine Learning, Helsinki*, vol. 1, pp. 1–8, 2008.

[60] H. Lutkepohl, *Introduction to multiple time series analysis.* Springer, Berlin Heidelberg New York, 1993.

[61] L. Faes and G. Nollo, "Extended causal modeling to assess partial directed coherence in multiple time series with significant instantaneous interactions," *Biological Cybernetics*, vol. 103, pp. 387–400, 2010.

[62] T. P. Jung, S. Makeig, C. Humphries, T. W. Lee, M. J. McKeown, V. Iragui, and T. J. Sejnowski, "Removing electroencephalographic artifacts by blind source separation," *Psychophysiology*, vol. 37, pp. 163–178, 2000.

[63] G. Gratton, M. Coles, and E. Donchin, "A new method for off–line removal of ocular artifact," *Electroencephalography and Clinical Neurophysiology*, vol. 55, pp. 468–484, 1983.

[64] J. Woestenburg, M. Verbaten, and J. Slangen, "The removal of the eye–movement artifact from the eeg by regression analysis in the frequency domain," *Biological Psychology*, vol. 16, pp. 127–147, 1983.

[65] O. G. Lins, T. W. Picton, P. Berg, and M. Scherg, "Ocular artifacts in recording EEGs and event-related potentials ii: Source dipoles and source components," *Brain Topography*, vol. 6, pp. 65–78, 1993.

[66] S. Romero, M. A. Mañanas, and M. J. Barbanoj, "A comparative study of automatic techniques for ocular artifact reduction in spontaneous eeg signals based on clinical target variables: A simulation case," *Computers in Biology and Medicine*, vol. 38, no. 3, pp. 348–360, 2008.

[67] K. J. Blinowska, M. Kaminski, R. Kus, and J. Ginter, "Transmission of brain activity in cognitive and motor tasks," in *Engineering in Medicine and Biology Society, 2008. EMBS 2008. 30th Annual International Conference of the IEEE*, pp. 3508 –3511, aug. 2008.

[68] F. Hummel and C. Gerloff, "Larger interregional synchrony is associated with greater behavioral success in a complex sensory integration task in humans," *Cerebral Cortex*, vol. 15, no. 5, pp. 670–678, May 2005.

[69] J. Classen, C. Gerloff, M. Honda, and M. Hallett, "Integrative visuomotor behavior is associated with interregionally coherent oscillations in the human brain," *J Neurophysiol*, vol. 79, pp. 1567–1573, 1998.

[70] J. Pardey, S. Roberts, and L. Tarassenko, "A review of parametric modelling techniques for eeg analysis," *Medical Engineering & Physics*, vol. 18, no. 1, pp. 2–11, 1996.

[71] L. Astolfi, F. Cincotti, D.Mattia, M. Mattiocco, F. D. V. Fallani, A. Colosimo, M. G. Marciani, W. Hesse, L. Zemanova, G. Z. Lopez, J. Kurths, C. Zhou, and F. Babiloni, "Estimation of the time-varying cortical connectivity patterns by the adaptive multivariate estimators in high resolution eeg studies," *Proceedings of the 2006 IEEE Engineering in Medicine and Biology 28th Annual Conference*, vol. 1, pp. 2446–2449, 2006.

[72] D. Kaplan and L. Glass, *Understanding Nonlinear Dynamics*, ch. 6, pp. 279–358. Springer–Verlag New York, 1995.

[73] A. Porta, G. D'Addio, S. Guzzetti, D. Lucini, and M. Pagani, "Testing the presence of non stationarities in short heart rate variability series," *Computers in Cardiology*, vol. 31, no. 1, pp. 645–648, 2004.

[74] S. Lopes da Silva, "Neural mechanisms underlying brain waves: from neural membranes to networks," *Electroencephalography and Clinical Neurophysiology*, vol. 79, no. 2, p. 81, 1991.

[75] R. S. Fisher, W. v. E. Boas, W. Blume, C. Elger, P. Genton, P. Lee, and J. Engel, "Epileptic seizures and epilepsy: Definitions proposed by the international league against epilepsy (ILAE) and the international bureau for epilepsy (IBE)," *Epilepsia*, vol. 46, no. 4, pp. 470–472, 2005.

[76] G. Chow, "Tests of equality between sets of coefficients in two linear regressions," *Econometrica*, vol. 28, no. 3, pp. 591–605, 1960.

[77] R. Quandt, "Tests of the hypothesis that a linear regression system obeys two separate regimes," *Journal of the American Statistical Association*, vol. 55, no. 290, pp. 324–330, 1960.

[78] H. Akaike, "A new look at the statistical model identification," *IEEE Transactions on Automatic Control*, vol. 19, pp. 716–723, December 1974.

[79] J. Hamilton, *Time series analysis.* Princeton University Press, NJ., 1994.

[80] L. Astolfi, F. Cincotti, D. Mattia, C. Babiloni, F. Carducci, A. Basilisco, P. Rossini, S. Salinari, L. Ding, Y. Ni, B. He, and F. Babiloni, "Assessing cortical functional connectivity by linear inverse estimation and directed transfer function: simulations and application to real data," *Clinical Neurophysiology*, vol. 116, no. 4, pp. 920–932, 2005.

[81] K. J. Blinowska, R. Kus, and M. Kaminski, "Granger causality and information flow in multivariate processes," *Phys. Rev. E*, vol. 70, pp. 0509021–0509024, 2004.

[82] H. Wang, S. Lu, K. Ju, and K. H. Chon, "A new approach to closed–loop linear system identification via a vector autoregressive model," *Annals of Biomedical Engineering*, vol. 30, pp. 1204–1214, 2002.

[83] S. Shimizu, P. O. Hoyer, A. Hyvärinen, and A. J. Kerminen, "A linear non–gaussian acyclic model for causal discovery," *Journal of Machine Learning Research*, vol. 7, pp. 2003–2030, 2006.

[84] G. E. P. Box and G. M. Jenkins, *Time series analysis: forecasting and control.* Holden-Day, San Francisco, 1970.

[85] G. M. Ljung and G. E. P. Box, "On a measure of lack of fit in time series models," *Biometrika*, vol. 65, no. 2, pp. 297–303, 1978.

[86] B. Schelter, M. Winterhalder, M. Eichler, M. Peifer, B. Hellwig, B. Guschlbauer, C. H. Lücking, R. Dahlhaus, and J. Timmer, "Testing for directed influences among neural signals using partial directed coherence," *Journal of Neuroscience Methods*, vol. 152, no. 1-2, pp. 210–219, 2006.

[87] R. Davidson and J. MacKinnon, *Econometric Theory and Methods*. Oxford University Press, New York, 2004.

[88] M. Kaminski, M. Ding, W. A. Truccolo, and S. L. Bressler, "Evaluating causal relations in neural systems: Granger causality, directed transfer function and statistical assessment of significance," *Biol Cybern*, vol. 85, pp. 145–157, August 2001.

[89] E. Florin, J. Gross, J. Pfeifer, G. R. Fink, and L. Timmermann, "Reliability of multivariate causality measures for neural data," *Journal of Neuroscience Methods*, vol. 198, no. 2, pp. 344–358, 2011.

[90] J. Theiler, S. Eubank, A. Longtin, B. Galdrikian, and J. D. Farmer, "Testing for nonlinearity in time series: the method of surrogate data," *Physica D*, vol. 58, pp. 77–94, 1992.

[91] T. Schreiber and A. Schmitz, "Surrogate time series," *Physica D*, vol. 142, pp. 346–382, 2000.

[92] L. Faes, G. Pinna, A. Porta, R. Maestri, and G. Nollo, "Surrogate data analysis for assessing the significance of the coherence function," *IEEE Transactions Biomed Eng*, vol. 51, no. 7, pp. 1156–1166, 2004.

[93] L. Faes, A. Porta, and G. Nollo, "Testing frequency-domain causality in multivariate time series," *Biomedical Engineering, IEEE Transactions on*, vol. 57, pp. 1897–1906, aug. 2010.

[94] G. M. Jenkins and D. G. Watts, *Spectral Analysis and Its Applications*. San Francisco, CA, 1968.

[95] D. Liberati, M. Cursi, T. Locateili, G. Comi, and S. Cerutti, "Total and partial coherence analysis of spontaneous and evoked EEG by means of multi-variable autoregressive processing," *Med. & Biol. Eng. & Comput.*, vol. 35, pp. 124–130, 1997.

[96] T. Mima, T. Matsuoka, and M. Hallett, "Functional coupling of human right and left cortical motor areas demonstrated with partial coherence analysis," *Neuroscience Letters*, vol. 287, no. 2, pp. 93–96, 2000.

[97] E. Niedermeyer and F. L. da Silva, *Electroencephalography: Basic Principles, Clinical Applications, and Related Fields*. Lippincott Williams and Wilkins, 5th ed., Nov. 2004.

[98] F. Babiloni, C. Babiloni, F. Carducci, L. Fattorini, P. Onorati, and A. Urbano, "Spline Laplacian estimate of EEG potentials over a realistic magnetic

resonance-constructed scalp surface model," *Electroencephalography and clinical Neurophysiology*, vol. 98, pp. 363–373, 1996.

[99] A. Gevins, J. Le, P. Brickett, B. Reutter, and J. Desmond, "Seeing through the skull: advanced EEGs use MRIs to accurately measure cortical activity from the scalp," *Brain Topogr*, vol. 4, no. 2, pp. 125–131, 1991.

[100] B. He, J. Lian, and G. Li, "High-resolution EEG a new realistic geometry spline Laplacian estimation technique," *Clin Neurophysiol*, vol. 112, pp. 845–852, 2001.

[101] C. M. Michel, M. M. Murray, G. Lantz, S. Gonzalez, L. Spinelli, and R. G. de Peralta, "EEG source imaging," *Clinical Neurophysiology*, vol. 115, pp. 2195–2222, 2004.

[102] S. Baillet, J. Mosher, and R. Leahy, "Electromagnetic brain mapping," *Signal Processing Magazine, IEEE*, vol. 18, pp. 14–30, nov 2001.

[103] C. Papadelis, V. Poghosyan, P. B. Fenwick, and A. A. Ioannides, "MEG's ability to localise accurately weak transient neural sources," *Clinical Neurophysiology*, vol. 120, no. 11, pp. 1958–1970, 2009.

[104] A. Isaksson, A. Wennberg, and L. H. Zetterberg, "Computer analysis of EEG signals with parametric models," *Proceedings of The IEEE*, vol. 69, pp. 451–461, 1981.

[105] K. J. Blinowska, L. T. Czerwosz, W. Drabik, P. J. Franaszczuk, and H. Ekiert, "EEG data reduction by means of autoregressive representation and discriminant analysis procedures," *Electroencephalography and Clinical Neurophysiology*, vol. 51, no. 6, pp. 650–658, 1981.

[106] R. Kus, M. Kaminski, and K. J. Blinowska, "Determination of EEG activity propagation: Pair-wise versus multichannel estimate," *IEEE Transactions Biomed Eng*, vol. 51, pp. 1501–1510, September 2004.

[107] X. Wang, Y. Chen, S. L. Bressler, and M. Ding, "Granger causality between multiple interdependent neurobiological time series: Blockwise versus pairwise methods," *Int. J. Neural Syst.*, vol. 17, pp. 71–78, 2007.

[108] S. J. Johnsen and N. Andersen, "On power estimation in maximum eentropy spectral analysis," *Geophysics*, vol. 43, no. 4, pp. 681–690, 1978.

[109] G. Baselli, A. Porta, O. Rimoldi, M. Pagani, and S. Cerutti, "Spectral decomposition in multichannel recordings based on multivariate parametric identification," *IEEE Transactions Biomed Eng*, vol. 44, no. 11, pp. 1092–1101, 1997.

[110] C. Braun, M. Staudt, C. Schmitt, H. Preissl, N. Birbaumer, and C. Gerloff, "Crossed cortico-spinal motor control after capsular stroke," *European Journal of Neuroscience*, vol. 25, pp. 2935–2945, 2007.

[111] C. Gerloff, C. Braun, M. Staudt, Y. L. Hegner, J. Dichgans, and I. Krägeloh-Mann, "Coherent corticomuscular oscillations originate from primary motor cortex: Evidence from patients with early brain lesions," *Human Brain Mapping*, vol. 27, no. 10, pp. 789–798, 2006.

[112] A. Battaglia-Mayer and R. Caminiti, "Optic ataxia as a result of the breakdown of the global tuning fields of parietal neurones," *Brain*, vol. 125, no. 2, pp. 225–237, 2002.

[113] A. Schnitzler and J. Gross, "Normal and pathological oscillatory communication in the brain," *Nature Reviews Neuroscience*, vol. 6, pp. 285–296, 2005.

[114] A. K. Engel, P. König, A. K. Kreiter, T. B. Schillen, and W. Singer, "Temporal coding in the visual cortex: new vistas on integration in the nervous system," *Trends in Neurosciences*, vol. 15, no. 6, pp. 218–226, 1992.

[115] W. Singer and C. Gray, "Visual feature integration and the temporal correlation hypothesis," *Annu Rev Neurosci*, vol. 18, pp. 555–586, 1995.

[116] A. K. Engel and W. Singer, "Temporal binding and the neural correlates of sensory awareness," *Trends in Cognitive Sciences*, vol. 5, no. 1, pp. 16–25, 2001.

[117] A. Engel, P. Fries, and W. Singer, "Dynamic predictions: oscillations and synchrony in top-down processing," *Nat Rev Neurosci.*, vol. 2, no. 10, pp. 704–716, 2001.

[118] P. Belardinelli, L. Ciancetta, V. Pizzella, C. D. Gratta, and G. Romani, "Localizing complex neural circuits with MEG data," *Cogn Process*, vol. 7, pp. 53–59, 2006.

[119] A. Von Stein and J. Sarnthein, "Different frequencies for different scales of cortical integration: from local gamma to long range alpha/theta synchronization," *International Journal of Psychophysiology*, vol. 38, no. 3, pp. 301–313, 2000.

[120] N. Kopell, G. Ermentrout, M. Whittington, and R. Traubi, "Gamma rhythms and beta rhythms have different synchronization properties," *PNAS*, vol. 97, pp. 1867–1872, February 2000.

[121] W. H. R. Miltner, C. Braun, M. Arnold, H. Witte, and E. Taub, "Coherence of gamma-band EEG activity as a basis for associative learning," *Nature*, vol. 397, pp. 434–436, 1999.

[122] A. Keil, T. Gruber, and M. M. Müller, "Functional correlates of macroscopic high-frequency brain activity in the human visual system," *Neuroscience Biobehavioral Reviews*, vol. 25, no. 6, pp. 527–534, 2001.

[123] S. Palva and J. M. Palva, "New vistas for alpha-frequency band oscillations," *Trends in Neurosciences*, vol. 30, no. 4, pp. 150–158, 2007.

[124] J. M. Kilner, Y. Paulignan, and D. Boussaoud, "Functional connectivity during real vs imagined visuomotor tasks: an EEG study," *Neuroreport*, vol. 15, pp. 637–642, Mar. 2004.

[125] R. A. Andersen and C. A. Buneo, "Intentional maps in posterior parietal cortex," *Annual Review of Neuroscience*, vol. 25, pp. 189–220, 2002.

[126] R. Caminiti, S. Ferraina, and A. B. Mayer, "Visuomotor transformations: early cortical mechanisms of reaching," *Current Opinion in Neurobiology*, vol. 8, no. 6, pp. 753–761, 1998.

[127] J. F. Kalaska, S. H. Scott, P. Cisek, and L. E. Sergio, "Cortical control of reaching movements," *Current Opinion in Neurobiology*, vol. 7, no. 6, pp. 849–859, 1997.

[128] W. P. Medendorp, S. M. Beurze, S. V. Pelt, and J. V. D. Werf, "Behavioral and cortical mechanisms for spatial coding and action planning," *Cortex*, vol. 44, no. 5, pp. 587–597, 2008.

[129] D. Thoenissen, K. Zilles, and I. Toni, "Differential involvement of parietal and precentral regions in movement preparation and motor intention," *The Journal of Neuroscience*, vol. 22, no. 20, pp. 9024–9034, 2002.

[130] S. Wise, D. Boussaoud, P. Johnson, and R. Caminiti, "Premotor and parietal cortex: corticocortical connectivity and combinatorial computations.," *Annual review of neuroscience*, vol. 20, pp. 25–42, 1997.

[131] R. C. Oldfield, "The assessment and analysis of handedness: The edinburgh inventory," *Neuropsychologia*, vol. 9, pp. 97–113, Mar. 1971.

[132] J. Vrba and S. E. Robinson, "Signal processing in magnetoencephalography," *Methods*, vol. 25, no. 2, pp. 249–271, 2001.

[133] G. G. Supp, A. Schloegl, N. Trujillo-Barreto, M. M. Mueller, and T. Gruber, "Directed cortical information flow during human object recognition: Analyzing induced EEG gamma-band responses in brain's source space," *PLoS ONE*, vol. 8, p. e684, August 2007.

[134] G. Gómez-Herrero, M. Atienza, K. Egiazarian, and J. L. Cantero, "Measuring directional coupling between EEG sources," *NeuroImage*, vol. 43, no. 3, pp. 497–508, 2008.

[135] S. Holm, "A simple sequentially rejective multiple test procedure," *Scand J Stat*, vol. 6, pp. 65–70, 1979.

[136] C. Babiloni, F. Vecchio, S. Cappa, P. Pasqualetti, S. Rossi, C. Miniussi, and P. M. Rossini, "Functional frontoparietal connectivity during encoding and retrieval processes follows hera model a high-resolution study," *Brain Res Bull*, vol. 68, pp. 203–212, 2006.

[137] H. Sakata, M. Taira, M. Kusunoki, A. Murata, and Y. Tanaka, "The tins lecture the parietal association cortex in depth perception and visual control of hand action," *Trends in Neurosciences*, vol. 20, no. 8, pp. 350–357, 1997.

[138] M. Jeannerod, M. Arbib, G. Rizzolatti, and H. Sakata, "Grasping objects: the cortical mechanisms of visuomotor transformation," *Trends in Neurosciences*, vol. 18, no. 7, pp. 314–320, 1995.

[139] G. Pfurtscheller and F. L. da Silva, "Event-related EEG/MEG synchronization and desynchronization: basic principles," *Clinical Neurophysiology*, vol. 110, pp. 1842–1857, 1999.

[140] M. Iacoboni, "Visuo-motor integration and control in the human posterior parietal cortex: Evidence from TMS and fMRI," *Neuropsychologia*, vol. 44, pp. 2691–2699, 2006.

[141] L. G. Ungerleider and M. Mishkin, *Two Cortical Visual Systems*, ch. 18, pp. 549–586. MIT Press, 1982.

[142] M. A. Goodale, "Visuomotor control: Where does vision end and action begin?," *Current Biology*, vol. 8, no. 14, pp. R489–R491, 1998.

[143] S. Robinson and J. Vrba, *Recent advances in biomagnetism*, pp. 302–305. Sendai: Tohoku University Press, 1998.

[144] K. Amunts and K. Zilles, "Advances in cytoarchitectonic mapping of the human cerebral cortex," *Neuroimaging Clin N Am*, vol. 11, pp. 151–169, 2001.

[145] C. Papadelis, S. B. Eickhoff, K. Zilles, and A. A. Ioannides, "BA3b and BA1 activate in a serial fashion after median nerve stimulation: Direct evidence from combining source analysis of evoked fields and cytoarchitectonic probabilistic maps," *NeuroImage*, vol. 54, no. 1, pp. 60–73, 2011.

[146] G. Rizzolatti, L. Fadiga, M. Matelli, V. Bettinardi, E. Paulesu, D. Perani, and F. Fazio, "Localization of grasp representations in humans by PET: 1. Observation versus execution," *Experimental Brain Research*, vol. 111, pp. 246–252, 1996.

[147] H. Ehrsson, A. Fagergren, T. Jonsson, G. Westling, R. Johansson, and H. Forssberg, "Cortical activity in precision versus power grip tasks: An fMRI study," *Journal of Neurophysiology*, vol. 83, pp. 528–536, 1999.

[148] S. T. Grafton, M. A. Arbib, L. Fadiga, and G. Rizzolatti, "Localization of grasp representations in humans by positron emission tomography," *Experimental Brain Research*, vol. 112, pp. 103–111, 1996.

[149] C. Babiloni, F. Vecchio, M. Bares, M. Brazdil, I. Nestrasil, F. Eusebi, P. Rossini, and I. Rektor, "Functional coupling between anterior prefrontal cortex (BA10) and hand muscle contraction during intentional and imitative motor acts," *Neuroimage*, vol. 39, pp. 1314–1323, 2008.

[150] R. Kawashima, M. Matsumura, N. S. N, E. Naito, A. Waki, S. Nakamura, K. Matsunami, H. Fukuda, and Y. Yonekura, "Regional cerebral blood flow changes in human brain related to ipsilateral and contralateral complex hand movements-a PET study," *Eur J Neurosci*, vol. 10, pp. 2254–60, 1998.

[151] L. Faes, G. Nollo, and A. Porta, "Information-based detection of nonlinear granger causality in multivariate processes via a nonuniform embedding technique," *Phys. Rev. E*, vol. 83, p. 051112, May 2011.

[152] P. Achermann, R. Hartmann, A. Gunzinger, W. Guggenbühl, and A. Borbély, "All-night sleep EEG and artificial stochastic control signals have similar correlation dimensions," *Electroencephalogr Clin Neurophysiol*, vol. 90, no. 5, pp. 384–387, 1994.

[153] K. J. Blinowska and M. Malinowski, "Non-linear and linear forecasting of the EEG time series," *Biol Cybern*, vol. 66, no. 2, pp. 159–165, 1991.

Summary of Papers

Multivariate Autoregressive Model with Instantaneous Effects to Improve Brain Connectivity Estimation

Silvia Erla, Luca Faes, Enzo Tranquillini, Daniele Orrico, and Giandomenico Nollo

International Journal of Bioelectromagnetism 11(2): 74-79, 2009.

The assessment of brain connectivity in the frequency domain is one of the major issues that are faced nowadays in the field of experimental neurosciences. This fact is attested, from the signal processing point of view, by the recent development of methods aimed at the estimation of the causal influences among different brain areas in humans. Among them, partial directed coherence (PDC) analysis is emerging as one the most widely used tools to estimate brain connectivity, thanks to the fact that it provides a direct frequency domain description of the concept of Granger causality. As well as with many other causality measures, the evaluation of PDC relies on fitting the available multichannel data set with a multivariate autoregressive (MVAR) model that describes, for each time series, the linear contribution coming from its past samples and the past samples of all other time series.
The MVAR model implemented in all neuroscience applications is strictly causal, in the sense that only lagged effects are modeled and instantaneous (i.e., not lagged) effects among the time series are not described by any model coefficients. However, zero-lag interactions are likely to occur among simultaneously recorded neural signals, and the impact of their exclusion on connectivity measures has not been investigated yet. Neglecting instantaneous effects in MVAR models implies that any zero-lag correlation among the time series is translated into a correlation among the model residuals. This prevents the use of tools such as coherence or directed coherence requiring uncorrelation of the model residuals to be accessible.
In this study we propose the use of an extended MVAR model including instantaneous effects, and compare its performance to that of the traditional MVAR approach using the Partial Directed Coherence (PDC). The new approach is based on the fact

that introducing coefficients which describe instantaneous effects into a MVAR model also changes the coefficients describing the lagged effects. Hence, different inferences about Granger causality in the frequency domain are made using PDC and the new iPDC.
We show by simulations that, in presence of zero-lag correlations, the PDC derived from traditional MVAR modeling may produce misleading frequency domain connectivity evaluation, and that in such situations the correct connectivity pattern is recovered using the extended MVAR model. Then we provide examples of multichannel EEG recordings from normal subjects in the resting eyes closed condition. In this dataset, instantaneous effects are found to be far from negligible. We observed that iPDC values describe the back-to-front propagation of the alpha activity better than PDC. Thus, extended MVAR modeling seems more suitable to elucidate direction and strength of the interactions among EEG rhythms.

An Identifiable Model to Assess Frequency-Domain Granger Causality in the Presence of Significant Instantaneous Interactions

Luca Faes, Silvia Erla, Enzo Tranquillini, Daniele Orrico, and Giandomenico Nollo

Proceedings of the 32nd Annual International Conference of the IEEE EMBS 2010 1:1699-1702, 2010.

We present a new approach for the investigation of Granger causality in the frequency domain by means of the partial directed coherence (PDC). The approach is based on the utilization of an extended multivariate autoregressive (MVAR) model, including instantaneous effects in addition to the lagged effects traditionally studied, to fit the observed multiple time series prior to PDC computation. Model identification is performed combining standard MVAR coefficient estimation with a recent technique for instantaneous causal modeling based on independent component analysis. The approach is first validated on simulated MVAR processes showing that, in the presence of instantaneous effects, only the extended model is able to interpret the imposed Granger causality patterns, while the traditional MVAR approach may yield strongly biased PDC estimates. The subsequent application to multichannel EEG time series confirms the potentiality of the approach in real data applications, as the importance of instantaneous effects led to significant differences in the PDC estimated after traditional and extended MVAR identification.

Measuring Connectivity in Linear Multivariate Processes: Definitions and Interpretation

Luca Faes, Silvia Erla and Giandomenico Nollo

Submitted to Computational and Mathematical Methods in Medicine, Methodological Advances in Brain Connectivity, 2011.

This tutorial paper introduces a common framework for the evaluation of widely used frequency domain measures of coupling (Coherence, Partial Coherence) and causality (Directed Coherence, Partial Directed Coherence) from the parametric representation of linear multivariate (MV) processes. After providing a comprehensive time-domain definition of the various forms of connectivity observed in MV processes, we particularize them to MV autoregressive processes and derive the corresponding frequency-domain measures. Then we discuss the theoretical interpretation of these measures, showing that each of them reflects a specific time-domain connectivity definition and how this results in the description of peculiar aspects of the information transfer in MV processes. Furthermore, issues related to process identification, limitations and recommendations for the practical utilization of these measures on real MV time series are pointed out. Finally, we report an example of estimation of the presented measures from multiple EEG signals recorded during a combined visuomotor task, showing how evaluation of coupling and causality in the frequency domain may help describing the neurophysiological mechanisms of integration involving different sensory and motor systems.

Robust Estimation of Partial Directed Coherence by the Vector Optimal Parameter Search Algorithm

Silvia Erla, Luca Faes, and Giandomenico Nollo

Proceedings of the 4th International IEEE EMBS Conference on Neural Engineering 734-737, 2009.

The study of brain connectivity, explored through the multivariate analysis of EEG and/or MEG signals simultaneously collected from different brain areas, is one of the main topics faced nowadays in the neuroscience field. Among the multitude of methods proposed for the estimation of brain connectivity, the Partial Directed Coherence (PDC) is recognized as one of the most effective frequency-domain estimators of the directional coupling in multivariate networks, as it is directly grounded on the notion of Granger causality.
The practical estimation of PDC requires a reliable fitting of a multivariate vector autoregressive (MVAR) model to the available multichannel data set. One major issue in MVAR model fitting is the determination of the model order, i.e. of the proper number of model coefficients to be used for the description of the multivariate process under analysis. Indeed, the accuracy of parameter estimation impinges on correct model order selection. The approach most commonly used in neuroscience studies for estimating the MVAR coefficients from multichannel recordings is based on Vector Least Squares (VLS) model identification, with utilization of the Akaike Information Criterion (AIC) to select the model order. However, this approach suffers from a number of limitations (tendency to overestimation of the true model order, inability to discern missing terms, high noise sensitivity) that leave room for the development of more accurate MVAR identification methods.
In this study we propose the utilization of a recently introduced method for MVAR model identification, named the Vector Optimal Parameter Search (VOPS), for accurate estimation of PDC in multichannel time series. The VOPS method is tested,

in comparison with the traditional VLS method combined with the AIC for model order selection, over simulated MVAR processes with different coefficients and noise conditions. We show that the VOPS provides more accurate PDC estimates than the VLS (either overall and single-arc errors) in presence of interactions with long delays and missing terms, and for noisy multichannel time series.

Studying Brain Visuo-Tactile Integration through Cross-Spectral Analysis of Human MEG Recordings

Silvia Erla, Christos Papadelis, Luca Faes, Christoph Braun, and Giandomenico Nollo

IFMBE Proceedings: XII Mediterranean Conference on Medical and Biological Engineering and Computing 29:73-76, 2010.

An important aim in cognitive neuroscience is to identify the networks connecting different brain areas and their role in executing complex tasks. In this study, visuotactile tasks were employed to assess the functional correlation underlying the cooperation process between visual and tactile regions. MEG data were recorded from eight healthy subjects while performing a visual, a tactile, and a visuo-tactile task. To define regions of interest (ROIs), event-related fields (ERFs) were estimated from MEG data related to visual and tactile areas. The ten channels with the highest increase in ERF variance, moving from rest to task, were selected. Cross-spectral analysis was then performed to assess potential changes in the activity of the involved regions and quantify the coupling between visual and tactile ROIs. A significant decrease ($p<0.01$) in the power spectrum was observed during performing the visuo-tactile task compared to rest, both in alpha and beta bands, reflecting the activation of both visual and tactile areas during the execution of the corresponding tasks. Compared to rest, the coherence between visual and tactile ROIs increased during the visuo-tactile task. These observations seem to support the binding theory assuming that the integration of spatially distributed information into a coherent percept is based on transiently formed synchronized functional networks.

Multivariate EEG Spectral Analysis evidences the functional link between motor and visual cortex during integrative sensorimotor tasks

Silvia Erla, Luca Faes, Giandomenico Nollo, Carola Arfeller, Christoph Braun, and Christos Papadelis

Biomedical Signal Processing and Control, 2011.

The identification of the networks connecting brain areas and the understanding of their role in executing complex tasks is a crucial issue in cognitive neuroscience. In this study, specific visuomotor tasks were devised to reveal the functional network underlying the cooperation process between visual and motor regions. Electroencephalography (EEG) data were recorded from twelve healthy subjects during a combined visuomotor task, which integrated precise grip motor commands with sensory visual feedback (VM). This condition was compared with control tasks involving pure motor action (M), pure visual perception (V) and visuomotor performance without feedback (V + M). Multivariate parametric crossspectral analysis was applied to ten EEG derivations in each subject to assess changes in the oscillatory activity of the involved cortical regions and quantify their coupling. Spectral decomposition was applied to precisely and objectively determine the power associated with each oscillatory component of the spectrum, while surrogate data analysis was performed to assess the statistical significance of estimated coherence values. A significant decrease of the alpha and/or beta power in EEG spectra with respect to rest values was assumed as indicative of specific cortical area activation during task execution. Indeed alpha band coherence increased in proximity of task-involved areas, while it was suppressed or remained unchanged in other regions, suggesting the activation of a specific network for each task. According to our coherence analysis, a direct link between visual and motor areas was activated during V + M and VM tasks. The ef-

fect of visual feedback was evident in the beta band, where the increase of coherence was observed only during the VM task. Multivariate analysis suggested the presence of a functional link between motor and visual cortex subserving sensorimotor integration. Furthermore, network activation was related to the sum of single task (M and V) local effects in the alpha band, and to the presence of visual feedback in the beta band.

Improving evaluation of functional causality network during visuomotor taks by MVAR model with istantaneous interaction

Silvia Erla, Christos Papadelis, Luca Faes, Carola Arfeller, Christoph Braun, and Giandomenico Nollo

In preparation, 2011.

The identification of communication patterns between different brain areas and their involvement in the execution of complex tasks is nowadays one of the most important aims in cognitive neurosciences. In the present study, we applied a novel signal processing approach for the study of brain connectivity between visual and motor brain regions during visuo-motor integration. The recently proposed definition of extended multivariate autoregressive (eMVAR) models including the instantaneous correlations was adopted and coupling and causality frequency-domain measures were computed in a visuo-motor paradigm.
EEG data were recorded from twelve healthy subjects during continuous integration of motor control in a precision grip task with sensory feedback from the visual system (VM). For each subject, extended multivariate autoregressive coefficients were identified. Coupling analysis was performed by computing coherence (COH) and partial coherence (PC), while causality was assessed through directed coherence (DC), partial directed coherence (PDC) and the novel extended corresponding measures (iDC, iPDC, eDC and ePDC), to test them on real data and discuss possible advantages and limitations. Surrogate data analysis was adopted to assess the statistical significance of the estimated measures. For each measure a specific approach for surrogate data generation was performed.
The connectivity analysis suggested (i) the usefulness of a combined analysis considering both the strength and the direct/non-direct nature of the interactions for a

full comprehension of the involved connectivity patterns; (ii) the efficacy of the new measures, which consider instantaneous effects, for real data analysis, since they detected important connections, which were not significant in the traditional MVAR measures; (iii) the possibility to better disentangle the causal relations between different cortical areas through eMVAR modeling, distinguishing between instantaneous and lagged effects.

The rostral inferior frontal gyrus monitors instructed visuomotor behaviour by linking the visual and motor cortices

Christos Papadelis, Carola Arfeller, Silvia Erla, Giandomenico Nollo, Luigi Cattaneo, Christoph Braun

Submitted to Plos, 2011.

Beyond its role in language processing, inferior frontal gyrus (IFG) seems to constitute a cortical interface area between perception and action. IFG has been shown to be active during imagery or execution of complex motor tasks involving sensorimotor interaction. However, little is known about its functional connections with other brain regions involved in the neural networks that integrate spatially distributed information in sensorimotor control. Here, we investigated the functional coupling between regional activations in the visual and motor cortex through the IFG in twelve healthy subjects using magnetoencephalography. Functional coupling was assessed on the basis of oscillatory brain activity during a simple visuomotor task that involved the continuous tracking of a predefined force varying in time. The task required the integration of precise grip motor commands with sensory feedback from the visual system. By combining well-established tools for source localisation, source identification based on probabilistic cytoarchitectonic maps, and multivariate autoregressive coherence analysis, we identified a complex brain network with activities oscillating in the alpha frequency band. This large-scale network was identified by examining the power decrease of magnetic brain activity during task performance compared to rest. It involved motor and visual areas as well as parts of the left and right IFG. Our results demonstrate a functional link between the motor and visual cortex through the IFG subserving sensorimotor integration. This link is in agreement with well-known anatomical connections, such as the inferior occipito-frontal fascicle that

mediates the communication between extrastriate areas and the prefrontal cortex.

Acknowledgements

I would like to express my sincere gratitude to all those supported me and collaborated to the work done during my PhD. I will mention here only some of them, but I will be forever grateful to everyone who shared with me his time and friendship.

Firstly to Giandomenico Nollo, who introduced me to the field of signal processing and gave me the opportunity to complete this thesis. Thank you for his advices in some crucial points of the work, and for the enthusiasm and never failing support.
Thank to my co-advisor, Christoph Braun, for introducing me to MEG recording and analysis techniques, for sharing his excellent knowledge in cognitive neurosciences, for his support and patience.

I am especially grateful to my "mentor", Luca Faes, for professionally teaching me what signals analysis is and for sharing his excellent knowledge in methodology. It is my pleasure to be a co-worker and a friend of him.
A warm thanks to Christos Papadelis, for his support and contribution to my work, for sharing his excellent knowledge in neurosciences and for the stimulating collaboration. His enthusiasm and friendship created a pleasant atmosphere during my research work.
Thank also to Carola Arfeller for sharing data and contributing to the research study.

I express my gratitude to Daniele Orrico, Enzo Tranquillini and Maria Lisanti at the Neurology Division of the S. Chiara Hospital, Trento, Italy, for giving me their time and clinical point of view, showing perspective and potential benefits of my research for patients.
A warm thank to Ferruccio Panzica, Giulia Varotto and Elisa Visani of the Unit of Neurophysiopathology, Istituto Neurologico Carlo Besta, Milano, Italy, for giving me the opportunity to test my algorithms on challenging data, and for the stimulating discussions.

A special thank to Michela Masè. Her precious friendship and kindly scientific guidance have been essential during these three years.
Furthermore, thank to Walter Mattei, Alessandro Cristoforetti, Nicola Pace, and Ulrike Richter, for the pleasure of sharing the office with them, interestingly discussing about science and daily news.

Thanks to all my friends, especially those of them sharing with me the passion

of photography and my "train-mornings" traveling to my working place. Thanks for encouraging me, for the nice time spent together and for remembering me that there are other good things in life than work.

To Francesco, for his support and patience, for believing in me and making my life colorful, even in "hard times".

Last but not least, thanks to my mother and my father, for loving me all life-long, for their extraordinary support and for being always present.

Silvia

About the author

Silvia Erla was born in Trento (Italy), in1983.

She received the Bachelor Degree in Physics, cum laude, in 2005, and the Msc. Degree in Physics and Biomedical Technologies, cum laude, in 2008 at the University of Trento, Italy.
She has been a research fellow of the Biophysics and Biosignal Laboratory, at the Department of Physics, University of Trento from April to August 2008. She moved to the Centre for Mind/Brain Sciences (CIMeC), University of Trento, in September 2008.

Her main research interest is the study of cortical complexity and connectivity in neurophysiological multichannel recordings (EEG and MEG) from healthy subjects (multisensory and visuo-motor integration processes) and patients (stroke, coma and ischemia).

List of publications

Extended publications

1. Faes L, Erla S, Nollo G: "Quantifying the Complexity of Short-Term Heart Period Variability through K-Nearest Neighbor Local Linear Prediction". Computers in Cardiology 2008; 35:549-552.

2. Erla S, Faes L, Nollo G: "Robust Estimation of Partial Directed Coherence by the Vector Optimal Parameter Search Algorithm". Proceedings of the 4th International IEEE EMBS Conference on Neural Engineering 2009; 734-737.

3. Erla S, Faes L, Tranquillini E, Orrico D, Nollo G: "Multivariate Autoregressive Model with Instantaneous Effects to Improve Brain Connectivity Estimation". International Journal of Bioelectromagnetism, 11(2): 74-79, 2009.

4. Erla S, Faes L, Nollo G: "Quantifying changes in EEG complexity induced by photic stimulation". Methods of Information in Medicine, 49: 496-500, 2010.

5. Erla S, Papadelis C, Faes L, Braun C, Nollo G: "Studying Brain Visuo-Tactile Integration through Cross-Spectral Analysis of Human MEG Recordings". IFMBE

Proceedings: XII Mediterranean Conference on Medical and Biological Engineering and Computing 2010, 29: 73-76, 2010.

6. Faes L, Erla S, Tranquillini E, Orrico D, Nollo G: "An Identifiable Model to Assess Frequency-Domain Granger Causality in the Presence of Significant Instantaneous Interactions". Proceedings of the 32nd Annual International Conference of the IEEE EMBS 2010, 1: 1699-1702, 2010.

7. Faes L, Nollo G, Erla S, Papadelis C, Braun C, Porta A: "Detecting Nonlinear Causal Interactions between Dynamical Systems by Non-uniform Embedding of Multiple Time Series". Proceedings of the 32nd Annual International Conference of the IEEE EMBS 2010, 1: 102-105, 2010.

8. Erla S, Faes L, Tranquillini E, Orrico D, Nollo G: "k-Nearest Neighbour Local Linear Prediction of scalp EEG activity during Intermittent Photic Stimulation". Medical Engineering and Physics, 33: 504-512, 2011.

9. Erla S, Faes L, Nollo G, Arfeller C, Braun C, Papadelis C: "Multivariate EEG Spectral Analysis evidences the functional link between motor and visual cortex during integrative sensorimotor tasks". Biomedical Signal Processing and Control, 2011 (in press).

10. Papadelis C, Arfeller C, Erla S, Nollo G, Braun C: "Inferior Frontal Gyrus Functionally Couples Visual and Motor Cortex in Sensorimotor Control". Submitted to Plos, 2011.

11. Faes L, Erla S, Nollo G: "Measuring Connectivity in Linear Multivariate Processes: Definitions and Interpretation". Submitted to Computational and Mathematical Methods in Medicine, Methodological Advances in Brain Connectivity, 2011.

12. Faes L, Erla S, Nollo G: "A framework for assessing frequency domain causality in multivariate linear processes with instantaneous interactions". In progress 2011.

13. Erla S, Faes L, Nollo G, Arfeller C, Braun C, Papadelis C: "Improving evaluation of functional causality network during visuomotor taks by MVAR model with istantaneous interaction". In progress 2011.

14. Erla S, Varotto G, Panzica F, Faes L, Nollo G: "Quantification of nonlinear complexity and connectivity in photosensitive idiopathic generalized epilepsy patients during photic stimulation". In progress 2011.

Other publications: congress acta

1. Erla S, Greiner S, Faes L, Orrico D, Tranquillini E, Lisanti M, Nollo G: "Predictability maps of the brain electrical activity". Proceedings of the Neuromath Workshop 2007.

2. Faes L, Erla S, Greiner S, Ki H Chon, Nollo G: "Time varying nonlinear prediction of EEG signals". Proceedings of the Neuromath Workshop 2007.

3. Erla S, Faes L, Greiner S, Lisanti M, Orrico D, Tranquillini E, Antolini R, Nollo G: "Quantification of the Complexity of the Cortical Electrical Activity during Visual Stimulation". Proceedings of the XIX Congresso Nazionale della Società Italiana di Biofisica Pura e Applicata (SIBPA) 2008; 45-46.

4. Greiner S, Tranquillini E, Erla S, Orrico D, Lisanti M, Faes L, Nollo G, Antolini R: "Detection of weak frequency coupling in EEG signals by combination of second order spectral analysis and statistical analysis". Proceedings of the XIX Congresso Nazionale della Società Italiana di Biofisica Pura e Applicata (SIBPA) 2008; 44-45.

5. Erla S, Faes L, Tranquillini E, Orrico D, Nollo G: "Multivariate Autoregressive Model with Instantaneous Effects to Improve Brain Connectivity Estimation". Proceedings of the 7th NFSI & ICBEM 2009 Conference (CD).

6. Erla S, Faes L, Nollo G: "Quantifying changes in EEG complexity induced by photic stimulation". Proceedings of the 6th International Workshop on Biosignal Interpretation 2009; 212-215.

7. Papadelis C, Arfeller C, Erla S, Nollo G, Plewnia C, Braun C: "Visuo-motor integration enhances coherent sources in the human brain". Conference Abstract: Biomag 2010, 17th International Conference on Biomagnetism.

8. Erla S, Faes L, Papadelis C, Borchers S, Arfeller C, Braun C, Nollo G: "Quantification of Power and Coherence of the Electrophysiological Activity of Brain Areas Involved in a Visuo-Tactile Task". Conference Abstract: Biomag 2010, 17th International Conference on Biomagnetism.

9. Erla S, Papadelis C, Braun C, Faes L, Nollo G: "Power changes due to visuomotor task in scalp EEG and MEG source signals". Conference Abstract: NeuroMath COST Action BM0601: Neurodynamic insight into functional connectivity, cognition, and consciousness 2010.

10. Erla S, Papadelis C, Faes L, Braun C, Nollo G: "Spectral and Coherence Analysis to investigate Multisensory Brain Integration Processes". Conference Abstract: XX Congresso Nazionale della Società Italiana di Biofisica Pura e Applicata (SIBPA), 2010.

11. Erla S, Faes L, Orrico D, Tranquillini E, Lisanti M, Nollo G: "EEG complexity analysis during photic stimulation in healthy subjects and patients with severe brain damages". Conference Abstract: XX Congresso Nazionale della Società Italiana di Biofisica Pura e Applicata (SIBPA), 2010.

12. Faes L, Erla S, Nollo G: "Investigating the impact of instantaneous causality on frequency domain connectivity measures". Conference Abstract: SAN 2011 Workshop, 2011.

13. Papadelis C, Arfeller C, Erla S, Nollo G, Cattaneo L, Braun C: "Rostral inferior frontal gyrus monitors visuomotor behaviour by linking visual and motor cortices". Conference Abstract: HBM Conference, 2011.